

CONTROL FOR AUTONOMOUS ALL-ELECTRIC SHIPS

INTEGRATING MANEUVERING, ENERGY MANAGEMENT, AND
POWER GENERATION CONTROL

CONTROL FOR AUTONOMOUS ALL-ELECTRIC SHIPS

**INTEGRATING MANEUVERING, ENERGY MANAGEMENT, AND
POWER GENERATION CONTROL**

Dissertation

for the purpose of obtaining the degree of doctor
at Delft University of Technology,
by the authority of the Rector Magnificus Prof.dr.ir. T.H.J.J. van der Hagen,
chair of the Board for Doctorates.
to be defended publicly on
Tuesday 3 December 2019 at 15:00 o'clock

by

Ali HASELTALAB

Master of Science in Electrical and Electronic Engineering, Boğaziçi University, Turkey
born in Tehran, Iran

This dissertation has been approved by the promotors.

Composition of the doctoral committee:

Rector Magnificus,	chairperson
Prof.dr. R.R. Negenborn,	Delft University of Technology, promotor
Prof.ir. J.J. Hopman,	Delft University of Technology, promotor

Independent members::

Prof.dr. A. Ferrara	University of Pavia, Italy
Prof.dr. M.A.D. Ayala Botto	University of Lisbon, Portugal
Prof.dr. M. Gibescu	Utrecht University
Prof.dr.ir. M. van Koningsveld	Delft University of Technology
Prof.dr.ir. P.M. Herder	Delft University of Technology



Keywords: Autonomous ships, DC all-electric, Power and propulsion systems, Model predictive control, Adaptive control

Printed by: Ipskamp printing

Cover by: Saba Saboursadeghzadeh

Front & Back: An autonomous all-electric vessel sails towards its destination

Copyright © 2019 by Ali Haseltalab

ISBN 978-94-6384-088-0

An electronic version of this dissertation is available at
<http://repository.tudelft.nl/>.

*To my parents, Hassan and Farideh
my brother, Omid
and my wife, Saba.
Thanks for all the support.*

CONTENTS

Summary	xi
Samenvatting	xiii
Preface	xv
Nomenclature	xvii
List of Figures	xxiii
List of Tables	xxv
1 Introduction	1
1.1 Autonomous shipping	1
1.2 Fuel efficiency	2
1.3 Stability and robustness.	4
1.4 Integrating maneuvering, energy management, and power generation control.	5
1.5 Problem statement and research questions	6
1.6 Thesis Outline	7
2 Literature Review	11
2.1 Maneuvering control	11
2.1.1 Path following control	12
2.1.2 Trajectory tracking control	14
2.1.3 Research opportunities	14
2.2 Energy management for DC-PPS	16
2.3 Power generation control	17
2.4 Conclusions.	21
3 Mathematical Modeling of Autonomous All-Electric Ships	23
3.1 3DoF maneuvering model	23
3.1.1 Thrust allocation.	25
3.2 DC power and propulsion system.	26
3.3 Energy consumption side	27
3.3.1 Propeller	27
3.3.2 Induction motor	28
3.3.3 State space modeling of energy consumption side	28

3.4	Energy generation side	29
3.4.1	Diesel engine	29
3.4.2	Synchronous generator	29
3.4.3	Rectifier and the DC-link.	30
3.4.4	Battery	31
3.4.5	Bidirectional converter.	31
3.4.6	State space modeling of energy generation side	32
3.5	The overall ship model	34
3.6	Conclusions.	35
4	Maneuvering Control in the Presence of Uncertainty	37
4.1	Introduction	37
4.2	The problem of uncertainty in propeller model	38
4.3	Problem formulation	40
4.4	Adaptive control strategy	42
4.4.1	Proposed control strategy	42
4.4.2	Stability analysis and the algorithm design.	43
4.4.3	The case of state dependent uncertainty	47
4.4.4	Application to autonomous ships	49
4.5	Simulation experiments and evaluation results	50
4.6	Conclusions.	60
5	Predictive Maneuvering Control	61
5.1	Model predictive maneuvering control	61
5.2	Scale-model experiments	64
5.2.1	Experiment I: circular trajectory	65
5.2.2	Experiment II: trajectory tracking in Oude Maas	67
5.3	Conclusions.	67
6	Energy Management for All-Electric Ships	71
6.1	Predictive energy management	71
6.2	Simulation experiments.	76
6.2.1	Experiment I: circular trajectory	76
6.2.2	Experiment II: voyage in the Port of Rotterdam	79
6.2.3	Experiment III: real operating profiles	79
6.3	Conclusions.	89
7	Control for Diesel-Generator-Rectifier Sets	91
7.1	State space modeling of DGR sets	92
7.2	The proposed control strategy	93
7.2.1	Input-output feedback linearization	93
7.2.2	Tube-based model predictive controller	95
7.2.3	Stability proof	97
7.2.4	Constraint linearization	98
7.2.5	Extension to diesel-generator shaft speed control	99

7.3	Integration with maneuvering control	100
7.4	Simulation experiments.	101
7.4.1	Model validation	101
7.4.2	Experiment I: voltage control under varying ship speed	104
7.4.3	Experiment II: fault-tolerance under a CPL	108
7.4.4	Experiment III: high speed voyage	108
7.5	Conclusions.	108
8	Multi-Level Control of Energy Generation Side	117
8.1	State space modeling of energy generation side.	118
8.2	Proposed Control strategy.	118
8.2.1	Control of the DGR sets	119
8.2.2	Control of the battery-converter set	123
8.2.3	Coordinator: control for the DC-link voltage	124
8.3	Simulation experiments.	126
8.3.1	Simulation model validation	126
8.3.2	Experiment I: voltage control under varying load	126
8.3.3	Experiment II: short circuit test	128
8.4	Conclusions.	132
9	Conclusions and Future Research	135
9.1	Addressing the research questions	135
9.2	Contributions of the thesis	138
9.3	Recommendations for future research direction	140
9.3.1	Maneuvering control of autonomous ships	140
9.3.2	Energy management for all-electric ships	141
9.3.3	Power generation control	141
	Bibliography	143
A	Appendix	153
A.1	Maneuvering model of Tito-Neri	153
A.2	Specifications of the low voltage PPS	153
A.2.1	Diesel engine	153
A.2.2	Synchronous generators	153
A.2.3	Rectifier	153
A.2.4	DC-link	153
A.2.5	Induction motor	155
A.2.6	Propelling actuators	155
A.2.7	Battery.	155
A.2.8	Bidirectional converter.	155
A.3	Specifications of the high voltage PPS.	156
	List of Publications	157
	Curriculum Vitae	159

SUMMARY

In the last few years, autonomous shipping has been under extensive consideration by academic and industrial communities as well as governmental organizations due to several potential advantages that it introduces. Furthermore, due to the drastic environmental consequences of transport over water, international organizations have enforced the shipping industry to reduce its emissions significantly. As a result, the emergence of sustainable autonomous shipping seems inevitable.

Autonomous ships are expected to yield advantage from several points of view such as reduced crew cost, higher safety, and more adaptability to different operating profiles. However, several challenges need to be addressed before fully operational autonomous ships can be enabled. These difficulties include problems with automatic path planning, navigation and trajectory tracking, cooperation with other vessels, power and energy management issues, and fault-detection, isolation and reconfiguration. Due to the expected reduced number of on-board crew members in autonomous vessels the role for automation and independent machine performance in all of the mentioned issues increases significantly and becomes more vital. For this purpose, the adoption of intelligent control and management schemes for diverse purposes is necessary.

There has been a great effort from shipping industry to reduce the environmental impact as well as increasing the fuel efficiency of ships. This has led to the arrival of modern power and propulsion architectures. The number and variety of components in these power and propulsion systems is significantly more compared to direct-diesel architectures. As a result, more advanced approaches are required to control the modern power and propulsion systems. In the literature, it has been shown that without the adoption of advanced control approaches, these modern power and propulsion systems are not as effective as they should be.

This dissertation aims at taking a step towards enabling autonomous ships with maximized fuel efficiency by proposing novel approaches for maneuvering, energy management, and power generation control. In the literature, these three problems have been studied independently from one another, while they are closely connected. Throughout this dissertation, a framework is proposed that does integrate maneuvering, energy management, and power generation control. The focus of this research work is on all-electric power and propulsion systems where the energy sources and propulsive actuators are connected through an electrical network.

The scientific contribution of this thesis starts with the modeling of all-electric ships. First, a maneuvering model is presented for the ship which captures the maneuvering dynamics in 3 degrees of freedom. In this thesis, the maneuvering model represents a non-affine in control system which encompasses the dynamics of the propelling actuators. For modeling of the power and propulsion system, a model is presented for each of the mechanical and electrical components. Then, these mathematical models

are merged to establish dynamical models for the energy generation and consumption sides.

For maneuvering control in the presence of uncertainties an adaptive control approach is proposed to steer the ship towards its desired trajectory by adopting neural networks that is used for estimating the dynamics of the propellers and handling hydrodynamical uncertainties. Considering that the maneuvering model of a vessel resembles a nonlinear non-affine in control system, the proposed neural-based adaptive control approach is designed to estimate the nonlinear influence of the input function which in this case is the dynamics of propellers and thrusters. It is also shown that the proposed methodology is capable of handling state dependent uncertainties within the ship maneuvering model. A Lyapunov-based technique and Uniform Ultimate Boundedness are used to prove the correctness of the algorithm. To assess the method's performance, several experiments are considered including trajectory tracking simulations in the port of Rotterdam.

Furthermore, a model predictive maneuvering control approach is proposed for constraint handling and prediction of future required propulsive power. This control approach is designed using Input-Output Feedback Linearization (IOFL). Through this approach, the required power for the ship mission is predicted and then, transferred to the energy management and power generation control modules.

To maximize the fuel efficiency of the vessel, an energy management approach is proposed which utilizes the predicted future required power to guarantee the optimal power split between energy sources. Using the proposed approach, it is ensured that if a diesel-generator is active, it is functioning around the optimal point on its specific fuel consumption curve. Several simulation cases have been considered for the evaluation of the proposed approach including a voyage in the port of Rotterdam waterways and operating profiles of a real tug.

To guarantee the stability of the power and propulsion system, a model predictive control approach is presented for the control of DGR sets. Later, this approach is extended to the case of controlling the energy generation side where multiple diesel-generator-rectifier sets and a battery-converter set are present. For power generation control, a multi-level MPC approach is proposed which utilizes the predicted future propulsive power as well as an approach to enable the use of quadratic programming schemes for solving the optimization problem of the model predictive controller. Several simulation cases are considered which are applied to a high fidelity model.

The results of this thesis indicate that using advanced control approaches, the efficiency, flexibility, and performance of autonomous all-electric ships can significantly be improved when facing different operating profiles.

SAMENVATTING

In de afgelopen paar jaar werd autonome scheepvaart door academische en industriële gemeenschappen uitgebreid overwogen evenals door overheidsorganisaties vanwege verschillende potentiële voordelen die het zal introduceren. Bovendien hebben internationale organisaties vanwege de drastische milieugevolgen van transport over water de scheepvaartsector gedwongen om de uitstoot aanzienlijk te verminderen. Als gevolg hiervan lijkt de opkomst van duurzame autonome scheepvaart onvermijdelijk.

De verwachting is dat autonome schepen vanuit verschillende gezichtspunten voordelen hebben, zoals lagere bemanningskosten, hogere veiligheid en meer aanpassingsvermogen aan verschillende bedrijfsprofielen. Er moeten echter verschillende uitdagingen worden aangepakt voordat volledig operationele autonome schepen kunnen worden ingeschakeld. Deze problemen omvatten automatische padplanning, navigatie en traject volgen, samenwerking met andere schepen, vermogen en energiebeheer, en foutdetectie, isolatie en herconfiguratie. Vanwege het verwachte verminderde aantal bemanningsleden aan boord in autonome schepen neemt de rol van automatisering en onafhankelijke machineprestaties in alle genoemde kwesties aanzienlijk toe en wordt ze vitaler. Voor dit doel is de toepassing van intelligente besturingschema's voor uiteenlopende doeleinden noodzakelijk.

Er is veel werk verzet van de scheepvaartindustrie om de milieueffecten te verminderen evenals het verhogen van de brandstofefficiëntie van schepen. Dit heeft geleid tot de komst van moderne vermogen- en voortstuwingsarchitecturen. Het aantal en de verscheidenheid van componenten in deze vermogen- en voortstuwingssystemen is, aanzienlijk groter in vergelijking met direct-diesel architecturen. Dientengevolge zijn geavanceerdere benaderingen vereist om de moderne vermogen- en voortstuwingssystemen te besturen. In de literatuur is aangetoond dat deze moderne vermogen- en voortstuwingssystemen zonder de invoering van geavanceerde regelmethoden, niet zo effectief zijn als ze zouden moeten zijn.

Deze dissertatie wil een stap zetten naar het mogelijk maken van autonome schepen met maximale brandstofefficiëntie, door het voorstellen van nieuwe benaderingen voor manoeuvreren, energiebeheer en energieopwekking. In de literatuur zijn deze drie problemen onafhankelijk van elkaar bestudeerd, terwijl ze nauw met elkaar verbonden zijn. In deze dissertatie wordt een raamwerk voorgesteld die het manoeuvreren, energiebeheer en het beheer van energieopwekking integreert. De focus van dit onderzoek ligt op volledig elektrisch vermogen- en voortstuwingssystemen waarbij de energiebronnen en voortstuwingsactuators zijn verbonden via een elektrisch netwerk.

De wetenschappelijke bijdrage van deze dissertatie begint met het modelleren van volledig elektrische schepen. Eerst wordt een manoeuvreermodel gepresenteerd voor het schip dat de manoeuvreerdynamiek vastlegt in 3 vrijheidsgraden. In deze dissertatie vertegenwoordigt het manoeuvreermodel een niet-affinaal controlesysteem dat de dynamiek van de aandrijvende actuators omvat. Voor het modelleren van het vermogen-

en het voortstuwingssysteem, wordt een model gepresenteerd voor elk van de mechanische en elektrische componenten. Vervolgens worden deze mathematische modellen samengevoegd om dynamische modellen op te stellen voor de energieopwekking en verbruik.

Voor manoeuvreerbesturing, in aanmerking nemend alle onzekerheden, wordt een adaptieve besturingsbenadering voorgesteld om het schip naar zijn gewenste traject te sturen door de aanname van neurale netwerken, die worden gebruikt voor het inschatten van de dynamiek van de schroeven en het omgaan met hydrodynamische onzekerheden. Gezien het feit dat het manoeuvreermodel van een vat lijkt op een niet-lineair niet-affien in controlesysteem, is de voorgestelde neurale gebaseerde adaptieve controle-aanpak ontworpen om de niet-lineaire invloed van de invoerfunctie te schatten, wat in dit geval de dynamiek van propellers en stuwkrachten is. Er wordt ook aangetoond dat de voorgestelde methodologie in staat is om van de toestand afhankelijke onzekerheden in het scheepsmanoeuvreermodel te handhaven. Een op Lyapunov gebaseerde techniek en Uniform Ultimate Boundedness worden gebruikt om de juistheid van het algoritme aan te tonen. Om de prestaties van de methode te beoordelen, worden verschillende experimenten overwogen, waaronder trajectory-tracking simulaties in de haven van Rotterdam.

Verder wordt een modelvoorspellende manoeuvreer besturingsaanpak voorgesteld voor het afhandelen van beperkingen en het voorspellen van in de toekomst vereist voortstuwingsvermogen. Deze besturingsaanpak is ontworpen met behulp van Input-Output Feedback Linearisation (IOFL). Door deze benadering wordt de vereiste kracht voor de scheepsmissie voorspeld en vervolgens overgedragen aan de regeleenheden voor energiebeheer en energieopwekking.

Om de brandstofefficiëntie van het schip te maximaliseren, wordt een benadering voor energiebeheer voorgesteld, die gebruikmaakt van de voorspelde toekomstige vereiste stroom, om de optimale vermogensverdeling tussen energiebronnen te garanderen. Met de voorgestelde aanpak wordt ervoor gezorgd, dat als een dieselgenerator actief is, deze rond het optimale punt op zijn specifieke brandstofverbruikcurve functioneert. Verschillende simulaties werden overwogen voor de evaluatie van de voorgestelde aanpak, inclusief een reis in de Rotterdamse waterwegen en operationele profielen van een echte sleepboot.

Om de stabiliteit van het vermogen en het voortstuwingssysteem te garanderen, wordt een modelvoorspellende besturingsaanpak gepresenteerd voor de besturing van DGR-sets. Later wordt deze aanpak uitgebreid tot het regelen van de energieopwekkingzijde waar meerdere diesel-generator -rectifier -sets en een batterij-omzetterset aanwezig zijn. Voor de controle van de stroomopwekking wordt een multi-level MPC-benadering voorgesteld, die gebruik maakt van de voorspelde toekomstige voortstuwingskracht als ook een benadering om het gebruik van kwadratische programmeringsschema's mogelijk te maken voor het oplossen van het optimalisatieprobleem van de modelvoorspellende regelaar. Verschillende simulatiegevallen worden overwogen die worden toegepast op een high fidelity-model. De resultaten van deze dissertatie geven aan dat het gebruik van geavanceerde besturingsmethoden, de efficiëntie, flexibiliteit en prestaties van autonome volledig elektrische schepen aanzienlijk kan worden verbeterd, wanneer zij worden geconfronteerd met verschillende operationele profielen.

PREFACE

First and foremost, I would like to thank my promotor Prof. Dr. Rudy Negenborn for putting his trust in me to carry out this project. His supervision, inclusive behavior, and patience were not only helpful and effective but also inspirational. I also would like to thank my other promotor Prof. ir. Hans Hopman for his supervision during this project, especially its second two years. I also wish to thank all the members of the doctoral committee for accepting our invitation and being part of the defense ceremony.

In the design of the proposed adaptive maneuvering controller in Chapter 4, the discussions with Dr. ir. Arthur Vrijdag and Dr. ir. Milinko Godjevac were very helpful. The trajectory of the real vessel in Section 4.5 has been provided by the Port of Rotterdam Authority in an automatic identification system data file. The content of the data file was categorized and arranged by Daan de Boer.

The Tito-Neri's maneuvering model in Chapter 5 is extracted by Daan Bruiggink, Quintin Cremer, Rik Groenewegen and Aernout Klokgieters under the supervision of Vittorio Garofano, Ali Haseltalab, and Rudy Negenborn. All are affiliated with Delft University of Technology.

For modeling of the DC-PPS components and the design of the proposed energy management approach, discussions with Dr. ir. Rinze Geertsma were very inspirational and useful. The operating profiles in Section 6.2.3 are provided by Damen Shipyards Gorinchem and through Rinze.

The power generation control approach in Chapter 7 is designed in collaboration with Prof. Dr. Miguel Ayala Botto. He was a great help during this part of my PhD project and hosted me for almost a month in Tecnico Lisboa. This part of the project is partially supported by Fundação para a Ciência e a Tecnologia (FCT), through IDMEC, under LAETA Pest-OE/EME/LA0022.

The components data of simulation models in Chapters 7 and 8 are provided by Piet Lievense of Damen Schelde Naval Shipbuilding. He has also been a great help during this PhD project. Our discussions on power and propulsion system stability and control have been very helpful and inspirational for me. Moreover, the ship model in Chapter 7 is provided by Damen Shipyards Gorinchem. The bidirectional converter model and its control scheme (presented in Chapter 8) are designed in collaboration with Faisal Wani. Our discussions on parallel control of DGR sets and the battery-converter set have been very useful for the ends of this project.

I would like to thank Saba Saboursadeghzadeh and Joost Verouden for translating the English summery into Dutch. Saba also designed the book cover (thanks honey!).

I would like to thank ShipDrive project colleagues Ioana Georgescu, Rinze Geertsma, Klaas Visser, Milinko Godjevac, Henk Polinder, Rudy Negenborn and Hans Hopman, and ShipDrive user committee members especially Gert-Jan Meijn, Erik-Jan Boonen, Benny Mestemaker, and Michiel Post for all the help and support during the project. I also would like to thank my colleagues in Maritime and Transport Engineering Department.

The supporting staff, secretariats, and the executive managers of the department have been a great help during past four years. Among them, I especially wish to thank Dineke Heersma, Patty Bokop-van der Stap, Anouk de Goede-Oosterhoff, Monique Gazendam, and Pauline de Ruijt-Franke. Finally, I would like to thank Vittorio Garofano who has helped me in different stages of this project, especially the parts related to maneuvering control.

This research is supported by the project “ShipDrive: A Novel Methodology for Integrated Modelling, Control, and Optimization of Hybrid Ship Systems” (project 13276) of the Netherlands Organization for Scientific Research (NWO), domain Applied and Engineering Sciences (TTW) and is supported by industrial partners Damen Schelde Naval Shipbuilding, Damen Shipyards Gorinchem, Bakker Sliedricht, HYPS, Royal IHC, RH Marine, Croonwouter&dros, and Royal Netherlands Navy.

*Ali Haseltalab
Delft, April 2019*

NOMENCLATURE

Greek Symbols

Δ Decoupling matrix

η_d Vector of desired position

η_i Cell efficiency

η_s Vector of position

$\kappa_{1,2}$ First element of MPC solution

ω Disturbance function

$\omega_{1,2}$ Disturbance functions

ω_{dg} Diesel-generator shaft speed

ω_e Electrical angular velocity

ω_p Rotor Speed of induction motors

ψ Flux (Wb)

ψ Vector of neural network activation function

$\tau_{1,2}$ Nominal system inputs

τ_{ac} Vector of generated propelling forces

τ_{drag} Vector of drag forces

τ_{en} Torque buildup constant (s)

τ_r Yaw moment

τ_s Vector of applied propelling forces to ship's center of gravity

τ_x Longitudinal applied propelling force

τ_y Lateral applied propelling force

θ_g Load angle (rad)

Ξ Thrust configuration matrix

ζ Transformed system state

Roman Symbols

- \hat{W} Estimation of weight matrix
- \tilde{W} Error of weight matrix estimation
- $A_{1,2}$ State matrices
- $B_{1,2}$ Input vectors
- C Capacitance (F)
- C_A Added Coriolis and centrifugal matrix
- C_n Nominal voltage of battery (V)
- C_s Coriolis and centrifugal matrix
- D Voltage ratio
- d Converter duty cycle
- D_L Linear damping matrix
- D_{NL} Nonlinear damping matrix
- D_s Damping matrix
- $e_{1,2}$ Errors between nominal and real systems
- f State transition function
- f_{en} Fuel index
- g Input function
- H Inertia constant
- h Output variables function
- I Vector of currents (A)
- i Current (A)
- I_a added moment of inertia (kg.m^2)
- i_b Battery current (A)
- i_L Converter current (A)
- I_z Ship's moment of inertia (kg.m^2)
- $K_{1,2}$ State feedback vectors
- K_d Derivative gain of PID controller

- K_{en} Diesel engine torque constant
- K_i Integral gain of PID controller
- K_m Acceleration feedback gain
- K_p Proportional gain of PID controller
- L Inductance (H)
- L_{mm} Mutual inductance of induction motor (H)
- L_{rm} Rotor inductance of induction motor (H)
- L_{sm} Stator inductance of induction motor (H)
- $L_x^k y$ k th lie derivative of y with respect to x
- m_{ax} Longitudinal added mass (kg)
- m_{ay} Lateral added mass (kg)
- M_A Added mass matrix
- m_b Ship weight (kg)
- M_{RB} Rigid-body mass matrix
- M_s Mass matrix
- M_v Mass of the vessel (kg)
- N Prediction horizon
- n_p Propeller speed (rps)
- O_{CV} Open circuit voltage (V)
- Q'_d Additive torque disturbance (N.m)
- Q_{en} Diesel engine torque (N.m)
- R Rotation matrix
- r Resistance (ohm)
- r_b Battery resistance (ohm)
- r_{rm} Rotor resistance of induction motor (ohm)
- r_{sm} Stator resistance of induction motor (ohm)
- R_v Resistance function
- S_{oC} State of charge

- S_w Speed matrix
- T_p Propeller thrust (N)
- T_p Propeller torque (N.m)
- U Ship speed (m/s)
- v Voltage (v)
- $\nu_{1,2}$ Transformed system inputs
- V_a Advance speed (m/s)
- ν_b Battery voltage (V)
- ν_d Direct-axis voltage (V)
- ν_d Quadratic-axis voltage (V)
- ν_s Speed vector
- ν_x Longitudinal speed (m/s)
- ν_y Lateral speed (m/s)
- W Weight matrix
- x_R Vector desired values
- X_G Inductance matrix
- $z_{1,2}$ Nominal system states

Subscripts

- d Direct-axis
- dc Direct current
- dg Diesel-generator
- drm Rotor direct-axis (induction motor)
- dsm Stator direct-axis (induction motor)
- en Diesel engine
- fd Field
- G Synchronous generator
- kd Direct-axis damper winding
- kq Quadratic-axis damper winding

q Quadratic-axis

qrm Rotor quadratic-axis (induction motor)

qsm Stator quadratic-axis (induction motor)

rec Rectifier

LIST OF FIGURES

1.1	Hybrid PPS configuration.	3
1.2	The DC-PPS under study.	4
1.3	The proposed hierarchy of controllers.	6
1.4	The scope of the thesis.	8
1.5	The outline of the thesis.	10
2.1	Path following control result of the Seabax vessel at Delft University of Technology [29].	12
2.2	Path following control result of Delfia-1 [35].	13
2.3	Delfia-1* in action [36].	13
2.4	SFC curve of two diesel engines with different power ratings.	18
2.5	Schematic view of centralized control approach.	19
2.6	Schematic view of decentralized control approach.	20
2.7	Schematic view of distributed control approach.	21
3.1	A vessel with two propellers, a bow thruster, and a stern thruster.	24
3.2	The DC-PPS under study.	27
4.1	Open water diagram for Wageningen B 5 75 with pitch ratio 0.96 where η_o is the open water efficiency [112].	39
4.2	The difference between measured propeller torque and the outcome of the model during a turn [57].	40
4.3	Results of Experiment 1.	52
4.4	Performance comparison of the proposed algorithm vs a conventional control scheme.	54
4.5	The effect of k on error bounds.	54
4.6	Dynamic positioning performance of the ship.	55
4.7	The considered trajectory in the Port of Rotterdam waterways.	57
4.8	Architecture of the considered power system [22].	57
4.9	Simulation results of Experiment 1.	58
4.10	Performance of the power and propulsion system.	59
4.11	Angular speed of propellers and thrusters.	60
5.1	The block diagram of the proposed maneuvering control strategy.	64
5.2	Tito-Neri: a harbor tug 1:30 replica model [121].	65
5.3	Trajectory tracking performance of the ship.	66
5.4	Trajectory tracking performance of the ship in Oude Maas river.	68
5.5	Vessel's speed and the applied forces.	69

5.6	Simulation results of Experiment II.	70
6.1	Combined SFC curve of the harbor tug from different angles.	77
6.2	Simulation results of the energy consumption side (Experiment I).	78
6.3	Simulation results of the energy generation side (Experiment I).	80
6.4	Stability results of the power system. (Experiment I).	81
6.5	Battery SOC and the fuel consumption rate (Experiment I).	82
6.6	Simulation results in battery discharge mode using PEM (Experiment I).	83
6.7	Simulation results using the rule-based approach (Experiment I).	84
6.8	Trajectory tracking result (Experiment II).	84
6.9	Simulation results of propelling actuators (Experiment II).	85
6.10	Simulation results using PEM and rule-based approaches (Experiment II).	86
6.11	Operating profiles (Experiment III).	87
7.1	The block diagram of the control strategy.	97
7.2	Synchronous generator's model results vs. emperical test results.	102
7.3	Three phase currents at 5535 kw load.	103
7.4	Short circuit current: model vs. datasheet.	103
7.5	The eigenvalues of the DGR set.	104
7.6	Open loop response of the system.	105
7.7	The ship speed vs the generated thrust and the propeller shafts speed in Experiment I.	106
7.8	The results of Experiment I using robust MPC approach.	107
7.9	The results of Experiment III.	109
7.10	The block diagram of the PI-based voltage controller.	110
7.11	The results of Experiment I using PI-based approach.	111
7.12	The results of Experiment I using PI-based approach.	112
7.13	The results of short circuit experiment (MPC vs. PI).	113
7.14	The results of short circuit experiment (MPC vs. PI).	114
7.15	Ship speed and propelling thrust during the voyage.	115
7.16	Results of Experiment III.	116
8.1	The block diagram of the proposed control approach.	120
8.2	The circuit diagram of the bidirectional converter.	123
8.3	Synchronous generator's model results versus emperical test results.	127
8.4	The varying load applied to the power system (Experiment I).	128
8.5	DC-link voltage stability simulation results (Experiment I).	129
8.6	Simulation results of the mechanical variables (Experiment I).	130
8.7	Simulation results of the mechanical variables (Experiment I).	131
8.8	The SOC of the battery during simulation (Experiment I).	132
8.9	Simulation results of Experiment II using the proposed two-level MPC controller.	133
8.10	Simulation results of Experiment II using the PI-based droop control scheme.	134
A.1	The graph of Tito-Neri drag forces.	154

LIST OF TABLES

2.1	A classification of different control approaches for trajectory tracking and path following control.	15
4.1	The model ASV parameters.	53
6.1	Overall fuel consumption and generated energy (Experiment I).	79
6.2	Performance comparison of algorithms (Experiment II).	82
6.3	Simulation results (Experiment III).	88
A.1	Maneuvering model parameters.	155

1

INTRODUCTION

The industrial revolution led to an increase in the production and transportation of goods. More jobs became available and more workforce were required to satisfy the ever increasing needs of marketized societies. Simultaneously, the automation of production and transportation methods started to increase cost efficiency, robustness, and flexibility. Addressing the environmental issues by technology owners and developers became a must starting in the final quarter of 20th century. The maritime industry is tackling its developments on both automation and addressing environmental concerns, ever since. Ships are becoming efficient and environment-friendly. The number of on-board crew is falling and new ships are more adaptive to different operating profiles. However, a long way remains to achieve fully autonomous -so called- green shipping.

In this thesis, several approaches are proposed to tackle the problem of enabling autonomous green shipping. Maneuvering, energy management and power generation control are studied in accordance with each other for the first time to propose a general methodology for controlling all-electric autonomous ships which enables more effective, efficient and environment-friendly vessels.

1.1. AUTONOMOUS SHIPPING

The domain of transport over water has been experiencing significant changes after the second world war. Although, with the advent of commercial airplanes, the transport of people over long-range waterways has declined, the transport of freight and goods has drastically been increasing. Containerization revolutionized the merchant shipping as more goods could be handled by the merchant fleets. The total number of merchant ships with at least 1000 gross registered tonnes raised from around 31,000 in 2005 to more than 39,000 in 2011, indicating a 26% increase [1]. A drastic increase in the number of inland vessels, tankers, ferries, cruise ships, tugboats, dredgers and supply vessels has happened as well. According to the international chamber of shipping more than 90 percent of the world trade is transported over water. The carriage of containers, dry cargo, bulk commodities, and oil and gas has increased three times in 2015 compared to 1980 [2].

Starting the second half of the twentieth century, the size of cargo and tanker vessels have been increasing significantly as a response to the rise of demands in consuming societies. However, this resulted in several disadvantages including overcapacity, extra cost of operation, idleness of smaller container carriers, and market monopoly. As a result and also due to the high costs of building giant ships, there is a shift towards manufacturing fleets of smaller vessels [3].

Reducing the operating costs of vessels has always been a goal for shipping companies. The crew cost has a very high share in operating cost of a vessel which usually increases on a yearly basis even if the on-board crew number does not increase. Therefore, decreasing the number of on-board crew has been one of the main reasons of technology development in shipbuilding industry. This resulted in a significant reduction of on-board crew number in the last few decades. Increasing the safety and reduction of maritime accidents are other concerns of ship operators. Nowadays, more than 70% of maritime incidents involve human operator mistakes. Moreover, operating in severe environmental conditions imposes risks on the lives of on-board crew.

From the 1990s, the research on fully autonomous ships has started as a reaction to the above mentioned concerns [4]. By definition, a fully autonomous ship is a ship that can observe and sense its environment, navigate and maneuver autonomously without human intervention. The adoption of autonomous ships is believed to result in crew cost reduction, reduction of operating costs, increased safety, addition of cargo capacity, and reduced emissions [4]. Autonomous shipping is considered as one of the solutions to congested waterways [5] and the problem of delay in cargo delivery [6].

The concept of autonomous shipping, its benefits, and future utilization are undergoing extensive study and investigation by both academic and industrial communities. However, several challenges need to be addressed before fully operational autonomous ships can be enabled. These difficulties include problems with automatic path planning [7, 8], navigation and trajectory tracking [5, 9], cooperation with other vessels [10–12], power and energy management issues [13–15], and fault-detection, isolation and reconfiguration [16–18]. Due to the expected reduced number of on-board crew members in autonomous vessels the role for automation and independent machine performance in all of the mentioned issues increases significantly and becomes more vital. For this purpose, the adoption of intelligent control and management algorithms for diverse purposes is necessary.

1.2. FUEL EFFICIENCY

Alongside with increased autonomy, and mainly due to environmental restrictions from international maritime authorities, there is a shift towards more efficient Power and Propulsion System (PPS) architectures as a replacement for direct-diesel propulsion configurations [13]. Based on the agreements made in the International Maritime Organization (IMO), the shipping industry agreed to reduce its emissions by 50% from 2008 to 2050 [19]. To address this, alternative energy sources are combined with innovative -and mainly- electric PPSes as the first step. Alongside with fuel efficiency and reduction of emissions, innovative PPS can also increase the adaptability of ships to different operating profiles [13, 14].

The complexity of the innovative on-board PPS architectures is increasing due to the

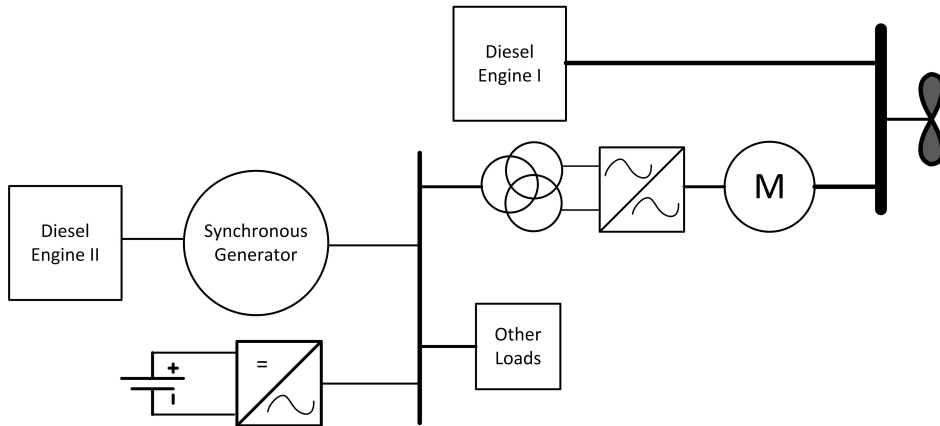


Figure 1.1: Hybrid PPS configuration.

addition of several components such as synchronous generators, induction motors, and power conversion modules. The innovative architectures can be divided into two different types: *hybrid* architectures in which the relationship between diesel engine and propellers is established directly and also through electrical machinery (Figure 1.1) [13, 20], and *all-electric* architectures in which this relationship is formed only through an electrical grid [21, 22]. It has been shown that such advanced architectures cannot be as efficient as expected unless advanced control and energy management algorithms are adopted [13, 14]. There have been several research works for increasing the fuel efficiency of ships with these architectures. For more information regarding these works see [13, 14, 23] and references therein.

Among the different architectures possible, in this thesis, the focus is on the DC Power and Propulsion System (DC-PPS) architectures which, with advances in the domain of semiconductors, are perceived as one of the most efficient architectures [23]. An architecture of a DC-PPS is shown in Figure 3.2. Several advantages of DC-PPS are the possibility for optimal engine loading, variable diesel engine speed, and fuel efficiency, which make this PPS suitable for ships with different operational profiles. Moreover, an increase of flexibility in the design stage and a decrease in the number of converting stages are among advantages of DC on-board microgrids [13, 21]. As a result, DC-PPS can be a proper power system candidate for autonomous ships. On the other hand, there are several challenges in taking full advantage of this architecture such as power system stability, fault tolerance, and optimal energy management issues [13, 23, 24]. As a result, the complexity of this architecture suggests performing more elaborate investigations to increase the performance and efficiency of this architecture.

The problem of optimal energy management in DC-PPS is mainly about finding a fuel-efficient optimal share between different energy sources. As a result, optimal engine loading during the operation of a diesel-generator set is the primary challenge which leads to fuel-efficient energy generation and reduction of emissions. Another issue is energy availability for the ship operation. A feasible energy management control ap-

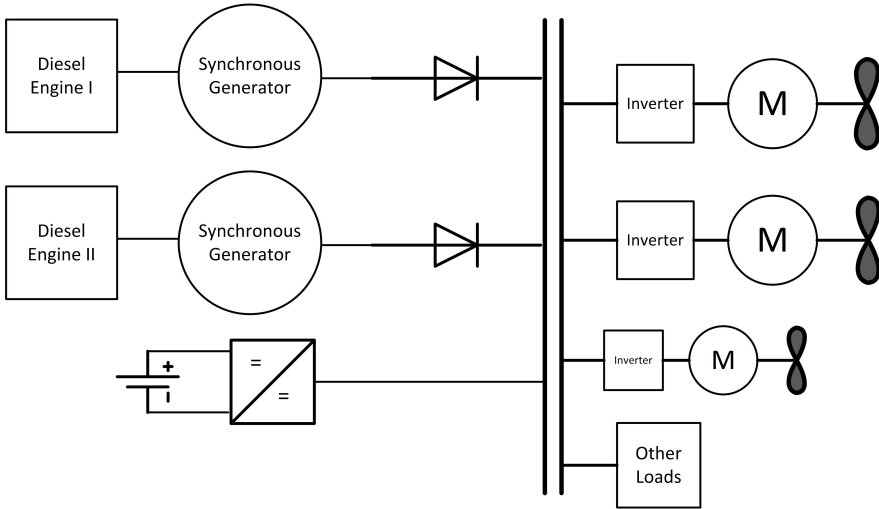


Figure 1.2: The DC-PPS under study.

proach must guarantee the availability of energy for propulsive and other loads. For this purpose, maneuvering control and energy management should be studied in accordance to each other and a general protocol should be defined to frame the relationship of maneuvering and energy management controllers for guaranteeing the availability of fuel-efficient propulsive energy.

1.3. STABILITY AND ROBUSTNESS

Propulsive power availability is dependent on the robustness and stability of the DC-PPS. The on-board energy sources should be able to generate power in parallel and harmonically to prevent blackouts.

One of the main drawbacks of DC-PPS is the problem of stability [25],[26]. In [13], the lack of a feasible control strategy is introduced as one of the main challenges in enabling DC-PPS. Adverse effects of Constant Power Loads (CPL), non-linearity in the dynamical model of electric machines and drives as well as fast changes in load conditions are among the issues that can lead to voltage oscillation and instability.

Therefore, strong measures should be devised and adopted to guarantee the generation of power throughout the operation time of the vessel. The robustness problem of power generation can be addressed from two perspectives; architectural and control. Architectural solutions include the methodologies that enhance the performance of the DC-PPS by adding, removing, changing or modifying power system components while control solutions mainly address the problem by the use of advanced control algorithms for power generation. In DC-PPS, the main purpose of power generation control is keeping the bus bar DC voltage stable around its nominal operating point. The frequency of generators and AC transmission lines between generators and rectifiers should be main-

tained around their nominal value.

The complexity of the DC-PPS architecture calls for the adoption of advanced cooperative approaches for power generation control. The problem of power generation stability and control should also be studied in accordance with energy management and maneuvering control. Communication between these three controllers, i.e., maneuvering, energy management, and power generation controllers, can lead to enhanced performance of the overall system and its adaptability to different operating profiles.

1.4. INTEGRATING MANEUVERING, ENERGY MANAGEMENT, AND POWER GENERATION CONTROL

In the design of conventional ships, even in autopilot modes, maneuvering, energy management, and power generation controllers have always been implemented isolated from each other. Proportional-Integral-Derivative (PID) control approaches are mostly considered for the control purposes, including, speed control or position control in dynamic positioning modes [22, 24]. Rule-Based (RB) energy management approaches are the most common methodologies for energy management and load sharing [27]. The information sharing between controllers has never been considered in the control hierarchy design stage. Power splits between different energy sources are approximated mainly at the beginning of operations and are rarely established based on data obtained during real-time operation [28]. Automatic voltage regulators are considered as isolated controllers which work with PID-based control approaches and only in few design cases communicate with each other, though not with the energy management and maneuvering controllers [21].

As will be discussed in Chapter 2, in the literature also, these three controllers are studied individually from each other and in very few cases, the interaction between two of them is considered. However, in this thesis, a new control hierarchy is proposed which is based on information exchange between these three controllers. It is shown, how these three controllers can benefit from each other by sharing the information and adapting themselves with the ship mission and loading conditions. These control modules and their operation is both studied individually and interactively using advanced control strategies and protocols. The proposed control hierarchy is shown in Figure 1.3.

In order to adjust the optimal power split between different energy sources during the operation, a rough approximation of the future required propulsive energy should be provided over a relatively a long horizon. Moreover, this data can be used by the power generation control modules to improve the performance of the power and propulsion system. The determined power split results can also be used by power generation modules for the control of energy sources.

In this thesis, for maneuvering control, Model Predictive Control (MPC) and adaptive control approaches are considered in order to extract the future power predictions, address model uncertainties, and handle environmental disturbances. The future required power is communicated with energy management and power generation controllers. For energy management, a predictive energy management approach is proposed to determine the optimal power split between different energy sources. Assigned power shares by the energy management controller and future required power is com-

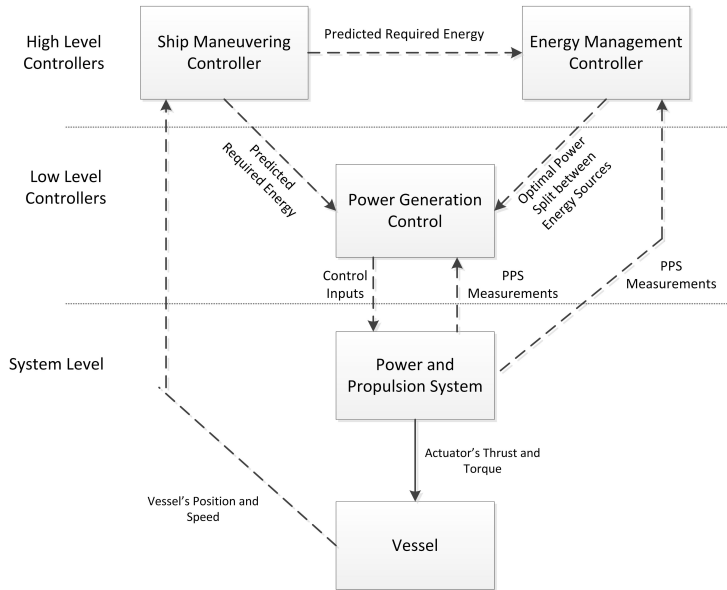


Figure 1.3: The proposed hierarchy of controllers.

municated with the power management control module where a robust MPC approach is introduced to guarantee robustness and stability, even in the presence of uncertainties and a range of electrical faults. These control approaches are introduced through out of this thesis and their relationship is discussed.

1.5. PROBLEM STATEMENT AND RESEARCH QUESTIONS

In this thesis, one aim is to enable the robust and efficient operation of autonomous all-electric ships. In this regard, the following research question is addressed:

How can the performance and efficiency of autonomous all-electric ships be improved using novel control approaches?

To answer the above question, the following set of sub-research questions is considered:

1. What are the feasible approaches for the maneuvering control of autonomous ships?
2. How to guarantee small trajectory tracking errors, constraints handling, and the prediction of future required propulsive energy?
3. How to handle environmental disturbances and model uncertainties in maneuvering control?
4. In what ways can the prediction of required future propulsive energy be used for increasing the operation robustness and efficiency of vessels?

5. How can optimal engine loading, fuel efficiency, and efficiency of energy generation be maximized?
6. How can propulsive power availability be guaranteed?
7. Can advanced control algorithms increase the stability of DC-PPS? If yes, what approach is suitable?
8. How can the adoption of cooperative control approaches lead to the increased stability and robustness of DC-PPS?
9. In what ways can maneuvering, energy management, and power generation controllers interact and how this interaction can lead to a more effective performance?

In this thesis, several solutions are discussed to address the above research questions. In the domain of maneuvering control, the problems of trajectory tracking in the presence of environmental disturbances and model uncertainties are considered. It is shown that with the proposed control approaches, the trajectory tracking error decreases, constraints handling is guaranteed, and environmental disturbances and model uncertainties are handled.

The optimal engine loading and fuel efficiency is achieved by adoption of a predictive energy management control approach which determines the optimal power split between energy sources, namely, diesel-generators and the battery, based on the predicted required power.

For the problem of power generation control, after modeling of the energy generation side, an approach is proposed for the control of a single Diesel-Generator-Rectifier (DGR) set and then, it is extended to cooperative control of multiple DGR sets as well as a battery-converter set.

Throughout the thesis, it is discussed and shown in what ways these different controllers can collaborate with each other and benefit from their interaction. The scope of this research work is illustrated in Figure 1.4, which includes trajectory tracking, energy management and control of the DC-PPS.

1.6. THESIS OUTLINE

The outline of this thesis is as follows:

- In Chapter 2, a literature review on the maneuvering, energy management, and power generation control of autonomous all-electric ships is provided where by discussing the shortcomings of the conventional control methods, potential feasible approaches for maneuvering, energy management, and power generation control are determined (Research Question 1).
- In Chapter 3, a mathematical model is presented for different components and then, the maneuvering and the DC-PPS models are presented in state space formats.
- In Chapter 4, the problem of model uncertainty in maneuvering control is addressed by proposing a novel neural network-based adaptive control approach.

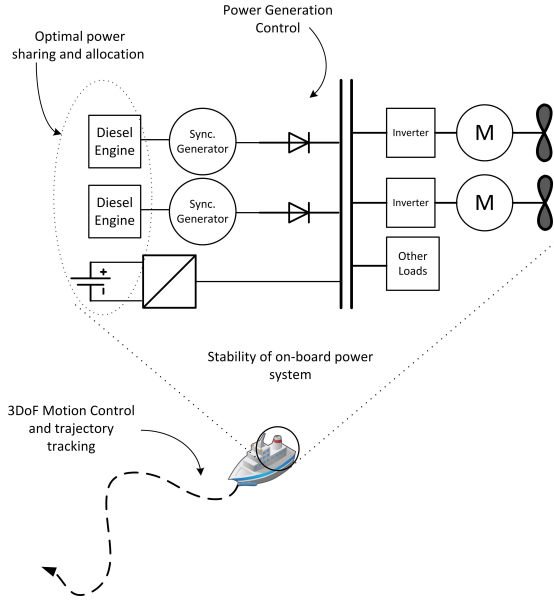


Figure 1.4: The scope of the thesis.

The correctness proof of the approach is carried out using a Lyapunov-based technique and uniform ultimate boundedness. To evaluate the performance of the approach several simulation experiments are carried out including trajectory tracking in the port of Rotterdam. Using the proposed approach environmental disturbances and model uncertainties can be handled (Research Question 3).

- In Chapter 5, an MPC-based approach is proposed for the trajectory tracking control of autonomous ships which guarantees constraints handling, small trajectory tracking error in the presence of environmental disturbances, and prediction of propulsive load. The approach is designed using Input-Output Feedback Linearization (IOFL) and a constraint linearization method so that the adoption quadratic programming approaches is enabled for solving the optimization problem of the model predictive controller. For simulation experiments in this chapter, maneuvering model of a replica scale model tug, known as *Tito-Neri* is adopted. Using the proposed approach, the prediction of the future propulsive load and constraint handling are enabled (Research Question 2).
- In Chapter 6, a predictive energy management scheme is proposed for determining the optimal power split between different energy sources on-board of a vessel during operation and based on the predicted future power. The approach is designed using Specific Fuel Consumption (SFC) curve of the diesel engines and guarantees optimal engine loading. To evaluate the performance of the proposed approach, many experiments are carried out including simulation of operating

profiles of real tugs which are provided by the ShipDrive project partners. For these experiments, a low voltage DC-PPS with two DGR sets and a battery-converter set is adopted which propels a tug boat. In this chapter, it is shown that a deterministic prediction of the future propulsive load can be used for energy management (Research Question 4). Moreover, the proposed energy management approach guarantees optimal engine loading and fuel efficiency (Research Questions 5 and 6).

- In Chapter 7, an MPC approach is introduced for the control of DGR sets. The proposed approach which is designed using an IOFL method, a tube-based MPC law, and a scheme to linearize the constraints, guarantees the stability of the power system during operation. High fidelity component models are considered for evaluation of the proposed approach which are provided by the ShipDrive project partners. Voltage control under varying loads and short circuit experiments are carried out for testing the proposed control approach. The DC-PPS for these experiments is a high voltage DGR set which generates power for a 90 m ship. In this chapter, it is shown that MPC approaches combined with robust control schemes are potential candidates for stabilizing DC-PPS (Research Question 7). The proposed approach guarantees power availability by stabilizing the DC-PPS under different loading conditions (Research Question 6).
- The results of Chapter 7 are extended in Chapter 8 where a multi-level control approach is proposed for power generation control on-board of all-electric ships. MPC schemes are used for the design of the approach and control of DGR sets and the battery-converter set. The performance of the proposed approach is evaluated using a high voltage DC-PPS model which is provided by ShipDrive project partners. Voltage control under varying loads and short circuit experiments are considered. The proposed approach in this chapter is a multi-level cooperative approach for power generation control which can be a potential replacement for conventional approaches (Research Question 8).
- In Chapter 9, the concluding remarks are given, the answers to research questions are summarized, and recommendations for future research directions are discussed. Throughout this thesis, several approaches are introduced for maneuvering, energy management, and power generation control. The necessity of integrating these approaches are explained and their integration schemes are explained (Research Question 9).

The outline of this thesis is illustrated in Figure 1.5.

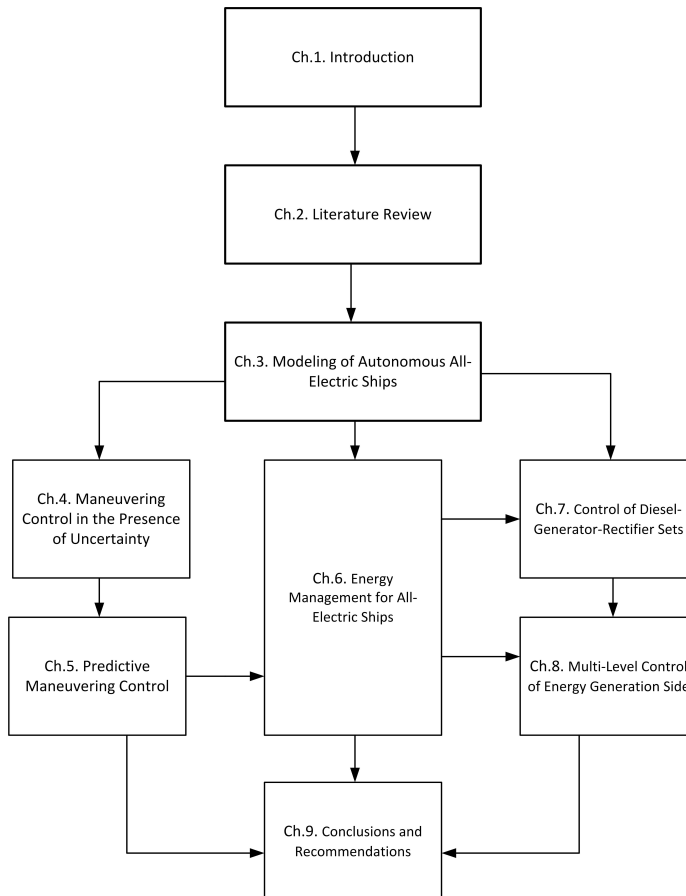


Figure 1.5: The outline of the thesis.

2

LITERATURE REVIEW

This chapter presents an overview of the literature relevant to maneuvering control, energy management and power generation control. In Section 2.1, the current state of affairs regarding maneuvering control of autonomous ships is discussed and novel control approaches proposed in the literature for trajectory tracking and path following are briefly discussed. Then, in Section 2.2, the DC-PPS is presented and different proposed energy management approaches for all-electric ships are introduced. In Section 2.3, the problem of stability in DC-PPS is explained and a literature review about control of DC-PPS is given.

2.1. MANEUVERING CONTROL

The problem of maneuvering control of autonomous vessels in the presence of environmental disturbances is one of the main challenges on the way to having fully autonomous ships. Intelligent controllers of autonomous ships should be capable of propelling the vessel towards an a priori planned path. Regardless of difficulties within controlling this complex system, one of the main issues is to keep the ship as close as possible to the planned path in the presence of environmental disturbances such as waves and currents. This problem is normally studied in two different methods depending on the path type. If the planned path is time independent, then the problem is called a path following control, and if the path is time dependent then it is a trajectory tracking control problem. The path following result of an autonomous model vessel is shown in Figure 2.1.

The problem of maneuvering control exposes its significance in or near port areas and hinterlands where the problem of waterway congestion exists. Maneuvering control of autonomous vessels is being studied extensively, where several approaches have been proposed for the trajectory tracking control including Model Predictive Control (MPC) [5, 30], adaptive schemes [9, 31–33] and nonlinear methods [30, 34]. The maneuvering control of autonomous ships using less advanced approaches including PID-based methods have been studied in theory and practice, extensively. See [34] and references therein.

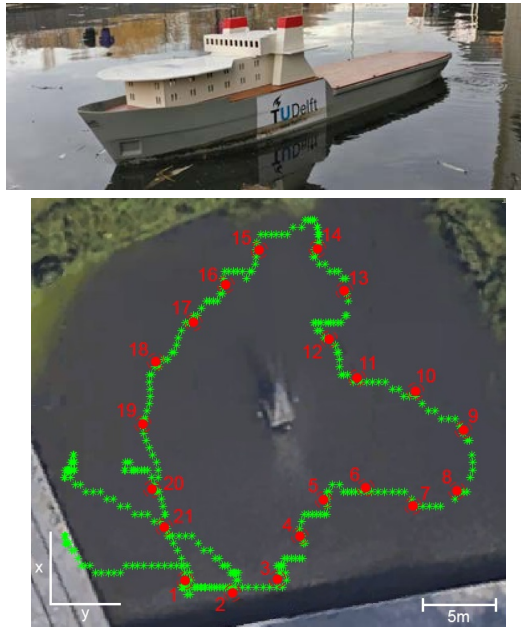


Figure 2.1: Path following control result of the Seabax vessel at Delft University of Technology [29].

2.1.1.1. PATH FOLLOWING CONTROL

Path following control using novel approaches is being studied extensively in academia. After the definition of the path by path planning algorithms, the vessel has to follow the generated path. However, the path is not time dependent, i.e., the vessel has no time dependent obligations.

The path following control problem using conventional PID-based approaches is being studied in practice [29, 35, 36]. In Figure 2.2, the path following result of an autonomous model vessel known as Delfia-1 is shown [35].

In the literature, this problem is well-addressed using novel control algorithms and in the presence of environmental disturbances and model uncertainties. In [37], an adaptive control algorithm is presented for path following where it is assumed that the information about hydrodynamic damping structure of the vehicle is not given. The uncertainties and disturbances are estimated and handled using a neural network. In [38], back-stepping techniques are combined with adaptive control approaches to handle uncertainties in the presence of constant and time-varying disturbances. Path following control problem is studied in [39] where a linear model is considered for the ship model and the model parameters are obtained using a least-square support vector regression.

Nonlinear control approaches are adopted for path following in several research works. In [40, 41], hierarchical control approaches are proposed for following continuous curves in the presence of disturbance. A nonlinear control approach is adopted in [42] to guarantee convergence to the reference path in the presence of unknown and constant currents. In Table 2.1, different path following schemes proposed in the literature are clas-

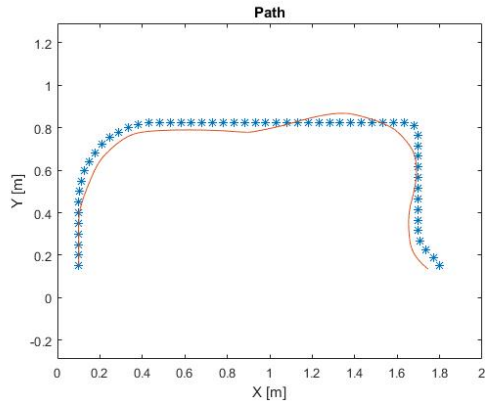


Figure 2.2: Path following control result of Delfia-1 [35].



Figure 2.3: Delfia-1* in action [36].

sified.

2.1.2. TRAJECTORY TRACKING CONTROL

The trajectory tracking control of autonomous vessels is under extensive study and several research papers have been published by the academic community. In most of the researches, MPC, adaptive control and nonlinear control approaches are used.

In [5], a Model Predictive Control (MPC) algorithm is proposed to address the problem of trajectory tracking control with knowledge over arrival time where the nonlinear model of the vessel is linearized to decrease computational complexity. Nonlinear MPC algorithms are adopted in [30, 43, 44] to address the problem of trajectory tracking.

A neural learning control strategy is adopted in [45] to guaranty trajectory tracking of an ASV with uncertainties in its model. In [32], the trajectory tracking problem is investigated using neural-adaptive control schemes in the existence of output constraints and parameter uncertainties in the craft model. The use of back-stepping control strategies is investigated in [46], where the estimator handles the model uncertainties as well as unknown disturbances. In [47], by solving systems of linear equations, the trajectory tracking problem is addressed. The use of fuzzy control approaches for adaptive track keeping is investigated in [48]. In [49], the performance of two different popular adaptive control algorithms for autonomous ships is compared where it is assumed that the vessel model is uncertain. In [50], a robust adaptive control strategy in combination with back-stepping and Lyapunov techniques is adopted to control the position of a ship in the presence of system uncertainties and unknown environmental disturbances.

The use of nonlinear control approaches are investigated in [51–53]. In [53], a sliding-mode tracking control approach for an underactuated vessel in the presence of parameter uncertainties is presented. A similar approach is implemented on a scaled model vessel in [54].

These control strategies are extended to multi-vessel applications where different vessels should collaborate with each other to fulfill diverse tasks [12, 55].

A classification of different approaches used for maneuvering control of autonomous ships is given in Table 2.1.

2.1.3. RESEARCH OPPORTUNITIES

Although, the maneuvering control of autonomous vessels has been studied extensively, still there is room for improvement.

Maneuvering in the presence of environmental disturbances is an issue that requires investigation. The effect of environmental forces appear as additive disturbances in different forms. While wave induced forces are bounded but varying, the current and wind forces appear in form of additive disturbances with constant values [34]. Precise trajectory tracking in the presence of these forces is challenging, specially in tight spaces.

The uncertainties within the maneuvering model is a problem which has been studied extensively. While conventional PID-based approaches are capable of controlling the vessel and they do not need any or precise knowledge of the vessel's hydrodynamical maneuvering model and parameters, the focus in the literature is to gain more precision in trajectory tracking and path following by handling uncertainties using adaptive control approaches [32, 46, 53]. However, in the literature, it is almost forgotten that a ship model

Research Article	Path Following	Trajectory Tracking	MPC	Nonlinear Control	Adaptive Control	Other Control Approaches	Maneuvering Model Uncertainties Considered	Environmental Disturbances Considered	Relation with PPS Considered
[56]	✓		✓					✓	
[37, 38]	✓				✓		✓		
[39]	✓					✓	✓	✓	
[40, 47]	✓					✓			
[34, 41, 42]	✓			✓				✓	
[5, 43, 44]		✓	✓						
[30]		✓	✓				✓		
[51, 52]		✓		✓				✓	
[53, 54]		✓		✓					
[32, 46, 48-50]		✓			✓		✓	✓	
[45]		✓			✓		✓		

Table 2.1: A classification of different control approaches for trajectory tracking and path following control.

is not an affine-in-control system and indeed it is non-affine. As a result, the effect control inputs, i.e., shaft speed of propellers and thrusters, appears nonlinearly in the maneuvering model. In conventional ships, the ship speed is considered proportional to the propeller's speed and that is how the captain controls the speed of the vessel [28]. However, this is not a precise estimation as the propellers model changes during maneuvering [57]. As a result more research should be carried out on maneuvering control while considering a ship as a non-affine in control system.

The relationship between maneuvering control and energy management should be studied as well [58]. In this regard, it should be investigated that how the relationship between energy management and maneuvering controllers should be framed? Can a maneuvering controller provide information on the future propulsive load which to be used by the energy management controller?

In this thesis, all of the above concerns are addressed by adopting adaptive control and MPC approaches. The model uncertainties, environmental disturbances and the relationship between different controllers are studied and different solutions are proposed for the challenges.

2.2. ENERGY MANAGEMENT FOR DC-PPS

Among different architectures, in this thesis, the focus is on the DC Power and Propulsion System (DC-PPS) architecture which, with advances in the domain of semiconductors, is perceived as one of the most efficient architectures [23]. Several advantages of DC-PPS are the possibility for optimal engine loading, variable diesel engine speed, and fuel efficiency, which make this PPS suitable for ships with different operational profiles. Moreover, the increase of flexibility in the design stage and a decrease in the number of converting stages are among advantages of DC on-board microgrids [13, 21]. As a result, DC-PPS can be a proper power system candidate for autonomous ships.

A DC-PPS can be regarded as a microgrid which has different types of energy sources on the energy generation side and propulsive loads plus hotel and other on-board facility loads on the energy consumption side. The adoption of this architecture for ships has started in the recent decades. DC-PPS has been widely used for submarines in combination with large battery packs before being vastly adopted for ships [28]. This architecture has been considered for naval ships of United States Navy and Royal Navy due to their increased efficiency and their applicability in combination with different types of loads [59, 60]. Research, development and implementation of DC-PPS for supply vessels and ferries has been under focus in past decade, extensively [28]. Siemens, ABB, Damen shipyards, Bakker, RH Marine, and Hybrid Marine are among companies that are investigating and applying DC-PPS to different types of vessels. On the other hand, there are several challenges in taking full advantage of this architecture such as power system stability, fault tolerance, and optimal energy management issues [13, 23, 24]. As a result, the complexity of this architecture suggests performing more elaborate investigations to increase the performance and efficiency of this architecture.

An on-board DC-PPS is modeled and the interaction between different components are investigated in [21]. This work is extended in [23] where an energy management algorithm is proposed to increase fuel efficiency under different loading conditions using an optimal energy management algorithm that uses the battery to achieve optimal

diesel engine loading. This is done by determining power ripples and filtering the high fluctuations. However, no prediction about the future demanded power is carried out.

In [15, 61], MPC-based algorithms are used for energy management where a combination of ultracapacitors and a battery is adopted for on-board energy storage. This combination is used in [15] to damp the adverse effects of load fluctuation. Using the proposed methodology, voltage fluctuation is decreased significantly, and the efficiency and battery life-time is increased. In [61], adaptive control approaches are combined with MPC to mitigate load fluctuations on-board of all-electric ships. The torque of the propulsive load is estimated using adaptive schemes and it is used by the energy management algorithm to increase reliability and efficiency.

RESEARCH OPPORTUNITIES

The research on energy management of DC-PPS is at its infancy. In most of the research works, the energy management approach has been studied individually and not in relation with other controllers or modules. The future required propulsive power as well as stability of the PPS can be studied through investigation of such relations [61].

A precise prediction of the future load can help to the reliability and stability of DC-PPS. Unlike [23], deterministic approaches should be investigated for this purpose. One way is using the a proper choice of approach for the maneuvering control[22]. Then, the integration of controllers should be studied.

Moreover, optimal loading of diesel engines should be investigated. Deterministic approaches should be investigated to increase fuel-efficiency, i.e., generating more energy with less fuel. For a DC-PPS with multiple diesel-generators and a battery set with offshore charging capability, the Specific Fuel Consumption (SFC) should be regarded as the main determinant of efficiency. As a result, the objective function of the energy management optimization problem should included SFC curves of the diesel engines (Figure 2.4) and its solution should indicate the power split between energy sources based on the SFC curves. Due to its fast transients, the load fluctuations can be handled by the battery-converter set and as a result, the diesel-generators loading condition does not undergo rapid changes. This leads to increased reliability and stability.

2.3. POWER GENERATION CONTROL

Power generation control is referred to the control of components in the energy generation side such that under different loading conditions, the power generation continues robustly.

Despite several advantages of DC on-board microgrids, there are some challenges in the implementation of these power and propulsion systems. One of the main drawbacks is the problem of stability [25, 26]. In [13], the lack of a feasible control strategy is introduced as one of the main challenges in enabling DC power and propulsion systems. Adverse effects of Constant Power Loads (CPL), non-linearity in the dynamical model of electric machines and drives as well as fast changes in load conditions are among the issues that can lead to voltage oscillation and instability. In the literature, several methods have been proposed to address the stability problem. These proposed methodologies range from architectural solutions to control solutions. Addition of filters for reducing oscillations [62, 63], employing energy storage devices [64] and load shedding [65] are

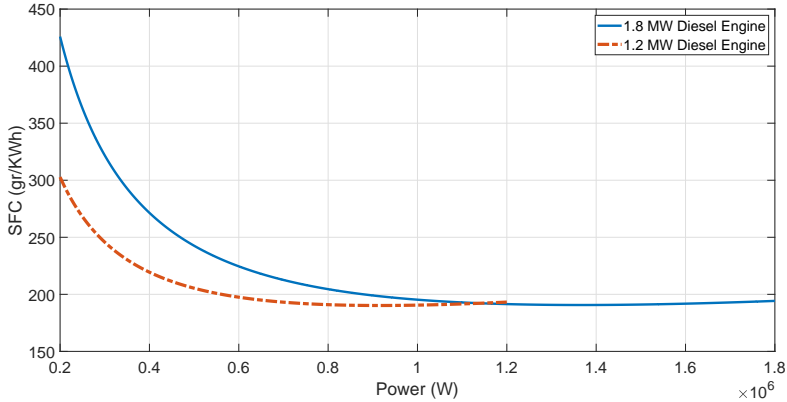


Figure 2.4: SFC curve of two diesel engines with different power ratings.

among the architectural solutions considered in the design stage. Moreover, in [66] after deriving a stability criterion for a synchronous generator connected to a diode-bridge rectifier, it is shown that the stability can be improved by establishing a short-circuited quadrature-axis winding on the rotor of a synchronous generator. In [67], a stability analysis is carried out for diode bridge rectifier-loaded synchronous generators with high values of reactance. A detailed review on architectural solutions is carried out in [62].

In the literature, a popular control solution is the adoption of linear controllers, mainly PID, to increase the robustness of the system [68, 69]. This controller is normally placed at a microgrid bus and controls the voltage by changing the duty cycles of line-regulating converters. As a result, implementation of these methodologies requires the use of controllable rectifiers.

There is also a shift towards more advanced control strategies due to incapability of conventional control strategies in guaranteeing the stability. In [70], a robust sliding mode control methodology is proposed to reduce destabilising effects of CPLs in a DC micro-grid where energy sources connected to boost converters are regarded as voltage sources. A disturbance observer-based feedforward scheme is proposed in [71], where the energy source is connected to a cascaded power converter and the observer is used to estimate the load current. Another feedforward scheme is presented in [72] to mitigate harmful effects of CPLs. In [25], after assessment of negative impedance instability effects of CPLs, different control strategies including sliding-mode control are presented to stabilize automotive power systems. State-feedback linearization is adopted in [73] to face CPLs destabilizing effects on-board of electric ships where an active control stage is considered between rectification stage and the DC-link. In [74], a semi-definite programming-based control algorithm is presented to increase stability of the power system by computing the stability region of attraction of the microgrid where the energy source is simplified to a constant voltage source. In [75], a methodology is proposed to stabilize the DC voltage by moving the states of the system into a previously found region of attraction. Nonlinear droop control and voltage regulation strategies are discussed in [76–78] where the objective is to keep the system stable when renewable energy sources

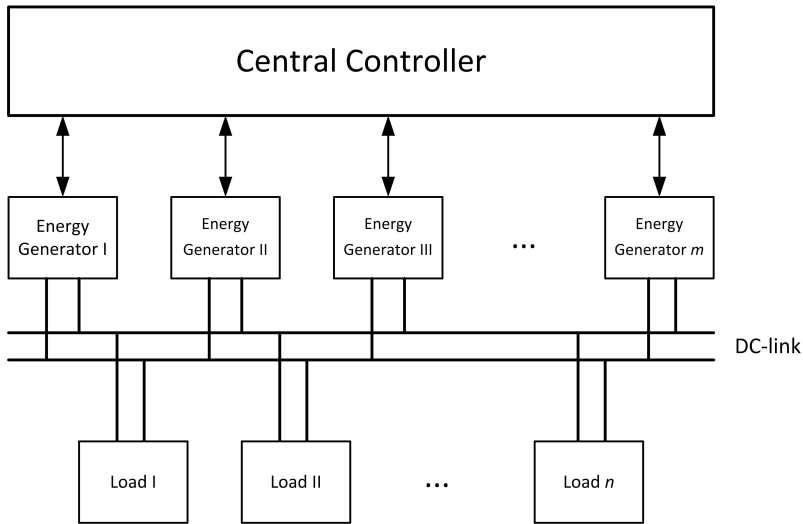


Figure 2.5: Schematic view of centralized control approach.

are connected to the grid using active rectification and converting devices.

A Model Predictive Control (MPC) strategy is proposed in [79] to enhance the transient stability of power systems by controlling the charge/discharge of superconducting magnetic energy storage systems. An MPC approach is proposed in [80] for power management and voltage regulation in isolated DC microgrids where the energy sources are a battery, supercapacitors, and a photovoltaic system. Consensus-based MPC approaches are considered in [81] for load sharing and voltage regulation.

The power generation control of DC microgrids can be classified into three different categories depending on the network architecture of controllers [82]. These categories are centralized, decentralized and distributed.

Centralized control of DC microgrids has been investigated in [83–86] where a central controller controls the energy generator units. In [84], a master-slave technique is used for the control of DC microgrid. A centralized control approach is proposed in [83] for microgrid operation optimization and coordination. However, centralized control has several drawbacks, including single point failure of the system, reduced flexibility, scalability, and reliability [82]. A schematic diagram of centralized control is shown in Figure 2.5.

Decentralized control is the most prevalent control approach in maritime applications where several control modules keep the microgrid stable without directly communicating [21]. Voltage droop control is one of the most popular strategies among decentralized schemes. In this strategy the output power is used as the droop feedback for controlling the DC-link voltage [87]. A schematic diagram of voltage droop control is depicted in Figure 2.6. The decentralized control approach suffers from several shortcomings including, load dependency of the DC-link voltage, unsuitability with nonlinear loads, and the lack coordinated performance by different on-board energy sources [82].

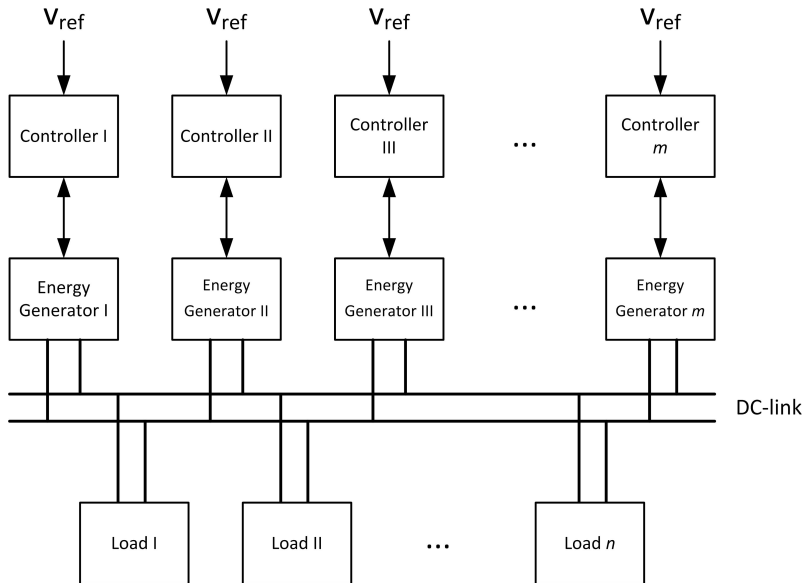


Figure 2.6: Schematic view of decentralized control approach.

Unlike a decentralized approach, in distributed architecture, the controllers communicate and coordinate based on the information that they share [88–90] (Figure 2.7). Distributed control of DC microgrids has the advantages of centralized and decentralized schemes. Moreover, immunity to single point of failure, ability of proportional load sharing, current sharing and SOC balancing are among other advantages of distributed control schemes [91–93]. Among distributed control approaches, consensus based [93] and agent-based approach are the most widespread [90, 94]. However, distributed control approach has never been considered for ships in the literature [13].

RESEARCH OPPORTUNITIES

In conventional ships, the energy sources are mainly diesel-generator sets and batteries [58, 61]. Recently, there is a shift towards other energy sources including gas turbines [95], fuel cells [96] and photovoltaics [97, 98]. With having different types of energy sources on-board which have different dynamics and transient behaviors, the problem of power generation control has become more challenging and as a result, there is greater need of having advanced control approaches, which by recognizing this difference between energy sources, enable robust power generation control under different loading conditions.

Voltage droop control [21] is the most popular control strategy for the control of DC-PPS. The strategy uses Proportional-Integral (PI) control techniques to control the voltage of the DC-link. The feedback of the DC-link voltage is sent to individual controllers proportionally compared to the overall load power. However, this methodology lacks

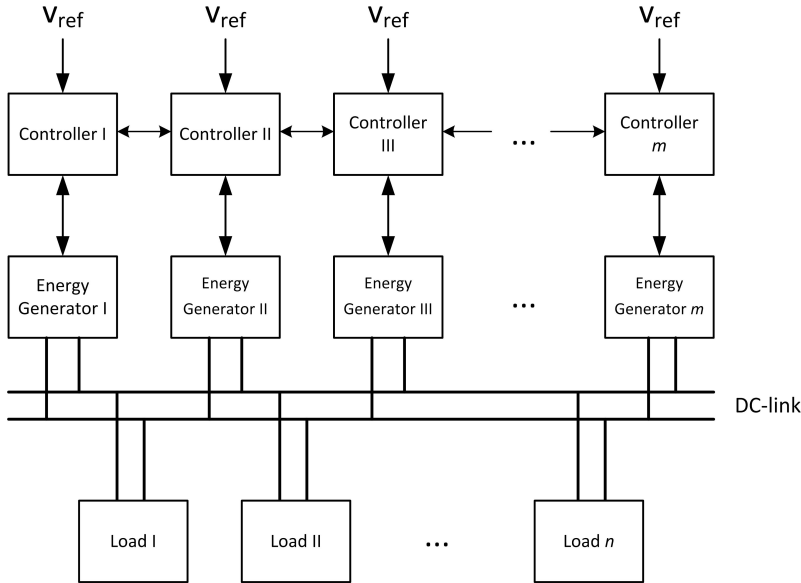


Figure 2.7: Schematic view of distributed control approach.

flexibility and robustness [24].

Among several issues, DC-PPS suffers from the lack of a coordinated control strategy to resolve stability issues and reach optimal performance [28]. Moreover, fault-protection as well as fault-tolerant control approaches should be investigated and adopted for robust performance of DC-PPS [24, 28]. The proposed approaches should be capable of guaranteeing stability in the presence of CPLs, varying loads as well as single point of failure.

The use of uncontrolled six-pulse bridge rectifiers is favorable in the maritime industry due to cost, maintenance and space saving concerns. In the most of the research works, it is assumed that the rectification stage is active, that is either a controlled rectifier is used or addition of a converter is suggested for DC voltage stabilization and control. However, stability studies in the presence of uncontrolled rectifiers has never been considered. In this thesis, the focus is on six-pulse uncontrolled bridge rectifiers and the objective is to regulate, stabilize and control the DC voltage by employing a feasible control algorithm.

2.4. CONCLUSIONS

In this chapter, a review on the current literature about maneuvering control, energy management and power generation control of all-electric ships with DC-PPS has been presented. Different control strategies have been introduced and their shortcomings have been explained, and research opportunities have been presented. It has also been

shown that several research questions presented in Chapter 1 cannot be answered by the current results in the literature. In this chapter, by discussing the shortcomings of the conventional control methods, necessary features of potential feasible approaches for maneuvering, energy management, and power generation control are determined which partly answers Research Question 1.

In the next chapter, mathematical models are presented for maneuvering and power and propulsion system of all-electric ships with DC configuration. Throughout this thesis, several control approaches for maneuvering, energy management, power generation control are proposed and the integration of these three control modules is discussed.

3

MATHEMATICAL MODELING OF AUTONOMOUS ALL-ELECTRIC SHIPS

In the previous chapter, a literature review on maneuvering, energy management, and power generation control has been given and shortcomings and research opportunities have been discussed. In this chapter, mathematical models are proposed for maneuvering, power generation, and propulsion of all-electric ships. First, a maneuvering model in 3 Degrees of Freedom (3DoF) is presented in Section 3.1. Then, in Section 3.2, the DC-PPS architecture is introduced. Mathematical models for components of energy consumption and energy generation sides are given in Sections 3.3 and 3.4, respectively. The results of this chapter have been partially included in several scientific papers ¹.

3.1. 3DOF MANEUVERING MODEL

In this thesis, the 3DoF maneuvering model is considered [33, 34] which is suitable for maneuvering control applications of surface vessels. The model includes information about the mass of the vessel and displacement, centrifugal and Coriolis forces, drag forces, and configuration of actuators. In Figure 3.1, the layout of a vessel with two propellers and two thrusters is illustrated.

¹The contents of this chapter have been published in:

1. A. Haseltalab, R. R. Negenborn, Model predictive maneuvering control and energy management for all-electric autonomous ships, *Applied Energy*, Volume 251, pp. 1-27, 2019.
2. A. Haseltalab, M. A. Botto, R. R. Negenborn, Model Predictive DC Voltage Control for All-Electric Ships, *Control Engineering Practice*, Volume 90, pp. 133-147, September 2019.
3. A. Haseltalab, R. R. Negenborn, G. Lodewijks, Multi-Level Predictive Control for Energy Management of Hybrid Ships in the Presence of Uncertainty and Environmental Disturbances, *IFAC-PapersOnLine*, Volume 49, Issue 3, 2016, Pages 90-95.

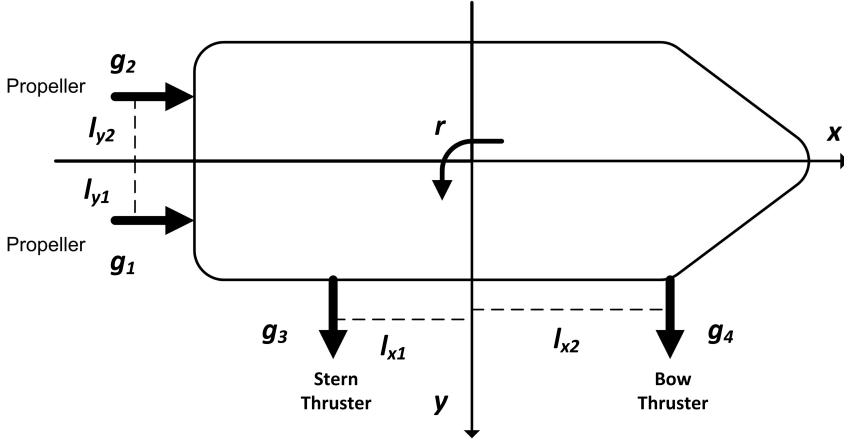


Figure 3.1: A vessel with two propellers, a bow thruster, and a stern thruster.

The maneuvering model of the ship can then be described as:

$$\begin{aligned}\dot{\eta}_s(t) &= R(\eta_s(t))v_s(t) \\ M_s \dot{v}_s(t) + C_s(v_s(t))v_s(t) &= \tau_s(t) + \tau_{\text{drag}}(v_s(t), \eta_s(t)),\end{aligned}\quad (3.1)$$

where $\eta_s(t) = [x(t), y(t), r(t)]^T$ is the ship position and orientation at time t , $v_s(t) = [v_x(t), v_y(t), v_r(t)]^T$ is the 3DoF ship speed and τ_s is the vector of forces applied to the ship center of gravity. M_s is the Inertial Mass matrix which consists of rigid body and added mass matrices:

$$M_s = M_{RB} + M_A \quad (3.2)$$

where

$$M_s = \begin{bmatrix} m_b & 0 & 0 \\ 0 & m_b & 0 \\ 0 & 0 & I_z \end{bmatrix}, M_A = \begin{bmatrix} m_{ax} & 0 & 0 \\ 0 & m_{ay} & 0 \\ 0 & 0 & I_a \end{bmatrix}. \quad (3.3)$$

Parameter m_b is the mass of the vessel, I_z is the moment of inertia, m_{ax} and m_{ay} are the added mass in x and y direction, respectively, and I_a represents the added moment of inertia.

Matrix $C_s(\cdot)$ is the Coriolis and Centrifugal matrix defined as:

$$C_s(v_s) = \begin{bmatrix} 0 & 0 & -m_b v_y \\ 0 & 0 & m_b v_x \\ m_b v_y & -m_b v_x & 0 \end{bmatrix}. \quad (3.4)$$

Function $\tau_{\text{drag}}(\cdot)$, which is a function of ship speed and course angle, represents drag forces in 3DoF applied to the craft. The details of this function are provided in Appendix A.1.

Another method to present drag forces is by establishing added Coriolis and damping matrices. In this regard,

$$\tau_{\text{drag}}(v_s(t), \eta_s(t)) = -C_A(v_s(t)) - D_s(v_s(t)) \quad (3.5)$$

where

$$C_A(v_s) = \begin{bmatrix} 0 & 0 & c_{13}(v_s) \\ 0 & 0 & c_{23}(v_s) \\ -c_{13}(v_s) & -c_{23}(v_s) & 0 \end{bmatrix}, \quad (3.6)$$

with $c_{13}(v_s) = Y_{\dot{v}} v_s + \frac{1}{2}(N_{\dot{v}} + Y_{\dot{r}})$ and $c_{23}(v_s) = -X_{\dot{u}} v_x$.

The damping matrix D_s is constructed by addition of a linear and a nonlinear matrices, i.e.,

$$D_s(V) = D_L + D_{\text{NL}}(v_s), \quad (3.7)$$

where

$$D_L = \begin{bmatrix} -X_u & 0 & 0 \\ 0 & -Y_v & -Y_r \\ 0 & -N_v & -N_r \end{bmatrix} \quad (3.8)$$

$$D_{\text{NL}}(v_s) = \begin{bmatrix} -d_{11}(v_s) & 0 & 0 \\ 0 & -d_{22}(v_s) & -d_{23}(v_s) \\ 0 & -d_{32}(v_s) & -d_{33}(v_s) \end{bmatrix},$$

with $d_{11}(v_s) = X_{|u|u}|v_x| + X_{uuu}v_x^2$, $d_{22}(v_s) = Y_{|v|v}|v_y| + Y_{|r|v}|v_r|$, $d_{23}(v_s) = Y_{|v|r}|v_y| + Y_{|r|r}|v_r|$, $d_{32}(V) = N_{|v|v}|v_r| + N_{|r|v}|v_r|$ and $d_{33}(v_s) = N_{|v|r}|v_x| + N_{|r|r}|v_r|$. For more information on the model and the parameters, see [33, 34].

Matrix $R(\eta_s)$ is a Jacobian matrix that transforms ship velocity from body-fixed into inertial velocities, defined as:

$$R(\eta_s) = \begin{bmatrix} \cos(r) & -\sin(r) & 0 \\ \sin(r) & \cos(r) & 0 \\ 0 & 0 & 1 \end{bmatrix}. \quad (3.9)$$

Vector τ_s is the vector of forces generated by propellers applied to the ship center of gravity, defined as:

$$\tau_s(t) = \begin{bmatrix} \tau_x(t) \\ \tau_y(t) \\ \tau_r(t) \end{bmatrix}, \quad (3.10)$$

where τ_x and τ_y are surge and sway forces and τ_r is the yaw moment.

3.1.1. THRUST ALLOCATION

Considering non-rotatable typical propellers, the relationship between the thrust produced by actuators (propellers and thrusters) and the vector of forces is [34]:

$$\tau_s = \Xi_{3 \times m} \begin{bmatrix} g_1(n_1) \\ \vdots \\ g_m(n_m) \end{bmatrix}, \quad (3.11)$$

where g_1, \dots, g_m are actuator dynamics, n_1, \dots, n_m are actuator shaft speeds, m is the number of actuators, and Ξ is the thrust configuration matrix defined as:

$$\Xi = [\gamma_1 \quad \dots \quad \gamma_m], \quad (3.12)$$

with $\gamma_1, \gamma_2, \dots, \gamma_m$ column vectors for standard actuators. If the actuator is a propeller, then:

$$\gamma_i = \begin{bmatrix} 1 \\ 0 \\ -l_y \end{bmatrix}; \quad (3.13)$$

if the actuator is a stern or bow thruster, then:

$$\gamma_i = \begin{bmatrix} 0 \\ 1 \\ l_x \end{bmatrix}, \quad (3.14)$$

where l_y and l_x represent the position of the actuator in the vessel's reference frame. Since, generally, Γ is not a square matrix the solution to the problem of unconstrained thrust allocation to non-rotatable actuators can be found using the pseudo-inverse of Γ :

$$\tau_{ac} = \Xi^T (\Xi \Xi^T)^{-1} \tau_s. \quad (3.15)$$

3.2. DC POWER AND PROPULSION SYSTEM

The fulfillment of the ship desired operation is not only dependent on the ship maneuvering control algorithm but it is also related to power availability during the operation. As a result, the PPS should be studied alongside to the ship maneuvering model.

On-board DC microgrids consist of prime-mover(s) and AC/DC conversion modules on the energy generation side and motor controller inverters, induction motors, propellers and other loads (like hotel loads, weaponry facilities, etc) on the consumption side. Diesel-generator sets act as prime-movers. The generators are connected to six-pulse rectifiers where the AC/DC conversion process is carried out. The DGR sets are connected to the consumption side through a DC-link which in our study consists of a capacitor. The schematic of the system under study is shown in Figure 3.2. Note that for redundancy and safety purposes in some variations of this architecture, more than one bus bar exists.

One of the main advantages of DC-PPS is enabling the use of variable speed generators. As a result, the diesel engine can run at variable speed which can lead to a reduction in fuel consumption [13]. This feature alongside with the other benefits of this architecture (mentioned in the introduction) increases the flexibility of this PPS which leads to increased adaptability to different operating profiles. On the other hand, one of the major challenges for enabling the DC-PPS is the problem of stability. In this thesis, the stability problem is addressed both through energy management as well as power generation control points of view.

The consumption side of DC-PPS contains induction motors that are connected to propellers and thrusters as well as non-propulsive loads such as hotel loads. The induction motors are connected to the DC bus using motor controller inverters. In the remainder of this chapter, mathematical models are proposed for the different components of the DC-PPS.

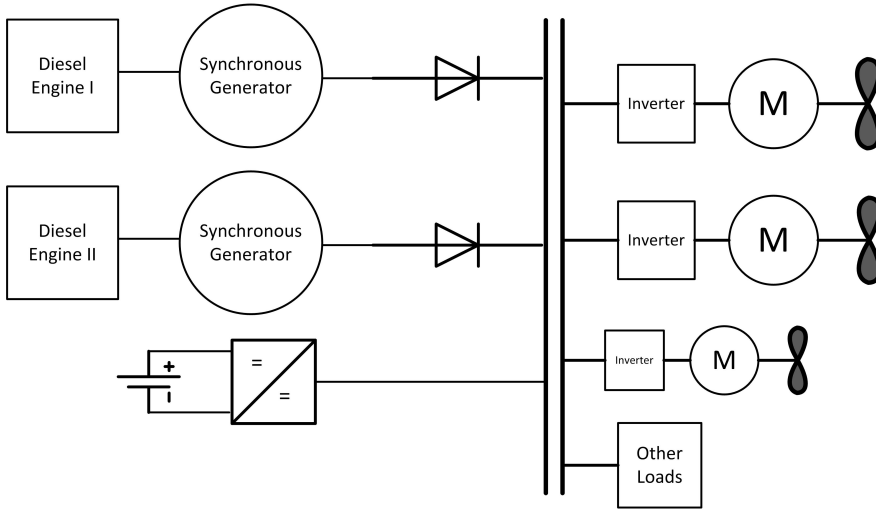


Figure 3.2: The DC-PPS under study.

3.3. ENERGY CONSUMPTION SIDE

In this section, mathematical models for different components of the energy consumption side are presented and then, the overall model is presented in a state space format.

3.3.1. PROPELLER

The relationship between the shaft speed and propeller torque and thrust is established using the following equations [99]:

$$T_p = K_T \rho D^4 |n_p| n_p \quad (3.16)$$

$$Q_p = K_Q \rho D^5 |n_p| n_p, \quad (3.17)$$

where D is the propeller diameter and ρ is the water density. Parameters K_T and K_Q are thrust and torque coefficients which are functions of propeller structure and advance ratio J_p [100] that is:

$$J_p = \frac{V_a}{n_p D},$$

where V_a is the advance speed of the ship.

3.3.2. INDUCTION MOTOR

The model of the induction motor is also represented in the dq-reference frame [101]. The dynamical equations of the squirrel-cage machine are:

$$\begin{aligned}
 \dot{\psi}_{\text{dsm}} &= v_{\text{dsm}} - \omega_p \psi_{\text{qsm}} + r_{\text{sm}} i_{\text{dsm}} \\
 \dot{\psi}_{\text{qsm}} &= v_{\text{qsm}} - \omega_p \psi_{\text{dsm}} - r_{\text{sm}} i_{\text{qsm}} \\
 \dot{\psi}_{\text{drm}} &= v_{\text{drm}} + \left(\frac{2}{p} \omega_p - \omega_e\right) \psi_{\text{qrm}} - r_{\text{rm}} i_{\text{drm}} \\
 \dot{\psi}_{\text{qrm}} &= v_{\text{qrm}} - \left(\frac{2}{p} \omega_p - \omega_e\right) \psi_{\text{drm}} - r_{\text{rm}} i_{\text{qrm}} \\
 Q_{\text{em}} &= 1.5p(\psi_{\text{dsm}} i_{\text{qsm}} - \psi_{\text{qsm}} i_{\text{dsm}}),
 \end{aligned} \tag{3.18}$$

where i_{dsm} and i_{qsm} are stator currents in the dq-reference frame, i_{drm} and i_{qrm} are rotor currents, ψ_{dsm} , ψ_{qsm} , ψ_{drm} and ψ_{qrm} are the stator and rotor fluxes, respectively. Parameter p represents the number of poles, ω_p is the rotor speed, ω_e is the electrical angular velocity and Q_{em} is the electric torque. The stator and rotor voltages in the dq-frame are shown as v_{dsm} , v_{qsm} , v_{drm} and v_{qrm} , respectively. The relationship between the machine currents and fluxes are established using the machine inductances L_{sm} , L_{rm} and L_{mm} as:

$$\begin{aligned}
 \psi_{\text{qsm}} &= L_{\text{sm}} i_{\text{qsm}} + L_{\text{mm}} i_{\text{qrm}} \\
 \psi_{\text{dsm}} &= L_{\text{sm}} i_{\text{dsm}} + L_{\text{mm}} i_{\text{drm}} \\
 \psi_{\text{qrm}} &= L_{\text{rm}} i_{\text{qrm}} + L_{\text{mm}} i_{\text{qsm}} \\
 \psi_{\text{drm}} &= L_{\text{rm}} i_{\text{drm}} + L_{\text{mm}} i_{\text{dsm}}.
 \end{aligned} \tag{3.19}$$

A voltage source inverter is used as a converting stage between the DC-link and the machine which controls the machine by adopting a direct torque control technique [101].

3.3.3. STATE SPACE MODELING OF ENERGY CONSUMPTION SIDE

Considering (3.17), (3.18), and (3.19) the state space model for an induction motor-propeller set can be written as:

$$\begin{aligned}
 \dot{I}_{\text{M}} &= X_{\text{M}}^{-1} v_{\text{M}} - X_{\text{M}}^{-1} w_{\text{M}} X_{\text{M}} I_{\text{M}} - X_{\text{M}}^{-1} R_{\text{M}} I_{\text{M}} \\
 \dot{\omega}_{\text{m}} &= \frac{1}{j} (1.5 p_{\text{m}} I_{\text{M}}^T X_{\text{M}}^T M_1 I_{\text{M}} - Q_{\text{p}}),
 \end{aligned} \tag{3.20}$$

where

$$w_{\text{M}} = \begin{bmatrix} \omega_p & 0 & 0 & 0 \\ 0 & \omega_p & 0 & 0 \\ 0 & 0 & -\left(\frac{2}{p_{\text{m}}} \omega_p - \omega_e\right) & 0 \\ 0 & 0 & 0 & \left(\frac{2}{p_{\text{m}}} \omega_p - \omega_e\right) \end{bmatrix}, \tag{3.21}$$

$$R_{\text{M}} = \begin{bmatrix} -r_{\text{sm}} & 0 & 0 & 0 \\ 0 & r_{\text{sm}} & 0 & 0 \\ 0 & 0 & r_{\text{rm}} & 0 \\ 0 & 0 & 0 & r_{\text{rm}} \end{bmatrix}, \tag{3.22}$$

$$X_M = \begin{bmatrix} L_{sm} & 0 & L_{mm} & 0 \\ 0 & L_{sm} & 0 & L_{mm} \\ L_{mm} & 0 & L_{rm} & 0 \\ 0 & L_{mm} & 0 & L_{rm} \end{bmatrix}, \quad (3.23)$$

$$M_1 = \begin{bmatrix} 0 & 1 & 0 & 0 \\ -1 & 0 & 0 & 0 \\ 0 & 0 & 0 & 0 \\ 0 & 0 & 0 & 0 \end{bmatrix}, \quad (3.24)$$

$I_M = [i_{dsm}, i_{qsm}, i_{rsm}, i_{qrm}]^T$, and $v_M = [v_{dsm}, v_{qsm}, v_{rsm}, v_{qrm}]^T$.

The energy consumption side and the maneuvering model are connected through the generated torque by propellers, i.e., Q_p . The combination of the dq currents of induction motors establishes the overall load current i_{load} .

3.4. ENERGY GENERATION SIDE

In this section, mathematical models for different components of the energy generation side are presented and then, the overall model is presented in a state space format.

3.4.1. DIESEL ENGINE

The diesel engine is the primary energy supplier by transforming chemical energy to mechanical energy. The produced power appears as torque generation. The diesel engine dynamics can be approximated by nonlinear or linear equations (see, e.g., [99],[102],[27]), depending on the level of accuracy needed. In this thesis, a linear model is adopted to accommodate the relationship between the fuel index and produced torque Q_{en} by means of a transfer function as below [103]:

$$\dot{Q}_{en} = -\frac{1}{\tau_{en}}(Q_{en} + K_{en}f_{en}), \quad (3.25)$$

where K_{en} is the torque constant, f_{en} is the governor setting (i.e., fuel index and flow) and τ_{en} is the torque buildup constant which determines the response speed of the diesel engine, a function of diesel-generator shaft speed:

$$\tau_{en} = \frac{0.9}{\omega_{dg}}, \quad (3.26)$$

where ω_{dg} represents the rotational speed [104].

3.4.2. SYNCHRONOUS GENERATOR

The mechanical energy is transformed to electrical energy by use of the synchronous generators. The relationship between a generator and a diesel engine is established through the shaft speed where the generated torque of the diesel engine is an input for the generator. In the context of this research, the Park equivalent Direct-Quadratic (dq) modeling approach is used to represent the dynamics of the synchronous generator. The

relationship between the voltages, fluxes, and currents in the dq reference frame is established using the following equations:

$$\begin{aligned}
 \dot{\psi}_d &= -v_d + \omega_{dg}\psi_q + r_s i_d \\
 \dot{\psi}_q &= -v_q + \omega_{dg}\psi_d + r_s i_q \\
 \dot{\psi}_{fd} &= v_{fd} - r_{fd} i_{fd} \\
 \dot{\psi}_{kd} &= -r_{kd} i_{kd} \\
 \dot{\psi}_{kq} &= -r_{kq} i_{kq},
 \end{aligned} \tag{3.27}$$

where r_s , r_{fd} , r_{kd} , and r_{kq} are stator, field circuit and damping resistances, respectively. Variables ψ_d and ψ_q are fluxes in the d and q axis, ψ_{kd} and ψ_{kq} are damper fluxes; field flux is represented by ψ_{fd} . In the above model, v_d and v_q are dq voltages and v_{fd} is the field voltage of the generator. The mechanical dynamics of the synchronous generator are given as:

$$\dot{\omega}_{dg} = \frac{1}{2H}(\psi_d i_q - \psi_q i_d + Q_{en}), \tag{3.28}$$

where ω_{dg} is the shaft speed of the diesel generator, Q_{en} is the mechanical torque produced by the diesel engine, and $H = \frac{J}{p}$ is the inertia constant per pole. Using the system inductances, the relationship between electrical currents and fluxes can be established as:

$$\begin{bmatrix} i_d \\ i_q \\ i_{fd} \\ i_{kd} \\ i_{kq} \end{bmatrix} = \begin{bmatrix} -L_d & 0 & L_{md} & L_{md} & 0 \\ 0 & -L_q & 0 & 0 & L_{mq} \\ -L_{md} & 0 & L_{fd} & L_{md} & 0 \\ -L_{md} & 0 & L_{md} & L_{kd} & 0 \\ 0 & -L_{mq} & 0 & 0 & L_{kq} \end{bmatrix}^{-1} \begin{bmatrix} \psi_d \\ \psi_q \\ \psi_{fd} \\ \psi_{kd} \\ \psi_{kq} \end{bmatrix}, \tag{3.29}$$

where L_d , L_{md} , L_{kd} , L_{fd} , L_q , L_{mq} and L_{kq} are per unit inductances [101].

3.4.3. RECTIFIER AND THE DC-LINK

We consider an average value model with constant parameters for the uncontrollable rectifier [105]. In our model, the rectifier is introduced with generator currents as input and DC current as the output. The DC current can be computed as:

$$i_{dc} = \beta_{rec} \sqrt{i_q^2 + i_d^2}. \tag{3.30}$$

The DC-link voltage is derived using the below Kirchhoff equation:

$$\dot{v}_{dc} = \frac{1}{C}(i_{dc} - i_{load}), \tag{3.31}$$

where i_{load} is the DC load current.

The dq-voltages from the rectifier to the generator are as follows:

$$\begin{aligned}
 v_q &= \alpha_{rec} v_{dc} \cos(\theta_g) \\
 v_d &= \alpha_{rec} v_{dc} \sin(\theta_g),
 \end{aligned} \tag{3.32}$$

where θ_g is the load angle and is computed as below:

$$\theta_g = \arctan\left(\frac{i_d}{i_q}\right) - \phi_{\text{rec}}. \quad (3.33)$$

Variables α_{rec} , β_{rec} and ϕ_{rec} are considered constant in this model.

3.4.4. BATTERY

A model from [106] is used for representing the battery dynamics. This is suitable for power and energy management purposes. The State-of-Charge (SoC) of the battery is determined using:

$$S_{\text{OC}}(k+1) = S_{\text{OC}}(k) - \left(\frac{\eta_i \Delta t}{C_n}\right) i_b, \quad (3.34)$$

where η_i is the cell Coulombic efficiency, i.e., $\eta_i = 1$ for discharge and $\eta_i \leq 1$ for charge. Parameter C_n is the nominal capacity of the battery, k is the sampling time, Δt is the sampling period, and i_b is the battery current. The battery voltage can be derived as:

$$v_b = O_{\text{CV}}(S_{\text{OC}}(k)) - r_b i_b, \quad (3.35)$$

where O_{CV} is the open circuit voltage of the battery and is a function of S_{OC} and r_b is the battery resistance.

3.4.5. BIDIRECTIONAL CONVERTER

A non-isolated bidirectional converter is considered for the DC-PPS. Non-isolated bidirectional converters are suitable for low and medium voltage DC microgrids. They are cheaper and have lower losses compared to isolated converters.

The dynamical model of the converter is adopted using Kirchhoff current and voltage laws:

$$\begin{aligned} \dot{i}_L &= \frac{d(t)}{L} v_{\text{dc}}(t) - \frac{v_b(t)}{L} \\ \dot{v}_{\text{dc}} &= \frac{D}{C} i_L(t) - \frac{i_{\text{load}}(t)}{C}, \end{aligned} \quad (3.36)$$

where $d(t)$ is the duty cycle of the switching operation, i_L is the current of the equivalent inductor on the low voltage side of the converter, v_b is the battery voltage and D is the voltage ratio. The converter is controlled using a cascaded PID control approach [107].

3.4.6. STATE SPACE MODELING OF ENERGY GENERATION SIDE

In this part, a state space model is presented by combining the components of the energy generation side. First, (3.27) is rewritten in matrix form as:

$$\begin{bmatrix} \dot{\psi}_d \\ \dot{\psi}_q \\ \dot{\psi}_{fd} \\ \dot{\psi}_{kd} \\ \dot{\psi}_{kq} \end{bmatrix} = \begin{bmatrix} 0 & \omega_{dg} & 0 & 0 & 0 \\ \omega_{dg} & 0 & 0 & 0 & 0 \\ 0 & 0 & 0 & 0 & 0 \\ 0 & 0 & 0 & 0 & 0 \\ 0 & 0 & 0 & 0 & 0 \end{bmatrix} \begin{bmatrix} \psi_d \\ \psi_q \\ \psi_{fd} \\ \psi_{kd} \\ \psi_{kq} \end{bmatrix} + \begin{bmatrix} r_s & 0 & 0 & 0 & 0 \\ 0 & r_s & 0 & 0 & 0 \\ 0 & 0 & -r_{fd} & 0 & 0 \\ 0 & 0 & 0 & -r_{kd} & 0 \\ 0 & 0 & 0 & 0 & -r_{kq} \end{bmatrix} \begin{bmatrix} i_d \\ i_q \\ i_{fd} \\ i_{kd} \\ i_{kq} \end{bmatrix} + \begin{bmatrix} v_d \\ v_q \\ v_{fd} \\ 0 \\ 0 \end{bmatrix}. \quad (3.37)$$

Then, by combining the above equation with (3.29) and (3.32), we obtain:

$$\begin{aligned} \dot{I}_G &= X_G^{-1} S_\omega(\omega_{dg}) X_G I_G + X_G^{-1} R_G I_G \\ &+ v_{dc} X_G^{-1} \begin{bmatrix} \alpha_{rec} \sin(\arctan(\frac{i_d}{i_q}) - \phi_{rec}) \\ \alpha_{rec} \cos(\arctan(\frac{i_d}{i_q}) - \phi_{rec}) \\ 0 \\ 0 \\ 0 \end{bmatrix} + X_G^{-1} b v_{fd} \end{aligned} \quad (3.38)$$

where I_G is the vector of currents, X_G is the matrix of per unit inductances, and R_G is the diagonal matrix of resistances. Moreover,

$$S_\omega(\omega_{dg}) = \begin{bmatrix} 0 & \omega_{dg} & 0 & 0 & 0 \\ \omega_{dg} & 0 & 0 & 0 & 0 \\ 0 & 0 & 0 & 0 & 0 \\ 0 & 0 & 0 & 0 & 0 \\ 0 & 0 & 0 & 0 & 0 \end{bmatrix}$$

and $b = [0 \ 0 \ 1 \ 0 \ 0]^T$.

The dynamics of a diesel-generator shaft speed can now be represented in matrix form as:

$$\begin{aligned} \dot{\omega}_{dg} &= \frac{1}{2H} (Q_{en} - I_G X_G^T G_1 I_G) \\ \dot{Q}_{en} &= -\frac{Q_{en}}{\tau_s} + K_{en} f_{en}, \end{aligned} \quad (3.39)$$

where

$$G_1 = \begin{bmatrix} 0 & 1 & 0 & 0 & 0 \\ -1 & 0 & 0 & 0 & 0 \\ 0 & 0 & 0 & 0 & 0 \\ 0 & 0 & 0 & 0 & 0 \\ 0 & 0 & 0 & 0 & 0 \end{bmatrix}.$$

The dynamics of the DC link voltage in the presence of m number of DGR sets can be written as:

$$\dot{v}_{dc} = \frac{1}{C} \left(\beta_{rec_1} \sqrt{I_{G_1}^T G_2 I_{G_1}} + \dots + \beta_{rec_m} \sqrt{I_{G_m}^T G_2 I_{G_m}} + D i_L - i_{load} \right) \quad (3.40)$$

where

$$G_2 = \begin{bmatrix} 1 & 0 & 0 & 0 & 0 \\ 0 & 1 & 0 & 0 & 0 \\ 0 & 0 & 0 & 0 & 0 \\ 0 & 0 & 0 & 0 & 0 \\ 0 & 0 & 0 & 0 & 0 \end{bmatrix}.$$

As a result, the overall dynamics of the energy generation side can be described using the following equations:

$$\begin{aligned} \dot{I}_{G_1} &= X_{G_1}^{-1} S_\omega(\omega_{dg_1}) X_{G_1} I_{G_1} + X_{G_1}^{-1} R_{G_1} I_{G_1} \\ &\quad + v_{dc} X_{G_1}^{-1} E_1 + X_{G_1}^{-1} b v_{fd_1} \\ \dot{\omega}_{dg_1} &= \frac{1}{2H_1} (Q_{en_1} - I_{G_1}^T X_{G_1}^T G_1 I_{G_1}) \\ \dot{Q}_{en_1} &= -\frac{Q_{en_1}}{\tau_{s_1}} + K_{en_1} f_{en_1} \\ &\quad \vdots \\ \dot{I}_{G_m} &= X_{G_m}^{-1} S_\omega(\omega_{dg_m}) X_{G_m} I_{G_m} + X_{G_m}^{-1} R_{G_m} I_{G_m} \\ &\quad + v_{dc} X_{G_m}^{-1} E_m + X_{G_m}^{-1} b v_{fd_m} \\ \dot{\omega}_{dg_m} &= \frac{1}{2H_m} (Q_{en_m} - I_{G_m}^T X_{G_m}^T G_1 I_{G_m}) \\ \dot{Q}_{en_m} &= -\frac{Q_{en_m}}{\tau_{s_m}} + K_{en_m} f_{en_m} \\ \dot{i}_L &= \frac{d}{L} v_{dc} - \frac{v_b(t)}{L} \\ \dot{v}_{dc} &= \frac{1}{C} (\beta_{rec_1} \sqrt{I_{G_1}^T G_2 I_{G_1}} + \dots + \beta_{rec_m} \sqrt{I_{G_m}^T G_2 I_{G_m}} + D i_L - i_{load}) \end{aligned} \quad (3.41)$$

where

$$E_j = \begin{bmatrix} \alpha_{rec_j} \sin(\arctan(\frac{i_{d_j}}{i_{q_j}}) - \phi_{rec_j}) \\ \alpha_{rec_j} \cos(\arctan(\frac{i_{d_j}}{i_{q_j}}) - \phi_{rec_j}) \\ 0 \\ 0 \\ 0 \end{bmatrix}. \quad (3.42)$$

For the control of energy generation side and load sharing, conventional PI-based schemes are adopted [23],[107].

3.5. THE OVERALL SHIP MODEL

Based on the proposed models in Sections 3.1, 3.3, and 3.4, the overall model of a ship with a DC-PPS is:

$$\begin{aligned}
 \dot{\eta}_s(t) &= R(\eta_s(t))v_s(t) \\
 \dot{v}_s(t) &= M_s^{-1} \left(\Xi_{3 \times m} \begin{bmatrix} \frac{K_{T1} Q_{p1}}{K_{Q1} D_1} \\ \vdots \\ \frac{K_{Tn} Q_{pn}}{K_{Qn} D_n} \end{bmatrix} + \tau_{\text{drag}}(v_s(t), \eta_s(t)) - C_s(v_s(t))v_s(t) \right) \\
 \dot{I}_{M_1} &= X_{M_1}^{-1} v_{M_1} - X_{M_1}^{-1} w_{M_1} X_{M_1} I_{M_1} - X_{M_1}^{-1} R_{M_1} I_{M_1} \\
 \dot{\omega}_{m_1} &= \frac{1}{j} (1.5 p_{m_1} I_{M_1}^T X_{M_1}^T M_1 I_{M_1} - Q_{p_1}) \\
 &\vdots \\
 \dot{I}_{M_n} &= X_{M_n}^{-1} v_{M_n} - X_{M_n}^{-1} w_{M_n} X_{M_n} I_{M_n} - X_{M_n}^{-1} R_{M_n} I_{M_n} \\
 \dot{\omega}_{m_n} &= \frac{1}{j} (1.5 p_{m_n} I_{M_n}^T X_{M_n}^T M_1 I_{M_n} - Q_{p_n}) \\
 \dot{I}_{G_1} &= X_{G_1}^{-1} S_\omega(\omega_{\text{dgl}}) X_{G_1} I_{G_1} + X_{G_1}^{-1} R_{G_1} I_{G_1} \\
 &\quad + v_{dc} X_{G_1}^{-1} E_1 + X_{G_1}^{-1} b v_{\text{fd}_1} \\
 \dot{\omega}_{\text{dgl}} &= \frac{1}{2H_1} (Q_{\text{en}_1} - I_{G_1}^T X_{G_1}^T G_1 I_{G_1}) \\
 \dot{Q}_{\text{en}_1} &= -\frac{Q_{\text{en}_1}}{\tau_{s_1}} + K_{\text{en}_1} f_{\text{en}_1} \\
 &\vdots \\
 \dot{I}_{G_m} &= X_{G_m}^{-1} S_\omega(\omega_{\text{dgm}}) X_{G_m} I_{G_m} + X_{G_m}^{-1} R_{G_m} I_{G_m} \\
 &\quad + v_{dc} X_{G_m}^{-1} E_m + X_{G_m}^{-1} b v_{\text{fd}_m} \\
 \dot{\omega}_{\text{dgm}} &= \frac{1}{2H_m} (Q_{\text{en}_m} - I_{G_m}^T X_{G_m}^T G_1 I_{G_m}) \\
 \dot{Q}_{\text{en}_m} &= -\frac{Q_{\text{en}_m}}{\tau_{s_m}} + K_{\text{en}_m} f_{\text{en}_m} \\
 \dot{i}_L &= \frac{d}{L} v_{dc} - \frac{v_b(t)}{L} \\
 v_{dc} &= \frac{1}{C} (\beta_{\text{rec}_1} \sqrt{I_{G_1}^T G_2 I_{G_1}} + \cdots + \beta_{\text{rec}_m} \sqrt{I_{G_m}^T G_2 I_{G_m}} + D i_L - i_{\text{load}})
 \end{aligned} \tag{3.43}$$

where n and m are the number of DGR sets and propelling actuators, respectively. Parameter i_{load} is the sum of DC current absorbed by the Induction motors and the other loads on-board of the ship.

3.6. CONCLUSIONS

In this chapter, the overall system under study has been modeled. A model for every component has been presented and then, the maneuvering model, energy generation side model, and the energy consumption side have been presented in state space format. The results of this chapter contribute to answering the research questions presented in Chapter 1 by proposing mathematical models which will be used in Chapters 4-8 to propose novel and effective approaches for maneuvering, energy management, and power generation control. In Chapters 4 and 5, control approaches are proposed for maneuvering control. Energy management and power generation control approaches are presented in Chapters 6, 7, and 8 to improve the fuel efficiency and stability of the power and propulsion system. The validation results of the components are presented throughout the thesis in computer-based evaluation sections where the components are adopted and introduced for simulation-based experiments.

4

MANEUVERING CONTROL IN THE PRESENCE OF UNCERTAINTY

One of the major challenges within the control of autonomous vessels is the problem of uncertainties in the craft and its components model. Recently, several research works have been published to address this problem. It has been shown in the literature that the dynamics of propellers experience a relatively large amount of uncertainty during maneuvering of the vessel [57]. This makes the speed and position control of autonomous vessels challenging. In this chapter, a control approach is proposed to handle the uncertainties within model of propeller as well as maneuvering model of the vessel. First, an introduction about the problem of uncertainty is presented in Section 4.1. In Section 4.2, the problem of uncertainty in propeller model is explained and then formulated in Section 4.3. The adaptive control scheme is proposed in Section 4.4 and in Section 4.5, simulation experiments results are presented and discussed. The results of this chapter have been partially included in several scientific papers.¹

4.1. INTRODUCTION

Considering the propellers shaft speed as the system input, the governing dynamical equation of the system is a non-affine in control system. As a result, the objective is to design a control algorithm that carries out the motion and position control of the ship by on-line approximation of propellers dynamics and handling hydrodynamical uncertainties within the vessel's model.

¹Parts of this chapter have been published in:

1. A. Haseltalab, R. R. Negenborn, Adaptive Control for a Class of Partially Unknown Non-Affine Systems: Applied to Autonomous Surface Vessels, IFAC-PapersOnLine, Volume 50, Issue 1, 2017, Pages 4252-4257.
2. A. Haseltalab, R. R. Negenborn, Adaptive Control for Autonomous Ships with Uncertain Model and Unknown Propeller Dynamics, Accepted for publication in Control Engineering Practice, 2019.

Considering the vessel model and by building up on our previous research results in [9], an adaptive control methodology for a class of non-affine-in-control systems is proposed where the unknown nonlinear influence of the system input is estimated using NN, so that the ASV can follow the given trajectory with the desired speed. In this chapter, it is also shown that the proposed methodology is capable of handling state dependent uncertainties within the hydrodynamical model of the ship. To achieve these goals, the results in [108] for adaptive control of affine-in-control systems are extended to control of partially unknown non-affine systems. An algorithm is proposed to address the problem of controlling a class of non-affine systems where the dynamics of the input function $g(\cdot)$ is unknown or uncertain where $g(\cdot)$ is the generated thrust by the propeller. By the adoption of Neural Networks (NN), particularly the results in [109] and the Weierstrass approximation theorem [110], the inverse of $g(\cdot)$ is calculated and by adopting a control law the stability of the system is guaranteed. For the stability analysis, the Lyapunov technique as well as *Uniform Ultimate Boundedness* are employed and it is then shown that the reference trajectory tracking error converges to a residual set. The algorithm transforms the system to an affine-in-control system and then, by approximating $g^{-1}(\cdot)$, estimates the feasible control input. It is also shown that this strategy is capable of handling state dependent uncertainties within the hydrodynamical model of the ship. In order to evaluate the performance of the algorithm, several experiments are carried out. Based on actual Automatic Identification System (AIS) data received from the Port of Rotterdam Authority, a maneuvering experiment is carried out. It is assumed that the ship model embeds a Direct Current (DC) power and propulsion system [22] in order to assess the interaction of the proposed algorithm with the on-board power and propulsion system. Moreover, a dynamic positioning experiment and a circular trajectory tracking experiment are performed.

4.2. THE PROBLEM OF UNCERTAINTY IN PROPELLER MODEL

The propellers and thrusters are the main components for the generation of required forces to propel a ship aligned to its given referenced trajectory. Based on the propeller model, the required forces can be determined by introducing a proper shaft speed to the propellers and thrusters. As a result, the propeller shaft speed is treated as the system input. These actuators are also the main link between on-board power and propulsion system and surrounding environment of the ship. To elaborate on the problem of propeller uncertainty, the propeller model in Section 3.3.1 is partially described again and then, the the problem of uncertainty is explained.

The relationship between the propeller shaft speed and the generated torque and thrust can be established based on the following relationships [99]:

$$T_p = K_T \rho D^4 |n_p| n_p \quad (4.1)$$

$$Q_p = K_Q \rho D^5 |n_p| n_p, \quad (4.2)$$

where D is the propeller diameter and ρ is the water density. Parameters K_T and K_Q are thrust and torque coefficients, which are functions of propeller structure and advance ratio J [100], defined as:

$$K_T = f_{K_T}(J, P/D, A_e/A_o, Z, R_n, t_c)$$

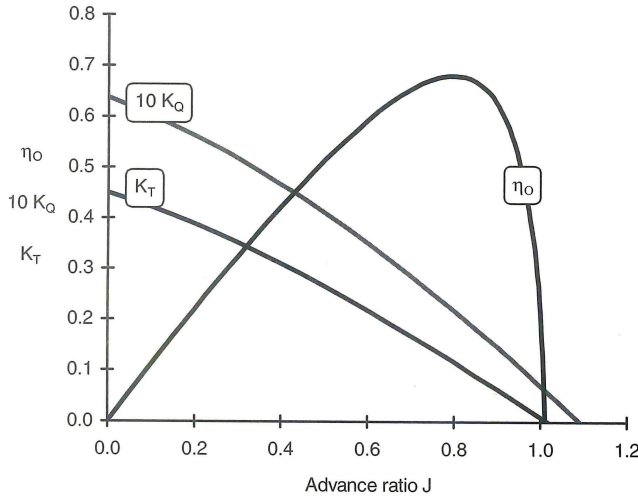


Figure 4.1: Open water diagram for Wageningen B 5 75 with pitch ratio 0.96 where η_o is the open water efficiency [112].

$$K_Q = f_{K_Q}(J, P/D, A_e/A_o, Z, R_n, t_c),$$

where P/D is the pitch ratio, A_e/A_o is the blade area ratio, Z is the number of propeller blades, R_n is the Reynolds number of a characteristic ratio and t_c is the ratio of maximum propeller thickness to the length of the cord at a characteristic radius. Moreover, the advance ratio is defined as:

$$J = \frac{V_a}{n_p D},$$

where V_a is the advanced speed that is the speed of water passing through propellers found using the following equation:

$$V_a = (1 - w)v_x, \quad (4.3)$$

with v_x the forward speed of the vessel and w the wake friction, depending on the shape of the hull.

Functions f_{K_T} and f_{K_Q} were estimated in [100, 111] in terms of very long and complex polynomials. However, typically, these functions are approximated using J and open water diagram where the performance of propellers are assessed, i.e., K_T and K_Q are functions of J . Figure 4.1 shows an open water diagram of a fixed pitch propeller belonging to the Wageningen B systematic series.

The modeling of propellers has always been a challenge in the maritime industry where a thorough model has not been proposed so far (for more information on this please refer to [57] and references therein). During maneuvering of a vessel, the propellers behave differently compared to when sailing straight. When a ship turns, due to the presence of lateral velocity, the inflow to the propellers is slanting and not axial. As a

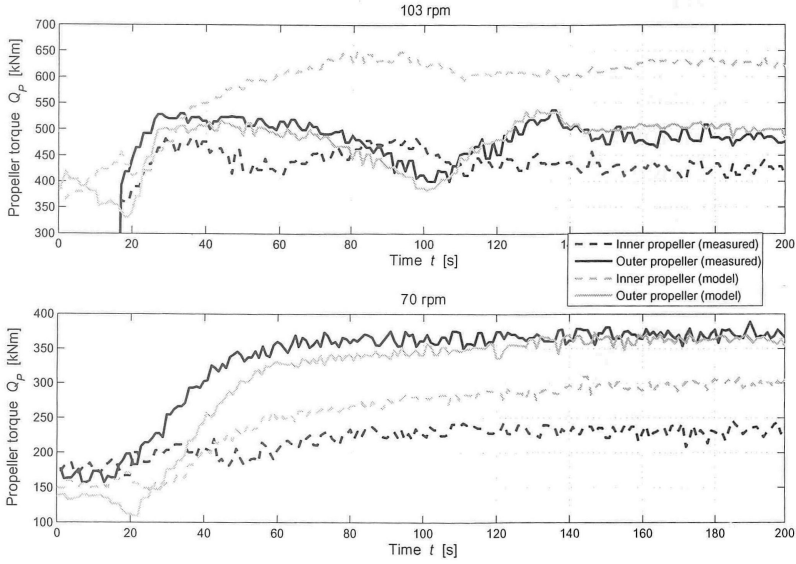


Figure 4.2: The difference between measured propeller torque and the outcome of the model during a turn [57].

result, the advance ratio J will decrease and more load is applied to propellers. Since, the open water diagram (and any other performance diagrams) is based on axial flow, they can not be used directly [57, 113]. Several analytical approaches have been proposed to solve this problem, however each of them contains a great amount of uncertainty.

Moreover, in a turn, the wake factor is also influenced. During straight courses, the wake is uniformly distributed but in a turn, the transversal velocity component is not dispersed uniformly and in the lower half of the propeller blade, the transversal velocity is way larger than the upper half [57, 114]. Figure 4.2 represents for a particular vessel the difference between the results of a propeller model and measured values [57], indicating the significant uncertainty in the model. In conventional ships, this problem might not be very critical since the control inputs are given by human operators. However in ASVs and during autopilot modes, this problem might result in inaccurate guidance. Since it has been shown in the literature that having an accurate and simple model for propellers is challenging, in this chapter, the objective is to design an algorithm to control the ship maneuvering by on-line approximation of propellers dynamics.

4.3. PROBLEM FORMULATION

In this chapter, it is assumed that g_1, \dots, g_m are unknown functions. For the algorithm design, the first step is to represent (3.43) in state space format. As a result, we have:

$$\begin{aligned} \dot{v}_s &= -M_s^{-1}(C_s(v_s)v_s + C_A(v_s)v_s + D_s(v_s)v_s - \tau_s) \\ \dot{\eta}_s &= T(\eta_s)v_s. \end{aligned} \quad (4.4)$$

Equation (4.4) can be rewritten in the following form:

$$\dot{x} = f(x) + \begin{bmatrix} M_s^{-1} \\ 0_{3 \times 3} \end{bmatrix} \tau_s, \quad (4.5)$$

where $x = [v_s^T \quad \eta_s^T]^T$ is the vector of states, $f : \mathbb{R}^6 \rightarrow \mathbb{R}^6$ is a nonlinear function. By combining (3.11) and (4.5) we obtain:

$$\dot{x} = f(x) + \begin{bmatrix} M_s^{-1} \Xi \\ 0_{3 \times m} \end{bmatrix} \begin{bmatrix} g_1(n_{p_1}) \\ \vdots \\ g_m(n_{p_m}) \end{bmatrix}, \quad (4.6)$$

$$\dot{x} = f(x) + g(u). \quad (4.7)$$

where $g : \mathbb{R}^m \rightarrow \mathbb{R}^6$ is a nonlinear function that contains the influence of input variables to the system and $u_s = [n_1, n_2, \dots, n_m]^T$ is the vector of actuators shaft speeds.

Consider the following class of non-affine systems:

$$\dot{x}(t) = f(x(t)) + g(u(t)) + \omega(t), \quad (4.8)$$

where $x(t) \in \mathbb{R}^n$ is the state of the system, $u(t) \in \mathbb{R}^m$ is the system input, $\omega(t) \in \mathbb{R}^n$ is the disturbance applied to the system, $f : \mathbb{R}^n \rightarrow \mathbb{R}^n$ is a Lipschitz continuous nonlinear function and $g : \mathbb{R}^m \rightarrow \mathbb{R}^n$ is a nonlinear continuously differentiable function with $g_1(0) = 0, \dots, g_n(0) = 0$. In the context of this paper, it is assumed that the function $g(\cdot)$ is unknown but satisfies the following assumption:

Assumption 1 *There exists a lower bound and an upper bound $\gamma_l, \gamma_u \in \mathbb{R}$, such that*

$$0 < \gamma_l < \left| J(g(u(t))) \right| < \gamma_u \quad (4.9)$$

for all $t \geq 0$.

Using the *Implicit Function Theorem* and assumptions on $g(\cdot)$, the existence of $g^{-1}(\cdot)$ can be demonstrated [115]. The above assumptions on the system dynamics are moderately mild and can be concluded for broad classes of nonlinear systems [115, 116].

Assumption 2 *The overall disturbance acting upon the system is bounded, i.e., there exists $\omega_M > 0$ such that $\|\omega(t)\| \leq \omega_M$ for all $t \geq 0$.*

Suppose $x_R(t)$ is the desired trajectory of the system. Then, one can write the trajectory tracking error of the system as:

$$e(t) = x_R(t) - x(t). \quad (4.10)$$

The objective is to design an adaptive controller that adopts state feedback to ensure that $x(t)$ follows $x_R(t)$ for all $t > 0$.

4.4. ADAPTIVE CONTROL STRATEGY

In this section, the proposed control strategy for the aforementioned class of non-affine systems is explained and the stability analysis and the proof of correctness are carried out.

4.4.1. PROPOSED CONTROL STRATEGY

The control strategy is based on transforming the non-affine system to an affine nonlinear system and then, keeping $e(t)$ in a residual set by approximating $g^{-1}(\cdot)$ and adopting a proper control law. Let

$$U(t) = g(u(t)), \quad (4.11)$$

where $U \in \mathbb{R}^n$ is treated as the control signal for the affine-in-control system, i.e.,

$$\dot{x}(t) = f(x) + U(t) + \omega(t). \quad (4.12)$$

Similarly as earlier research works in adaptive control (such as [117, 118]), we define the following control law for the above system:

$$U(t) = ke(t) - f(x), \quad (4.13)$$

where k is the controller gain, which will be determined below using a Lyapunov technique. By adopting the above control rule, it can be shown that (4.12) can follow the desired trajectory $x_R(t)$. However, in the problem considered in this chapter, one of the main challenges is that $U(t)$ is not recognizable for the non-affine system (4.8), i.e., generally, $u(t)$ cannot be computed using $U(t)$. Therefore, the objective is to estimate $u(t)$ using the trajectory tracking error of the system and a well-tuned controller gain.

Based on the results in the literature [109] and similar to the methodology used in [108], feed-forward NNs with one hidden layer are capable of approximating any continuous function on a compact set, regardless of the nature of NN activation functions and input space dimensions. Assume $g^{-1}(\cdot)$ as the inverse of $g(\cdot)$. Let us define $g^{-1}(\cdot)$ as:

$$g^{-1}(U) = \text{diag}^{-1}(W^T \psi(U)) + \epsilon, \quad (4.14)$$

where $\psi(U) \in \mathbb{R}^{N \times n}$ is known as the vector of NN activation functions, $W \in \mathbb{R}^{N \times n}$ is the ideal approximation weight vector, ϵ is the approximation error and N is the number of neurons. In the presented methodology, the controller updates its set of weights \hat{W} based on the tracking error $e(t)$ to approximate $g^{-1}(\cdot)$. As a result, at each time $t \geq 0$, the estimation of $g^{-1}(\cdot)$ can be written as:

$$\hat{g}^{-1}(U) = \text{diag}^{-1}(\hat{W}^T \psi(U)), \quad (4.15)$$

where $\hat{g}^{-1}(\cdot)$ and \hat{W} are estimates of $g^{-1}(\cdot)$ and W , respectively. The $\text{diag}(\cdot)$ operator is defined as:

$$\text{diag}(A) = \begin{bmatrix} a_1 & 0 & \dots \\ 0 & a_2 & \dots \\ 0 & 0 & \ddots \end{bmatrix}$$

Algorithm 1 Adaptive Control Algorithm for Non-Affine Systems:

Initialization: Obtain $x(0)$ and $x_R(t)$. Assign initial values to the elements in the vector of weights.

- 1: Calculate $e(t)$ using (7.19).
 - 2: Compute U using (4.13) at each time t .
 - 3: Estimate u by adopting (4.15).
 - 4: Apply u to the system.
 - 5: Update the vector of weights based on (4.19).
 - 6: Obtain the state of the system and go to 1.
-

where $A = [a_1, a_2, \dots]^T$ and $\text{diag}^{-1}(\text{diag}(A)) = A$. The error in the estimation of $g^{-1}(\cdot)$ can be defined as:

$$\tilde{g}^{-1}(U) = g^{-1}(U) - \hat{g}^{-1}(U) = \text{diag}(\tilde{W}^T \psi(U)) + \epsilon, \quad (4.16)$$

where

$$\tilde{W} = W - \hat{W} \quad (4.17)$$

is the weight approximation error. Furthermore, using (4.15), the error dynamics of system (4.8) can be determined as:

$$\dot{e}(t) = -\left(f(x(t)) + g(\text{diag}^{-1}(\hat{W}^T \psi(U))) + \omega(t) - \dot{x}_R(t)\right). \quad (4.18)$$

Consider the following update rule for \hat{W} :

$$\dot{\hat{W}} = -\Gamma \psi(U) \text{diag}(e(t)) - \mu \Gamma \hat{W}, \quad (4.19)$$

where Γ is a diagonal $N \times N$ matrix with positive diagonal elements and $\mu \in \mathbb{R}$ is the NN tuning gain. The complete proposed adaptive control algorithm for the non-affine system (4.8) is described in Algorithm 1.

4.4.2. STABILITY ANALYSIS AND THE ALGORITHM DESIGN

In this section, the stability analysis of the algorithm is carried out. By employing uniform ultimate boundedness, it is shown that the error $e(t)$ converges to a residual set and states stay bounded for all $t \geq 0$.

Definition 1 (Uniform Ultimate Boundedness) *The solution to system (4.8) is Uniformly Ultimately Bounded (UUB) with the ultimate bound $b \in \mathbb{R}$, if there exists a positive constant $c \in \mathbb{R}$, independent of $t_0 \geq 0$, and if for all $a \in (0, c)$, there is $\tau = \tau(a, b)$ such that:*

$$\|x(t_0)\| \leq a \Rightarrow \|x(t)\| \leq b, \forall t \geq t_0 + \tau.$$

If the above statement holds for arbitrarily large a then the solution is Globally Uniformly Ultimately Bounded.

The above definition can be extended also to the trajectory tracking error $e(t)$. Indeed, our intention is to show that the error is uniformly ultimately bounded and that the state $x(t)$ is contained for all $t \geq 0$. Therefore, considering the boundedness of ϵ , i.e., there exists a positive real value ϵ_M such that $\epsilon(t) < \epsilon_M$ for all $t \geq 0$ [110], there exists a vector of activation functions $\psi(\cdot)$ and a set of weights, both with dimension $N \times 1$, such that as $N \rightarrow \infty$, ϵ converges to zero [108–110].

Before presenting the main result of this chapter, the following assumptions must be considered, in order to prove the correctness of Theorem 1.

Assumption 3 *The desired trajectory $x_R(t)$ and its derivative $\dot{x}_R(t)$ are bounded, i.e., there exists $x_M \in \mathbb{R}$ such that $\max\{|x_R(t)|, |\dot{x}_R(t)|\} \leq x_M$, for all $t \geq 0$.*

Assumption 4 *The elements in the vector of ideal weights W are bounded, i.e., there exists $W_M \in \mathbb{R}$ such that $\|W\| \leq W_M$.*

Assumption 5 *The NN activation functions are bounded. As a result, there is a positive real value ψ_M such that $\|\psi(\cdot)\| \leq \psi_M$.*

It is worthy to mention that for designing the controller, having the knowledge over the bounds discussed in Assumptions 1-4 is not required.

Next, we analyze the stability of the proposed method and demonstrate the feasibility of the choices for control law (4.13) and the update rule for the NN weights (4.19).

Theorem 1 *Suppose the control and the NN weight update laws are:*

$$\begin{aligned} U &= ke(t) - f(x(t)) \\ \dot{W} &= \Gamma \psi(U) \text{diag}(e(t)) + \mu \Gamma \hat{W}. \end{aligned}$$

If

$$k > \frac{\frac{1}{4}(M+1)^2 \psi_M^2}{\mu}, \quad (4.20)$$

where M is the Lipschitz constant of $g(\cdot)$, then the trajectory tracking error $e(t)$ and NN weights estimation error \tilde{W} are UUB and there exists a set of NN activation functions and a vector of weights with which the nonlinearities of $g^{-1}(\cdot)$ can be approximated.

Proof 1 *Consider the following Lyapunov function:*

$$V = \frac{1}{2} e^T e + \frac{1}{2} \text{Tr}(\tilde{W}^T \Gamma^{-1} \tilde{W}) \quad (4.21)$$

with $\text{Tr}(\cdot)$ as the trace operator. Then, the derivative of V is:

$$\dot{V} = \dot{e}^T e + \text{Tr}(\dot{\tilde{W}}^T \Gamma^{-1} \tilde{W}). \quad (4.22)$$

From (4.18),

$$\begin{aligned} \dot{V} = & -\left(f(x(t)) + g(\text{diag}^{-1}(\hat{W}^T \psi(U))) + \omega(t) - \dot{x}_R(t)\right)^T e \\ & + \text{Tr}(\dot{\tilde{W}}^T \Gamma^{-1} \tilde{W}). \end{aligned} \quad (4.23)$$

Since, in this chapter, it is assumed that $f(x)$ is determined, using (4.11) and (4.13), the above equation can be rewritten as:

$$\begin{aligned}\dot{V} &= - \left(ke - g(u) + g(\text{diag}^{-1}(\hat{W}^T \psi(U))) + \omega(t) - \dot{x}_R(t) \right)^T e \\ &\quad + \text{Tr} \left(\dot{\hat{W}}^T \Gamma^{-1} \tilde{W} \right) \\ &= - ke^T e + \left(g(u) - g(\text{diag}^{-1}(\hat{W}^T \psi(U))) \right)^T e + \omega(t)^T e \\ &\quad - \dot{x}_R(t)^T e + \text{Tr} \left(\dot{\hat{W}}^T \Gamma^{-1} \tilde{W} \right).\end{aligned}$$

Using (4.19), we have:

$$\begin{aligned}\dot{V} &= - ke^T e + \left(g(u) - g(\text{diag}^{-1}(\hat{W}^T \psi(U))) \right)^T e + \omega(t)^T e \\ &\quad - \dot{x}_R(t)^T e + \text{Tr} \left((\psi(U) \text{diag}(e(t)) + \mu \hat{W})^T \tilde{W} \right)\end{aligned}$$

and by adopting (4.17),

$$\begin{aligned}\dot{V} &= - ke^T e + \left(g(u) - g(\text{diag}^{-1}(\hat{W}^T \psi(U))) \right) e + \omega(t)^T e \\ &\quad - \dot{x}_R(t)^T e + \text{Tr} \left((\psi(U) \text{diag}(e(t)) + \mu(W - \tilde{W}))^T \tilde{W} \right).\end{aligned}$$

Taking into account the smoothness of $g(\cdot)$ which indicates its Lipschitz continuity and Assumptions 2, 4 and 5, it can be concluded that

$$\begin{aligned}\dot{V} \leq & -k \|e\|^2 + M \|e\| \|u - \hat{W}^T \psi(U)\|_F + \omega_M \|e\| + x_M \|e\| \\ & + \psi_M \|e\| \|\tilde{W}\|_F + \mu W_M \|\tilde{W}\|_F - \mu \|\tilde{W}\|_F^2,\end{aligned}\quad (4.24)$$

where M is the Lipschitz constant and $\|\cdot\|_F$ is the Frobenius norm operator. Considering (4.14), one can rewrite the above equation as:

$$\begin{aligned}\dot{V} \leq & -k \|e\|^2 + M \|e\| \|W^T \psi(U) + \epsilon - \hat{W}^T \psi(U)\|_F \\ & + \omega_M \|e\| + x_M \|e\| + \psi_M \|e\| \|\tilde{W}\|_F \\ & + \mu W_M \|\tilde{W}\|_F - \mu \|\tilde{W}\|_F^2\end{aligned}\quad (4.25)$$

$$\begin{aligned}\dot{V} \leq & -k \|e\|^2 + M \psi_M \|e\| \|\tilde{W}\|_F + M \epsilon_M \|e\| + \omega_M \|e\| \\ & + x_M \|e\| + \psi_M \|e\| \|\tilde{W}\|_F + \mu W_M \|\tilde{W}\|_F - \mu \|\tilde{W}\|_F^2.\end{aligned}\quad (4.26)$$

The above non-equality can be represented in matrix form, i.e.,

$$\begin{aligned}\dot{V} \leq & - \begin{bmatrix} \|e\| \\ \|\tilde{W}\|_F \end{bmatrix}^T \begin{bmatrix} k & -\frac{1}{2}(M+1)\psi_M \\ -\frac{1}{2}(M+1)\psi_M & \mu \end{bmatrix} \begin{bmatrix} \|e\| \\ \|\tilde{W}\|_F \end{bmatrix} \\ & + [M\psi_M + \omega_M + x_M \quad \mu W_M] \begin{bmatrix} \|e\| \\ \|\tilde{W}\|_F \end{bmatrix}\end{aligned}\quad (4.27)$$

which can be rewritten as:

$$\dot{V} \leq -z^T Q z + P z. \quad (4.28)$$

The necessary and sufficient conditions for correctness of $\dot{V} \leq 0$ are Q to be positive definite and

$$\|z\| > \frac{\|P\|}{\sigma_m(Q)} \quad (4.29)$$

where $\sigma_m(Q)$ is the minimum singular value of Q . For positive definiteness of Q ,

$$k > \frac{\frac{1}{4}(M+1)^2 \psi_M^2}{\mu}.$$

The minimum singular value Q can be calculated as:

$$\sigma_m(Q) = \frac{\sqrt{S_1 - S_2}}{2},$$

where

$$S_1 = k^2 + \frac{1}{2}(M+1)^2 \psi_M^2 + \mu^2$$

$$S_2 = \sqrt{(k^2 - \mu^2)^2 + (k + \mu)^2 (M+1)^2 \psi_M^2}.$$

For ease of calculation, take $\mu = k$. Then,

$$\sigma_m(Q) = k + \frac{1}{2}(M+1)\psi_M. \quad (4.30)$$

From (4.30) and (7.29),

$$\|z\| > \frac{M\psi_M + \omega_M + x_M + \mu W_M}{k + \frac{1}{2}(M+1)\psi_M}. \quad (4.31)$$

Therefore, if

$$\|\tilde{W}\|_F > \frac{M\psi_M + \omega_M + x_M + \mu W_M}{k + \frac{1}{2}(M+1)\psi_M} \quad (4.32)$$

or

$$\|e\| > \frac{M\psi_M + \omega_M + x_M + \mu W_M}{k + \frac{1}{2}(M+1)\psi_M}, \quad (4.33)$$

then (4.31) holds. (4.33) and (4.32) specify that e and/or \tilde{W} will always converge to a residual set if (4.20) holds. Moreover, the size of the residual set can be decreased by increasing k . The above result indicates that e and \tilde{W} are uniformly ultimately bounded. Therefore, it can be concluded that the state is bounded for all $t \geq 0$. Based on the results in [109, 110] there exists a set of activation functions and a vector of weights that can approximate the nonlinearities of $g^{-1}(\cdot)$.

Theorem 1 implies the correctness of the method and shows that trajectory tracking and weight estimation errors will converge to the set provided in (4.31) for all $t \geq 0$. Moreover, the size of the set can be reduced by increasing the controller gain.

There are several cases where the input function is partially known, i.e., it consists of a known part with an explicit inverse and an unknown part, such as vessels where the unknown part appears, mostly, during turns. As a result, the inverse of $g(\cdot)$ can be written as:

$$g^{-1}(U) = g'^{-1}(U) + \text{diag}^{-1}(\hat{W}^T \psi(U)), \quad (4.34)$$

where $g'^{-1}(\cdot)$ is the inverse of the known part of $g(\cdot)$ and U is calculated using (4.13). It can be shown that Theorem 1 is extendable to this case.

Corollary 1 *With the control law and the NN weights update rule defined in Theorem 1, the unknown part of $g^{-1}(\cdot)$ in (4.34) can be estimated and the trajectory tracking and the weight estimation errors are uniformly ultimately bounded.*

Proof 2 *Taking into account the Lipschitz continuity of $g(\cdot)$ and by combining (4.34) and (4.24), (4.25) can be concluded. The remainder of the proof is similar to the proof of Theorem 1.*

Remark 1 *Since the weight matrix \hat{W} is being updated online, the presented algorithm is capable of handling the possible changes that might happen in $g^{-1}(\cdot)$ during the ship operation. As a result, the algorithm can be used for both fixed pitch propellers and controllable pitch propellers.*

4.4.3. THE CASE OF STATE DEPENDENT UNCERTAINTY

In the previous sections, it is assumed that the knowledge over $f(x)$ is certain and there is no state dependent uncertainty in the system. However, in many applications, this is not the case, as the ship hydrodynamical model may face some degrees of uncertainty during sailing. Moreover, hydrodynamical modeling of ships for maneuvering purposes is a laborious process. In this section, it is shown that using the same strategy and by making a small change in the previously presented algorithm, state dependent uncertainties can be handled as well. This is also proved by presenting a theorem. For this purpose let us rewrite the governing equation of the system (4.8) as follows:

$$\dot{x}(t) = \hat{f}(x(t)) + g(u(t)) + \omega(t) + \omega_f(x(t)), \quad (4.35)$$

where \hat{f} is an estimate of f (which is known) and ω_f is the state dependent uncertainty (that is unknown). It can be concluded that:

$$f(x(t)) = \hat{f}(x(t)) + \omega_f(x(t)). \quad (4.36)$$

The above equation indicates that $\omega_f(x(t))$ is also Lipschitz continuous. Similar to g^{-1} , let us introduce an approximation method for f , i.e.,

$$f(x(t)) = \text{diag}^{-1}(W_f^T \psi(x(t))) + \epsilon_f \quad (4.37)$$

and

$$\hat{f}(x(t)) = \text{diag}^{-1}(\hat{W}_f^T \psi(x(t))), \quad (4.38)$$

where W_f is the approximation weight matrix, \hat{W}_f is its estimate and ϵ_f is the estimation error. Then, similar as in the previous section, it can be deduced that,

$$\omega_f(x(t)) = \text{diag}(\tilde{W}_f^T \psi(x(t))), \quad (4.39)$$

where \tilde{W}_f is the weight approximation error. As a result, the error dynamics are:

$$\dot{e}(t) = -\left(f(x(t)) + g(\text{diag}^{-1}(\hat{W}_f^T \psi(x(t)))) + \omega_f(x(t)) + \omega(t) - \dot{x}_R(t)\right). \quad (4.40)$$

Theorem 2 Suppose that the adaptive control law for system (4.35) is:

$$U = ke(t) - \hat{f}(x(t)). \quad (4.41)$$

Using the NN weights update rule (4.19) and the following update rule for \hat{W}_f :

$$\dot{\hat{W}}_f = -\Gamma_f \psi(x(t)) \text{diag}(e(t)) - \mu_f \Gamma_f \hat{W}_f, \quad (4.42)$$

if

$$k > \frac{\frac{1}{4}(M+1)^2 \psi_M^2}{\mu} + \frac{\psi_M^2}{\mu_f},$$

then the trajectory tracking error $e(t)$ is UUB.

Proof 3 Let us consider the following Lyapunov function:

$$V = \frac{1}{2} e^T e + \frac{1}{2} \text{Tr}(\tilde{W}^T \Gamma^{-1} \tilde{W}) + \frac{1}{2} \text{Tr}(\tilde{W}_f^T \Gamma_f^{-1} \tilde{W}_f) \quad (4.43)$$

After derivation we obtain:

$$\begin{aligned} \dot{V} = & -\left(\hat{f}(x(t)) + g(\text{diag}^{-1}(\hat{W}_f^T \psi(x(t)))) + \omega_f(x(t))\right. \\ & \left. + \omega(t) - \dot{x}_R(t)\right)^T e + \text{Tr}(\dot{\tilde{W}}^T \Gamma^{-1} \tilde{W}) \\ & + \text{Tr}(\dot{\tilde{W}}_f^T \Gamma_f^{-1} \tilde{W}_f). \end{aligned} \quad (4.44)$$

Using a similar approach as for the proof of Theorem 1 and by adopting (4.39) and (4.41), the following relationship can be obtained:

$$\begin{aligned} \dot{V} \leq & -k \|e\|^2 + M\psi_M \|e\| \|\tilde{W}\|_F + (M\epsilon_M + \omega_M) \|e\| \\ & + x_M \|e\| + 2\psi_M \|e\| \|\tilde{W}_f\|_F + \psi_M \|e\| \|\tilde{W}\|_F \\ & + \mu W_M \|\tilde{W}\|_F - \mu \|\tilde{W}\|_F^2 + \mu_f W_{fM} \|\tilde{W}_f\|_F - \mu_f \|\tilde{W}_f\|_F^2. \end{aligned} \quad (4.45)$$

By representing the above inequality in matrix form, we have:

$$\begin{aligned} \dot{V} \leq & - \begin{bmatrix} \|e\| \\ \|\tilde{W}\|_F \\ \|\tilde{W}_f\|_F \end{bmatrix}^T \begin{bmatrix} k & -\frac{1}{2}(M+1)\psi_M & -\psi_M \\ -\frac{1}{2}(M+1)\psi_M & \mu & 0 \\ -\psi_M & 0 & \mu_f \end{bmatrix} \\ & \begin{bmatrix} \|e\| \\ \|\tilde{W}\|_F \\ \|\tilde{W}_f\|_F \end{bmatrix} + \begin{bmatrix} M\epsilon_M + \omega_M + x_M \\ \mu W_M \\ \mu_f W_{fM} \end{bmatrix}^T \begin{bmatrix} \|e\| \\ \|\tilde{W}\|_F \\ \|\tilde{W}_f\|_F \end{bmatrix}, \end{aligned} \quad (4.46)$$

Algorithm 2 *Adaptive Control Algorithm for Non-Affine Systems with State Dependent Uncertainties:*

Initialization: Obtain $x(0)$ and $x_R(t)$. Assign initial values to the elements in the vector of weights.

1: Calculate $e(t)$ using (7.19).

2: Compute U using (4.41) at each time t .

3: Estimate u by adopting (4.15) and f by (4.38).

4: Apply u to the system.

5: Update the matrices of weights based on (4.19) and (4.42).

6: Obtain the state of the system and go to 1.

which can be rewritten in the following form:

$$\dot{V} \leq -z_f^T Q_f z_f + P_f z_f. \quad (4.47)$$

If matrix Q_f is positive definite then $\dot{V} \leq 0$ holds. As a result,

$$k > \frac{\frac{1}{4}(M+1)^2 \psi_M^2}{\mu} + \frac{\psi_M^2}{\mu_f}.$$

The remainder of the proof can be carried out with the same approach as used in the proof of Theorem 1.

It can be concluded from the above theorem that the overall system can be uncertain and that with a small change in Algorithm 1, using the same strategy, the state dependent uncertainties can also be handled. The proposed methodology for this case is represented in Algorithm 2. In the next section, the presented algorithm is applied to an ASV with unknown actuator dynamics and state dependent uncertainties.

4.4.4. APPLICATION TO AUTONOMOUS SHIPS

In this part, the proposed adaptive control strategy is presented for control of ASVs with uncertainty in the maneuvering model and unknown propellers dynamics.

Suppose the desired trajectory, the initial position of the vessel, and its initial speed in 3DoF are denoted by $\eta_d(t)$, $\eta_s(0)$ and $V(0)$, respectively. If Δt is the duration from one time step to the next, then the preferred speed of the vessel in its body-fixed coordinates can be calculated as:

$$V_d(t) = \frac{1}{\Delta t} R^{-1}(\eta_s)(\eta_d(t) - \eta_s(t)). \quad (4.48)$$

Using this, the speed error vector is found as:

$$e_s(t) = v_d(t) - v_s(t). \quad (4.49)$$

By adopting (4.13) and (4.4), the control law is established as:

$$\tau_s = k e_s(t) + M_s^{-1}(C_s(v_s) v_s + D_s(v_s) v_s). \quad (4.50)$$

Algorithm 3 Adaptive Control Algorithm for ASVs:**Initialization:** Obtain $\eta_s(0)$, $V(0)$ and $\eta_d(t)$. Initialize NN weight matrix.**1:** Compute $V_d(t)$ using (4.48).**2:** Calculate $e(t)$ by adopting (4.49).**3:** By use of (4.50) and (4.51), compute the ship control law.**4:** By exploiting (4.52), estimate the required actuators shaft speeds and apply them to the system.**5:** Update the NN weights matrix.**6:** Obtain the system states and go to 1.

4

If the system model contains state dependent uncertainty then:

$$\tau_s = ke_s(t) - \hat{f}(x(t)). \quad (4.51)$$

The thrust allocation problem is solved using (3.15) with which the vector of desired forces generated by actuators is found, denoted by τ_d . Based on the length of the NN, the matrix of squashing functions $\psi(\tau_d)$ is computed. Note that the NN weight matrix \hat{W} and $\psi(\tau_d)$ have similar sizes, i.e., $N \times m$, where m is the number of actuators. The estimated actuators shaft speeds are found as follows:

$$n = \begin{bmatrix} n_1 \\ \vdots \\ n_m \end{bmatrix} = \text{diag}^{-1}(\hat{W}^T \psi(\tau_d)). \quad (4.52)$$

After this step, the NN weight matrices are updated. The NN weight matrix update rules are regulated as below:

$$\begin{aligned} \dot{W} &= -\Gamma \psi(U) \text{diag}(T^T (TT^{-1})^{-1} e_s(t)) - \mu \Gamma \hat{W} \\ \dot{W}_f &= -\Gamma_f \psi(x(t)) \text{diag}(e_s(t)) - \mu_f \Gamma_f \end{aligned} \quad (4.53)$$

The overall algorithm for the adaptive control of ASVs is presented in Algorithm 3.

4.5. SIMULATION EXPERIMENTS AND EVALUATION RESULTS

The chosen ASV for evaluating the performance of the algorithm is Cybership II from [33], which is a 1:70 scale replica of an Offshore Support Vessel. It is assumed that the ASV has four actuators: two propellers, one stern thruster and a bow thruster as illustrated in Figure 3.1. As a result,

$$\tau_s = \Xi_{3 \times 4} \begin{bmatrix} K_{T_1} \rho D_1^4 | n_{p_1} | n_{p_1} \\ K_{T_2} \rho D_2^4 | n_{p_2} | n_{p_2} \\ K_{T_3} \rho D_3^4 | n_{p_3} | n_{p_3} \\ K_{T_4} \rho D_4^4 | n_{p_4} | n_{p_4} \end{bmatrix} \quad (4.54)$$

and

$$T = \begin{bmatrix} 1 & 1 & 0 & 0 \\ 0 & 0 & 1 & 1 \\ -0.1 & 0.1 & 0.2 & 0.5 \end{bmatrix}. \quad (4.55)$$

Note that the vector of actuator dynamics in (4.54) is unknown to the controller. Moreover, it is supposed that the knowledge over inertial mass, Coriolis and centrifugal and damping matrices are uncertain. The parameters of the model vessel are summarized in Table 1.

To assess the performance of the algorithm, three simulation scenarios are considered:

1. Trajectory tracking of a circular path.
2. Dynamic positioning in the presence of environmental disturbances.
3. Trajectory tracking simulation in the port of Rotterdam.

For these experiments the length of the NN is opted to be $N = 300$ and the chosen activation function with which the matrix of activation functions $\psi(\cdot)$ is constructed, is as the following:

$$y = 0.05 \left(\frac{1 - e^{-x}}{1 + e^{-x}} \right). \quad (4.56)$$

For all experiments, based on (4.20), $k = 500$ is considered for the control law and $\mu = 0.1$ and Γ is chosen to be an identity matrix. Simulations are carried out using Matlab 2017b in a computer which has a core i7 2.6 GHz CPU and 8 GB of RAM.

EXPERIMENT I: CIRCULAR TRAJECTORY TRACKING

For the first experiment, the considered trajectory is assumed to be circular with the following specifications:

$$\eta_d(t) = \begin{bmatrix} \eta_{d_x}(t) \\ \eta_{d_y}(t) \\ \text{atan2}(\dot{\eta}_{d_x}, \dot{\eta}_{d_y}) \end{bmatrix} \quad (4.57)$$

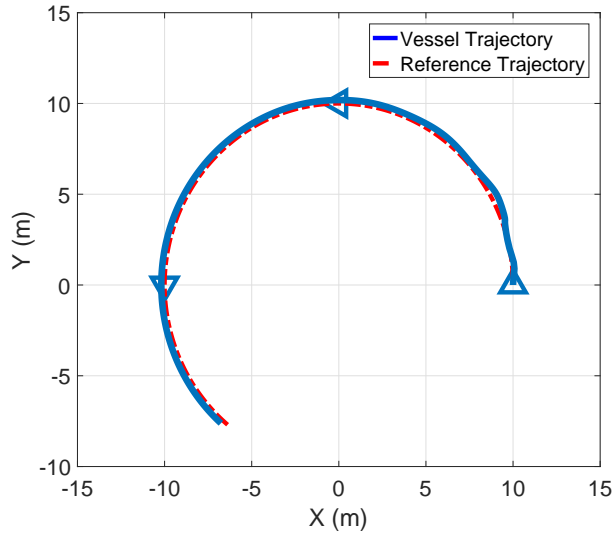
$$\eta_{d_x}(t) = \alpha \cos\left(\frac{\beta t}{\alpha}\right), \quad \eta_{d_y}(t) = \alpha \sin\left(\frac{\beta t}{\alpha}\right) \quad (4.58)$$

where α and β are the radius of the circular trajectory and traveling speed, respectively. It is assumed that $V(0) = [0, 0, 0]^T$, $\eta_s(0) = [10, 0, 1.57]^T$, $\alpha = 10$ and $\beta = 0.2$ m/s. Note that in this experiment the reference speed is constant.

The results for the circular trajectory tracking case are shown in Figure 4.3. It can be inferred from the figures that after the transient and training time of the NN that take few seconds, the ship can smoothly follow the reference trajectory and actuators generated thrust as well as ship speed converge to steady state values.

In this experiment, the proposed algorithm is compared with MIMO nonlinear PID control scheme [34] where the control law is:

$$\tau = -K_m \dot{V} + R^{-1}(\eta_s(t)) \tau_{\text{PID}} \quad (4.59)$$



(a) The ship trajectory vs the reference trajectory.

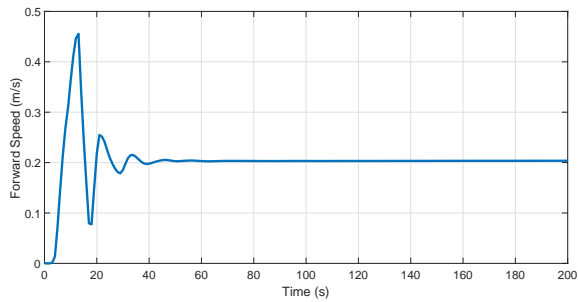
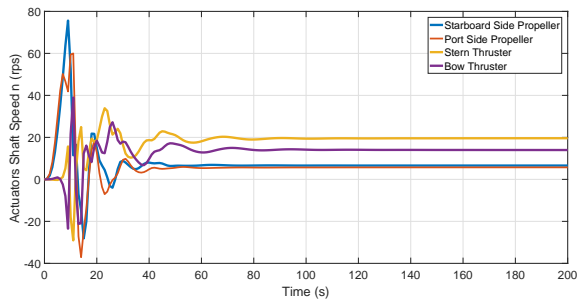
(b) Forward speed of the ship ($u(t)$).(c) Shaft speed of actuators ($(n(t))$).

Figure 4.3: Results of Experiment 1.

Table 4.1: The model ASV parameters.

Parameter	Value	Parameter	Value
m	23.8	$Y_{ r v}$	-0.805
x_g	0.046	$N_{ r v}$	0.13
I_z	1.76	Y_r	-7.25
$X_{\dot{u}}$	-2	N_r	-1.9
$Y_{\dot{v}}$	-10	$Y_{ v r}$	-0.845
$Y_{\dot{r}}$	0	$N_{ v r}$	0.08
$N_{\dot{v}}$	0	$Y_{ r r}$	-3.45
X_u	-0.722	$N_{ r r}$	-0.75
Y_v	-0.889	K_{T_1}	0.08
$X_{ u u}$	-1.327	K_{T_2}	0.08
$Y_{ v v}$	-36.472	K_{T_3}	0.07
X_{uuu}	-5.866	K_{T_4}	0.07
N_v	0.03130	D_{p_1}	0.08
$N_{ v v}$	3.956	D_{p_2}	0.08
ρ	1024	D_{p_3}	0.05
		D_{p_4}	0.05

and

$$\tau_{\text{PID}} = -K_p(\eta_d - \eta) - K_d\dot{\eta} - K_i \int_0^t (\eta_d - \eta) d\tau. \quad (4.60)$$

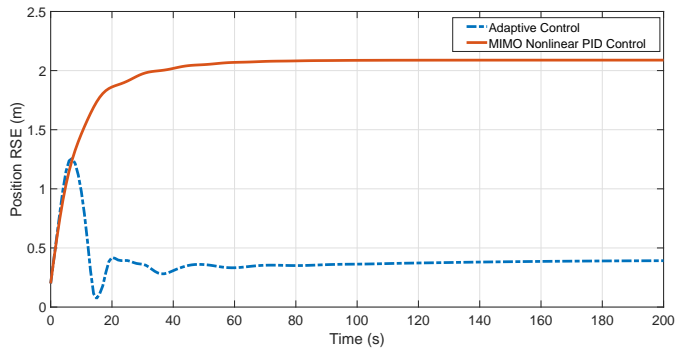
Parameter K_m is the acceleration feedback gain. As suggested in [34], $K_i = 0$. Other parameters are chosen as $K_p = 0.8$, $K_d = 1$ and $K_m = 4$. As explained in Section 2, it is assumed that the precise knowledge over actuators model is not available during the operation. As a result, thrust coefficients are presumed to be $K_{T_1} = K_{T_2} = 0.12$ and $K_{T_3} = K_{T_4} = 0.1$. On the other hand, for the adaptive control simulations, it is assumed no knowledge about the model exist. The experiment results are shown in Figure 4.4. Simulation results are represented in terms of Root-Square Error (RSE). It can be inferred that by using the proposed methodology the ship can stay closed to the reference trajectory.

As mentioned in the previous section, as k increases the size of the residual sets (4.31) and (4.32) decreases which leads to the decrease in error. Figure 4.5 shows the value of RSE for different k values. It is seen that as k increases, the bounds of error decreases.

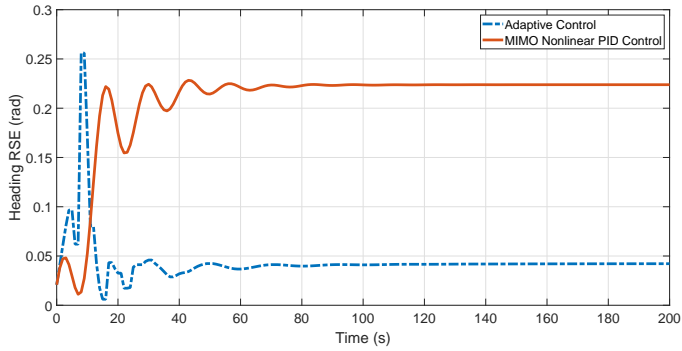
EXPERIMENT II: DYNAMIC POSITIONING

The second experiment is a dynamic positioning scenario where the ship has to maintain its position at $\eta_d(t) = [0, 0, 1.57]^T$. Furthermore, it is assumed that there exists a current in the environment with the inertial velocities $V_c(t) = [0.1, 0.1, 0]^T$.

Figure 4.6 shows the experiment results. Similar to the previous case, the position of the ship is stabilized and actuators shaft speeds converge after the transient time and the training time of NN. This indicates that the NN-based adaptive controller succeeded in handling the uncertainties within propellers dynamics and the ship model.

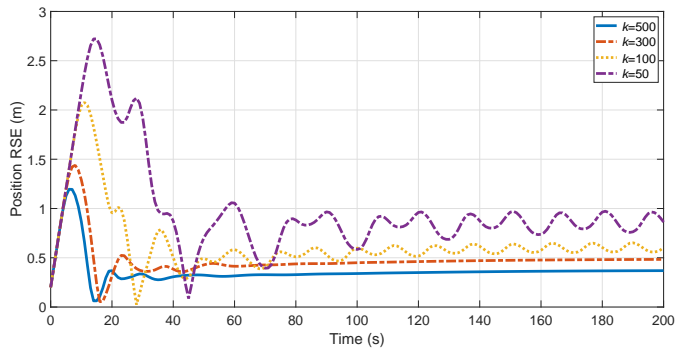


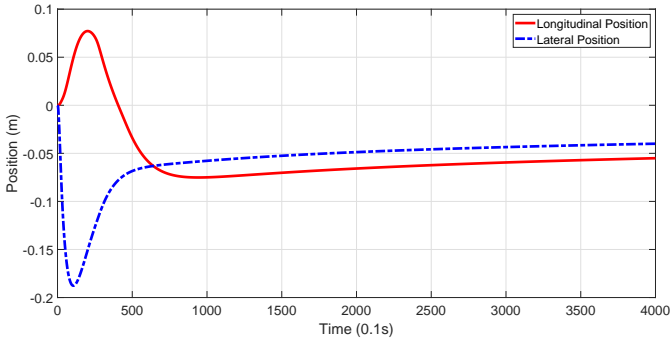
(a) Position RSE during the maneuver.



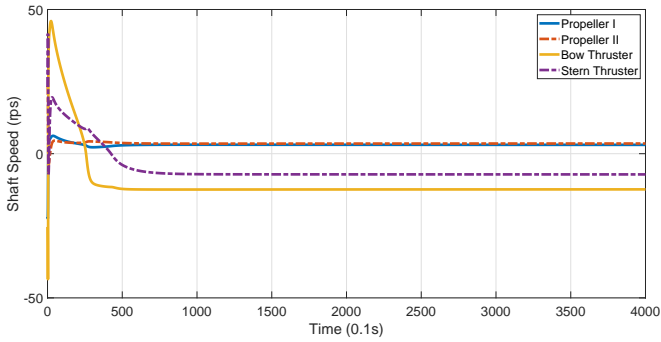
(b) Heading RSE during the maneuver.

Figure 4.4: Performance comparison of the proposed algorithm vs a conventional control scheme.

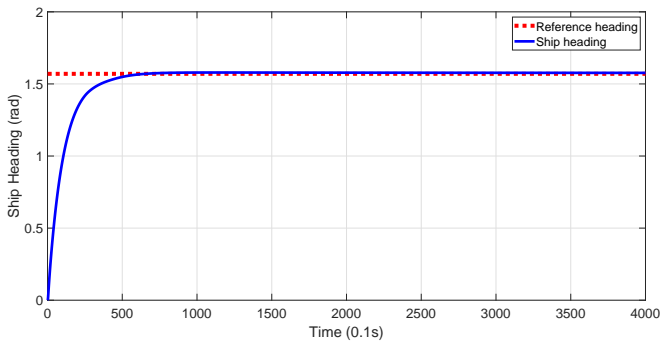
Figure 4.5: The effect of k on error bounds.



(a) Ship position keeping performance.



(b) Actuators shaft speeds ($n(t)$).



(c) The ship heading ($\eta_\theta(t)$).

Figure 4.6: Dynamic positioning performance of the ship.

EXPERIMENT III: TRAJECTORY TRACKING IN THE PORT OF ROTTERDAM

In the third experiment, the real trajectory of a vessel is considered in Oude Maas river in port of Rotterdam using AIS data received from the Port of Rotterdam authority. The considered path is the trajectory of an inland tanker vessel during two hours of voyage. Using Froude scaling the trajectory is scaled down to be aligned with the dimensions of the model ship with $C_{\text{Froude}} = 70$. During this voyage, the ship should sail with different course speeds. In simulations, it is also assumed that there is a stream in the river which applies force to the replica model ship hull. This force is considered to be $\tau_c = [0.1, -0.1, 0]^T$ in global reference frame. The trajectory of the ship is depicted in Figure 4.7.

The experiment results are shown in Figure 4.9. The trajectory tracking performance of the vessel is depicted in Figure 4.9a and the course speed of the vessel is compared with the scaled reference speed of the ship in Figure 4.9b. The applied thrust by the actuators are represented in Figure 4.9c. It is seen that after the transient and NN training time the ship can follow the planned trajectory.

One of the main concerns regarding novel methods for trajectory tracking control of ships is the applicability of these algorithms to real ships and the interaction of the on-board power and propulsion system with the trajectory tracking algorithm. In this regard, the power and propulsion system should be able to generate requested thrust by the controller with a rough approximation. To examine this issue, a model of a power and propulsion system has been adopted. The applied thrust in Figure 4.9c is scaled up using Froude scaling to be fitting for a real size vessel and then, it is used as the reference thrust for the power and propulsion system. The propellers and thrusters of the on-board propulsion system should be able to follow the reference thrust roughly.

The architecture of the considered power and propulsion system is presented in Figure 4.8. The prime movers are connected to a DC-link through converters. The electric motors that rotate the actuators are fed and controlled by motor inverter-controllers. The reader is referred to [22] for more information regarding configuration and modeling of the power system. In this model, the propulsion drive-train specifications are as follows:

Port side and starboard side propellers: $K_T = 0.8$, $K_Q = 0.08$, $D = 2\text{m}$, 1.8 MW, 60 Hz, 460 V.

Bow and stern thrusters: $K_T = 0.8$, $K_Q = 0.08$, $D = 1\text{m}$, 500 kW, 60 Hz, 460 V.

The Matlab Simscape 2017b toolbox is partially used for the modeling. Due to highly demanding data logging of this toolbox, the simulation can not be done for the whole voyage time which is approximately 6400 seconds. As a result, the focus is on period which fastest transients with highest peaks happen and in this case, this period is at the beginning of the simulation.

The simulation results are shown in Figure 4.10. Figures 4.10a to 4.10d show the generated thrust by the actuators vs the requested thrust by the controllers. The angular speed of electric motors is shown in Figure 4.11. The results suggest that the transients are traceable by the propulsion system and it can generate the requested thrust. Therefore, the algorithm is potentially applicable to real-size vessels.

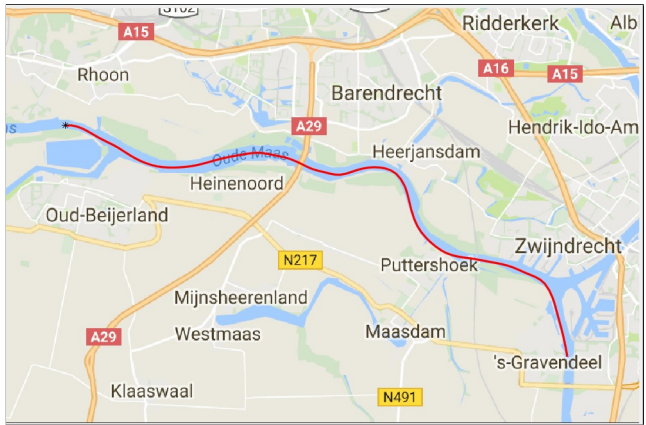


Figure 4.7: The considered trajectory in the Port of Rotterdam waterways.

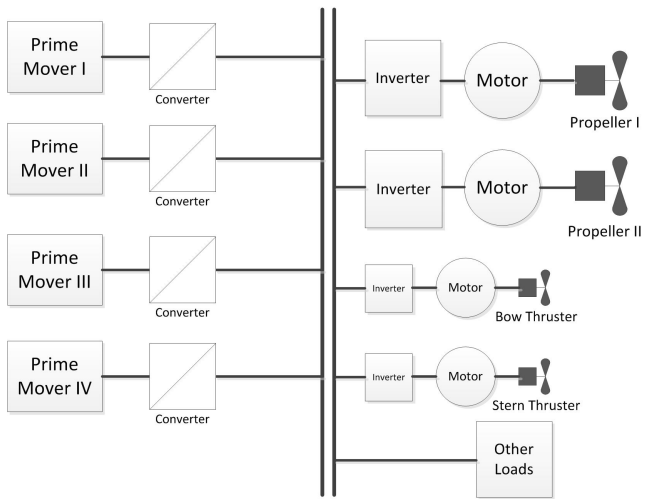
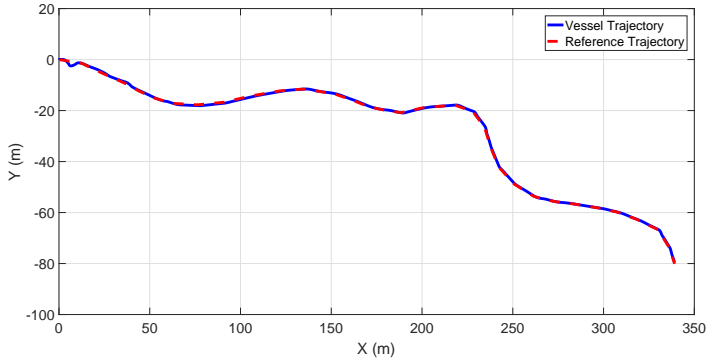


Figure 4.8: Architecture of the considered power system [22].



(a) Trajectory tracking result.

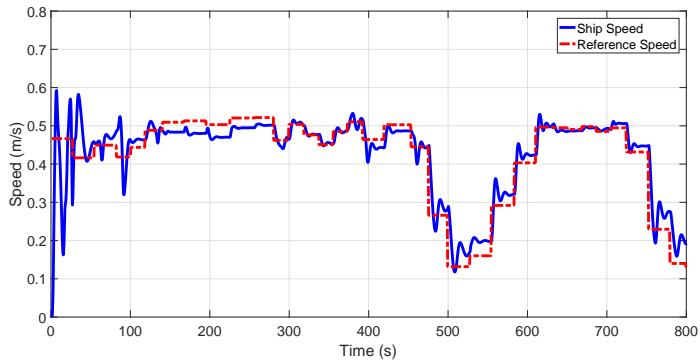
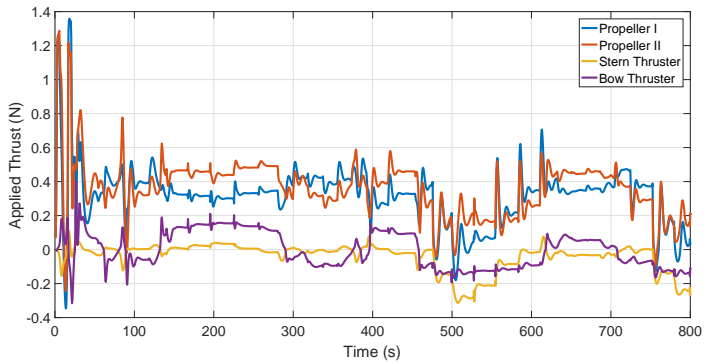
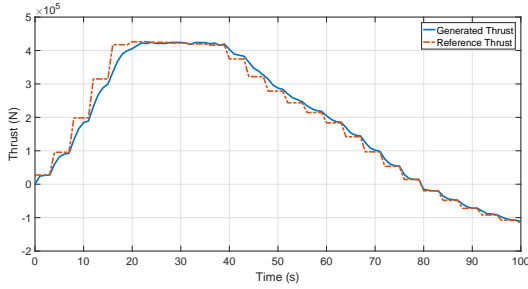
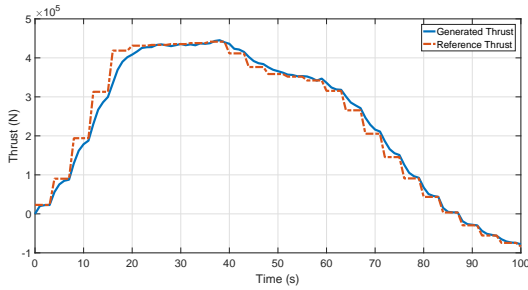
(b) Forward speed of the vessel ($u(t)$).(c) Applied thrust by actuators ($\tau_{act}(t)$).

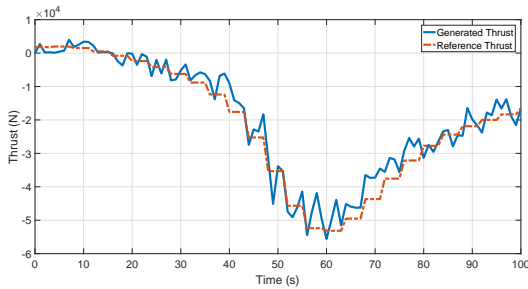
Figure 4.9: Simulation results of Experiment 1.



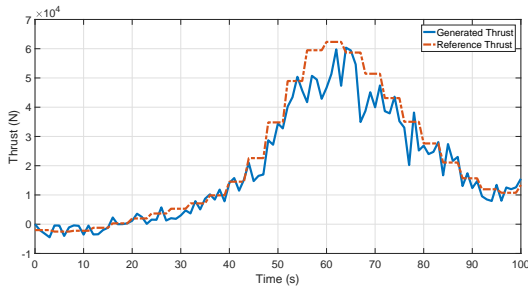
(a) Port side propeller: generated thrust vs requested thrust.



(b) Starboard side propeller: generated thrust vs requested thrust.



(c) Stern thruster: generated thrust vs requested thrust.



(d) Bow thruster: generated thrust vs requested thrust.

Figure 4.10: Performance of the power and propulsion system.

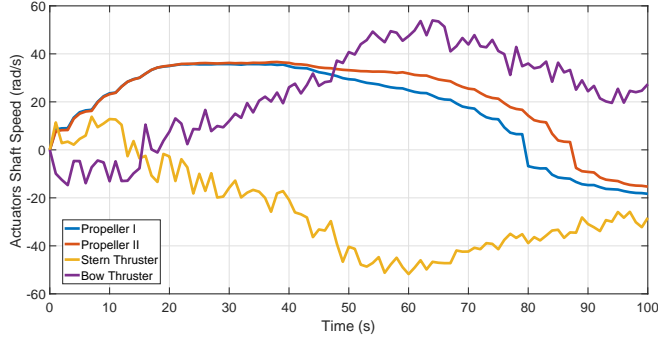


Figure 4.11: Angular speed of propellers and thrusters.

4.6. CONCLUSIONS

In this chapter, a novel Neural Networks-based (NN-based) adaptive control algorithm has been proposed for motion and position keeping control of ASVs with unknown actuators dynamics and state dependent uncertainties. For the correctness proof of the algorithm, uniform ultimate boundedness, a Lyapunov technique and Weierstrass approximation theorem have been adopted. For the numerical analysis, three cases have been considered; trajectory following and dynamic positioning. It has been illustrated that the control approach is successful in terms of keeping the overall system stable and following the desired trajectory.

The results in this chapter address the concerns raised in Research Questions 1 and 3 by proposing a control approach for maneuvering control which is capable of handling uncertainties and environmental disturbances. In the next chapter, a maneuvering control approach is proposed that is capable of the predicting the required propulsive power over a finite horizon.

5

PREDICTIVE MANEUVERING CONTROL

In the previous chapter, a control approach is proposed for maneuvering in the presence of uncertainties. In this chapter, a Model Predictive Control (MPC) approach is proposed for the purpose of trajectory tracking control and the prediction future required propelling power. The MPC approach is designed based on Input-Output Feedback Linearization (IOFL) that is established by using the results in [119, 120]. By adopting this technique, quadratic programming methods can be applied for solving the optimization problem which leads to a significant decrease in computational costs. Then, using the propeller dynamics and the efficiency curve of induction motors [14], the predicted required power is estimated over a finite horizon. In Section 5.1, the approach is introduced and in Section 5.2, its performance is evaluated through simulation-based experiments. The content of this chapter have been partially published in a scientific paper.¹

5.1. MODEL PREDICTIVE MANEUVERING CONTROL

MPC approaches enable constraint handling and predicting future values of states and control inputs. These features are advantageous for ship maneuvering control purposes and interaction with the PPS as they can lead to safer and more fuel-efficient ship operations. In this section, an MPC algorithm is proposed for maneuvering control of autonomous ships in 3DoF. The proposed algorithm is based on IOFL where by introduction of an auxiliary control input, a linear relationship is established between the system outputs and auxiliary inputs. Moreover, by adoption of the methodology introduced in [119, 120], the constraints are linearized which leads to the possibility of using quadratic

¹Parts of this chapter have been published in:

1. A. Haseltalab, R. R. Negenborn, Model predictive maneuvering control and energy management for all-electric autonomous ships, *Applied Energy*, Volume 251, pp. 1-27, 2019.

programming methods for solving the optimization problem of the MPC algorithm. As a result, the computational costs of the algorithm reduce significantly compared to the algorithms presented in [5, 30]. We use the speed dynamics in (3.43) of Chapter 3 for the trajectory tracking control. The position dynamics in (3.43) are used for determining the desired speed of the ship.

Let us rewrite the speed dynamics of the ship as:

$$\dot{v}_s(t) = M_s^{-1} \left(\tau_s + \tau_{\text{drag}}(v_s(t), \eta_s(t)) - C_s(v_s(t)) v_s(t) \right). \quad (5.1)$$

With the following IOFL law the above system can be linearized:

$$\tau_s = M_s \left(-\tau_{\text{drag}}(v_s(t), \eta_s(t)) + C_s(v_s(t)) v_s(t) + A_s v_s + B_s v_s \right) \quad (5.2)$$

where v_s is the input vector of linearized system, ζ_s represents its states and A_s and B_s are states and input matrices of the linear system, respectively. As a result, the transformed linear system can be written as:

$$\dot{v}_s = A_s v_s + B_s v_s. \quad (5.3)$$

After discretization, MPC is applied where the objective is to keep the ship as close as possible to the reference trajectory. In this regard, the following MPC problem is defined with sample time T_k :

$$\mathbb{P}(v_s) : \min_{v_s} \left(V_N(v_s, v_s) = \sum_{i=0}^{N-1} l(v_s(k+i), v_s(k+i)) \right) \quad (5.4)$$

subject to:

$$\begin{aligned} v_s(k+i+1) &= A_s(T_k) v_s(k+i) + B_s(T_k) v_s(k+i) \\ v_{\min}(k+i) &\leq v_s(k+i) \leq v_{\max}(k+i) \\ v_{\min}(k+i-1) &\leq v_s(k+i-1) \leq v_{\max}(k+i-1), \forall i \in [0, N] \end{aligned} \quad (5.5)$$

where

$$l(v_s(k), v_s(k)) = (v_s(k) - v_{s_{\text{ref}}}(k))^T W_s (v_s(k) - v_{s_{\text{ref}}}(k)) + v_s^T(k) v_s(k). \quad (5.6)$$

In the above MPC problem, parameter N is the prediction horizon and W_s is the weight matrix of the cost function and is a positive definite matrix.

The reference ship speed $v_{s_{\text{ref}}}(k)$ is approximated using (3.43) as:

$$v_{s_{\text{ref}}}(k+1) = R^{-1}(\eta_s(k)) \left(\frac{\eta_{\text{ref}}(k+1) - \eta_s(k)}{T_k} \right). \quad (5.7)$$

The adoption of IOFL for MPC results in clear advantages since the optimization problem is simplified, however, due to non-linearity of input constraints, quadratic programming cannot be adopted for solving the optimization problem. In the following, using the results in [120], we adopt a methodology for linearizing the input constraints in (7.16) to further simplify the optimization problem which leads to major reduction of computational costs.

The main idea behind this methodology is linear estimation of non-linear constraints. Let us present the constraints acting on the thrust vector τ_s :

$$\tau_{\min} \leq \tau_s(k) \leq \tau_{\max}. \quad (5.8)$$

If the IOFL rule is rewritten as:

$$\begin{aligned} v_s(t) = \Psi_s(v_s(t), \tau_s(t)) = \\ B_s^{-1} \left(M_s^{-1} \tau_s(t) + \tau_{\text{drag}}(v_s(t), \eta_s(t)) - C_s(v_s(t)) v_s(t) - A_s v_s(t) \right), \end{aligned} \quad (5.9)$$

then, v_s can be approximated around $(v_s(t_0), \tau_s(t_0))$ as:

$$\begin{aligned} v_s(t) \approx \hat{\Psi}_{s_0}(v_s(t), \tau_s(t)) = \Psi_s(v_s(t_0), \tau_s(t_0)) \\ + \frac{\partial \Psi_s}{\partial v_s} \Big|_{(v_s(t_0), \tau_s(t_0))} (v_s(t) - v_s(t_0)) \\ + \frac{\partial \Psi_s}{\partial \tau_s} \Big|_{(v_s(t_0), \tau_s(t_0))} (\tau_s(t) - \tau_s(t_0)). \end{aligned} \quad (5.10)$$

Let $v_s(k+i|k)$ denotes the value of v_s at time $(k+i)t_k$ predicted at time kt_k , then using (5.10), the linear constraints can be found as:

$$\begin{aligned} v_{\min}(k+i-1) &= \min_{\tau_s(k+i-1)} \hat{\Psi}_{s_{k+i|k-1}}(v_s(k+i|k-1), \tau_s(k+i-1)) \\ v_{\max}(k+i-1) &= \max_{v_s(k+i-1)} \hat{\Psi}_{s_{k+i|k-1}}(v_s(k+i|k-1), \tau_s(k+i-1)) \end{aligned} \quad (5.11)$$

subject to,

$$\tau_{\min} \leq \tau_s(k+i-1) \leq \tau_{\max}, \forall i \in [0, N-1]. \quad (5.12)$$

Note that for time instant $(k+N-1)t_k$, we have:

$$\begin{aligned} v_{\min}(k+N-1) &= v_{\min}(k+N-2) \\ v_{\max}(k+N-1) &= v_{\max}(k+N-2). \end{aligned} \quad (5.13)$$

Note also that, due to the linearity of $\hat{\Psi}_{s_{k+i|k-1}}(\cdot)$, the optimization problems in (7.34) are trivial to solve.

The adoption of this methodology leads to simplification of the optimization problem within MPC and to the possibility of using a quadratic programming scheme. The block diagram of the proposed control approach is depicted in Figure 5.1.

At every sample time k , the proposed control algorithm generates a set of control inputs $v_s(k|k), \dots, v_s(k+N-1|k)$ and $v_s(k|k), \dots, v_s(k+N-1|k)$. Using these sets and (5.2), the set of future control inputs $\tau_s(k|k), \dots, \tau_s(k+N-1|k)$ can be estimated. By adoption of (3.16) and (3.17), the set of future power demand for propelling the ship over horizon N can be approximated that is $P_s(k|k), \dots, P_s(k+N-1|k)$. In the next section, we propose an energy management strategy that will utilize this set.

The maneuvering control algorithm steps can be described as below:

- **Initialization:** Let $\eta_s(0) = \eta_0$, $v_s(0) = v_0$.

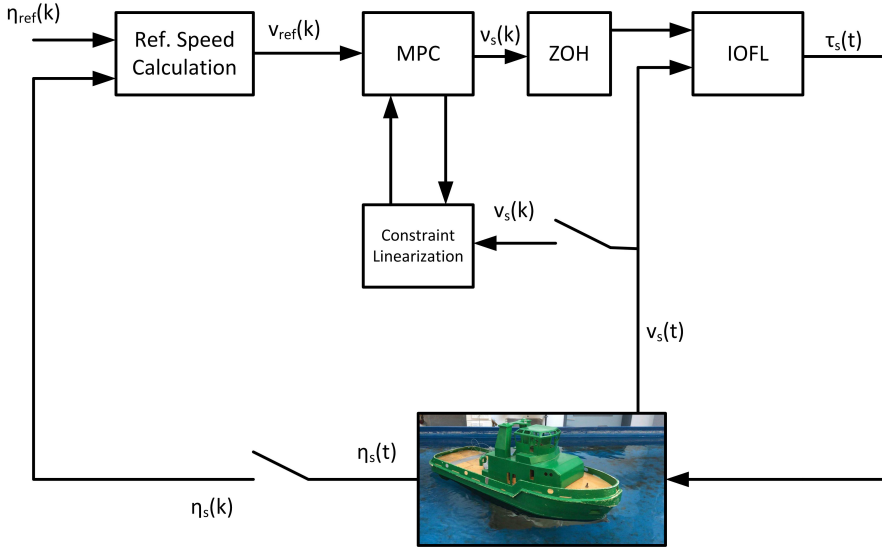


Figure 5.1: The block diagram of the proposed maneuvering control strategy.

1. Compute $v_{\text{ref}}(k+i) = \frac{\eta_{\text{ref}}(k+i) - \eta_0}{iT_s}$, for all $i = 0, \dots, N-1$ where T_s is the sample time of predictive maneuvering controller.
2. Solve the optimization problem in (5.4) using the constraint linearization approach in (7.34).
3. Gather the predicted required thrust over the horizon $\tau_s(k), \dots, \tau_s(k+N-1)$, solve the thrust allocation problem in (3.15) to determine the desired speed of propellers.
4. Using the model of propellers in (3.16) and (3.17) and the efficiency curve of inductions motors estimate the future power demand P_d over the horizon N .
5. Send P_d to the energy management controller and desired speed of actuators to induction motor controllers. Go to 1.

5.2. SCALE-MODEL EXPERIMENTS

For the trajectory tracking control experiments, a model vessel known as *Tito-Neri* (Figure 5.2) is chosen which represents a 1:30 replica model of a harbor tug [121].



Figure 5.2: Tito-Neri: a harbor tug 1:30 replica model [121].

5.2.1. EXPERIMENT I: CIRCULAR TRAJECTORY

In this experiment, a circular trajectory is considered in which the vessel increases its speed. The specifications of the considered trajectory is:

$$\eta_{\text{ref}}(t) = \begin{bmatrix} \eta_{\text{ref}_x}(t) \\ \eta_{\text{ref}_y}(t) \\ \text{atan2}(\dot{\eta}_{\text{ref}_x}, \dot{\eta}_{\text{ref}_y}) \end{bmatrix} \quad (5.14)$$

$$\eta_{\text{ref}_x}(t) = \gamma \cos\left(\frac{\beta t}{\gamma}\right), \quad \eta_{\text{ref}_y}(t) = \gamma \sin\left(\frac{\beta t}{\gamma}\right) \quad (5.15)$$

where γ and β are the radius of the circular trajectory and traveling speed, respectively. It is assumed that $V(0) = [0, 0, 0]^T$, $\eta_s(0) = [0, 0, 0]^T$, $\gamma = 10$ and $\beta = 0.2 \text{ m/s}$. Note that in this experiment the reference speed is constant. It is assumed that there is a current in the environment with $[-0.04, 0.05, 0]^T$ speed vector.

In this experiment, the proposed algorithm is compared with a MIMO nonlinear PID control scheme [34] where the control law is:

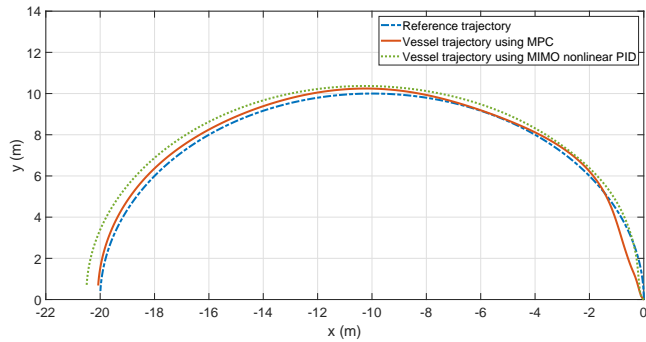
$$\tau = -K_m \dot{V} + R^{-1}(\eta_s(t)) \tau_{\text{PID}} \quad (5.16)$$

and

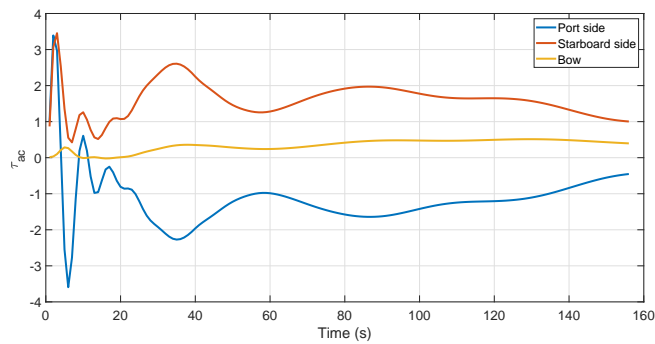
$$\tau_{\text{PID}} = -K_p(\eta_d - \eta) - K_d \dot{\eta} - K_i \int_0^t (\eta_d - \eta) d\tau. \quad (5.17)$$

Parameter K_m is the acceleration feedback. Other parameters are chosen as $K_p = 0.8$, $K_d = 1$ and $K_i = 4$.

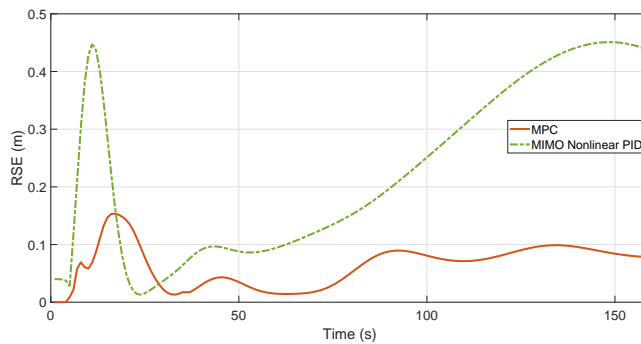
The experiment results are given in Figure 5.3. Simulation results of trajectory tracking are compared in terms of Root-Square Error (RSE). From Figure 5.3c, it can be inferred that by using the proposed methodology the ship can stay closer to the reference trajectory.



(a) Vessel trajectory compared to the reference trajectory.



(b) Generated thrust by the actuators (using MPC).



(c) Trajectory tracking error.

Figure 5.3: Trajectory tracking performance of the ship.

5.2.2. EXPERIMENT II: TRAJECTORY TRACKING IN OUDE MAAS

In this experiment, the trajectory of a tanker vessel in Oude Maas river is extracted using AIS (Figure 4.7). The trajectory is scaled down using Froude scaling so it is applicable to the vessel. It is assumed that the sampling time of the controller is 1s and the prediction horizon is $N = 10$. Moreover, the river current is considered in this experiment which applies -0.1 N and 0.1 N force in x and y coordinate directions, respectively.

The tracking experiment results are provided in Figure 5.4. In Figure 5.4a, the trajectory tracking result is shown in comparison with the reference trajectory. The ship heading versus the reference heading is presented in Figure 5.4b. The tracking error is provided in Figure 5.4c which indicates that the tracking error is less than 1.5 m throughout the experiment.

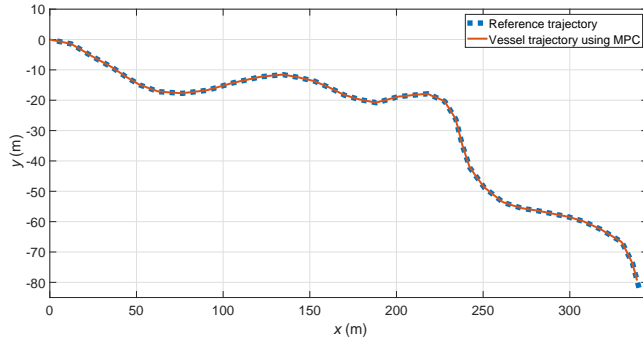
The speed of the vessel in 3DoF is shown in Figure 5.5a. The propelling forces are presented in Figure 5.5b and the disturbance forces applied to the ship's Center of Gravity (CoG) is provided in Figure 5.5c.

In Figure 5.6a, the actuator forces applied to the ship's CoG are shown and in Figure 5.6b, the real-time constraint handling of the controller is illustrated which indicates the success of the control approach in keeping the system within the bounds.

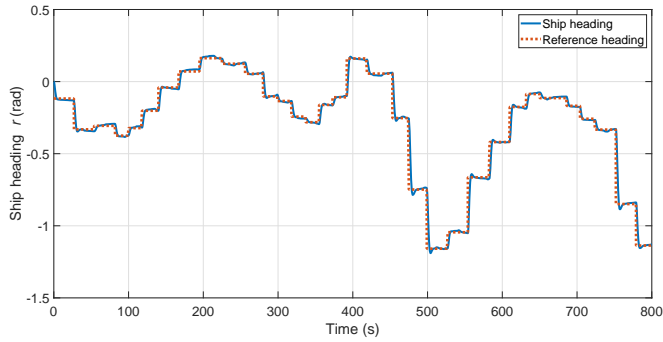
5.3. CONCLUSIONS

In this chapter, an MPC approach is presented for maneuvering control which employs IOFL. It is shown that using the proposed approach, the future required energy for propelling the ship can be predicted and constraints can be handled. Therefore, the results of this chapter provide an answer to Research Question 2 in Section 1.5 by proposing a control approach which guarantees small trajectory tracking (less than 1.5 m in the simulation experiments), constraint handling in the presence of environmental disturbances, and prediction of future propulsive load.

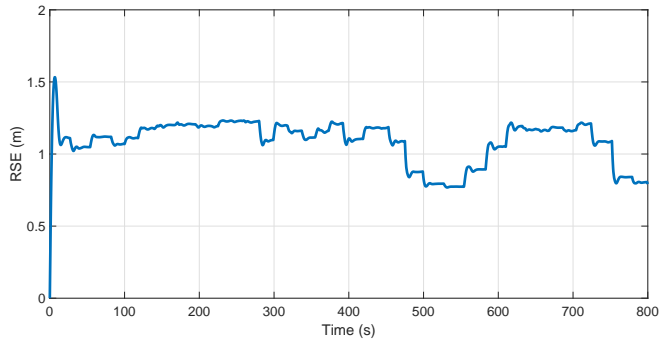
The future required propulsive power predicted by the proposed approach can be utilized by energy management and power generation control modules. This is shown in Chapters 6, 7, and 8.



(a) Vessel trajectory compared to the reference trajectory.

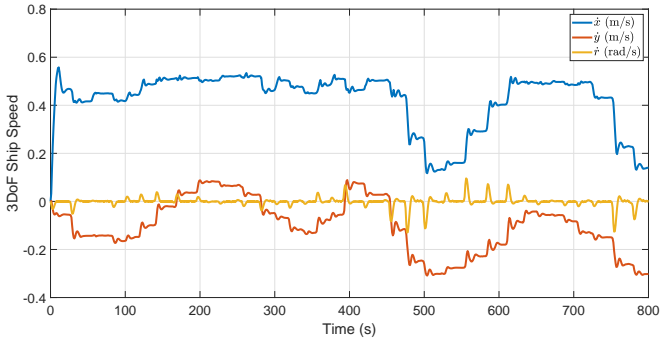


(b) Ship heading versus the reference heading.

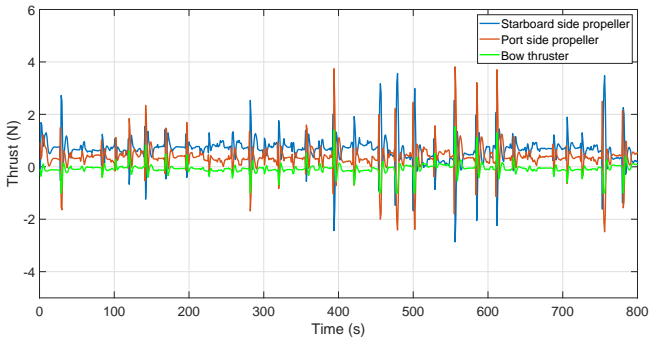


(c) Trajectory tracking Root Square Error (RSE).

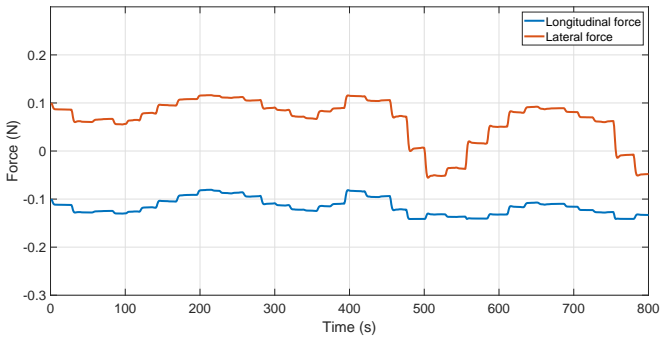
Figure 5.4: Trajectory tracking performance of the ship in Oude Maas river.



(a) Vessel speed during the voyage.

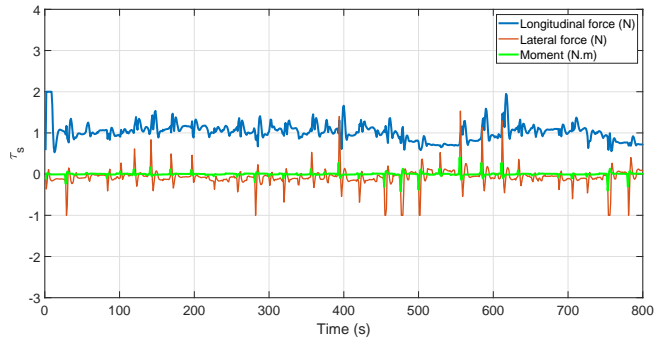


(b) Generated thrust by the propelling actuators.

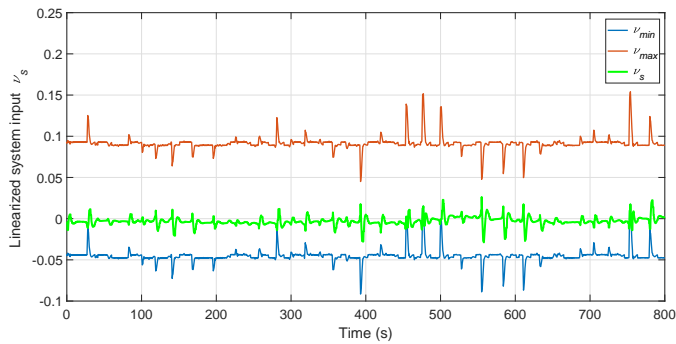


(c) Disturbance forces applied to the vessel's CoG.

Figure 5.5: Vessel's speed and the applied forces.



(a) Propelling actuator forces applied to the ship's CoG.



(b) Constraint handling result of the MPC controller.

Figure 5.6: Simulation results of Experiment II.

6

ENERGY MANAGEMENT FOR ALL-ELECTRIC SHIPS

In the previous chapter, a trajectory tracking control scheme has been introduced which is capable of extracting the future required propulsive load. In this chapter, an energy management algorithm is proposed for the purpose of finding the optimal split between the different energy sources, namely, the DGR sets and the battery-converter set by utilizing the propulsive load predicted. The objective is to keep the diesel-generators functioning around their optimal point in the Specific Fuel Consumption (SFC) curve which leads to an efficient performance. As a result, maximize fuel efficiency can be guaranteed. Furthermore, the proposed approach limits DGR sets to experience sudden changes in loading condition which results in higher robustness of the DC-PPS. In Section 6.1, the proposed energy management approach is presented and in Section 6.2, the performance of the approach is evaluated using several simulation-based experiments including sailing in the port of Rotterdam and operating profiles of real-size tugs. The DC-PPS used for simulation-based experiments is established by adopting the models introduced in Chapter 3. The results in this chapter have been partially published in two scientific papers.¹

6.1. PREDICTIVE ENERGY MANAGEMENT

In this section, the predictive energy management approach is introduced. This approach utilizes the prediction of the propulsive load, that is extracted by the model pre-

¹Parts of this chapter have been published in:

1. A. Haseltalab, R. R. Negenborn, "Model predictive maneuvering control and energy management for all-electric autonomous ships," *Applied Energy*, Volume 251, 2019.
2. A. Haseltalab, R. R. Negenborn, "Predictive on-board power management for all-electric ships with DC distribution architecture," in the proceedings of OCEANS 2017, Aberdeen, pp. 1-8.

dictive maneuvering control scheme (introduced in Chapter 5), to determine the optimal split between different energy sources. As a result, optimal engine loading and maximized fuel efficiency are guaranteed.

To construct the approach, first, the cost function of the Predictive Energy Management (PEM) problem that is based on the SFC curve of diesel engines is derived. SFC curve is an indicator for fuel-efficient power and energy generation. The SFC curve of a diesel engine can be represented as:

$$SFC(P_{DE}) = \frac{a}{P_{DE}} + bP_{DE} + c \quad (6.1)$$

where P_{DE} is the delivered mechanical power and a , b and c are parameters dependent on the diesel engine specifications.

The electrical losses in energy generation side of the power network are functions of the output power of the diesel engine [101]. In this chapter, based on the results in [23], the copper, iron, mechanical and rectifier losses of the generator-rectifier set are included in the problem by a constant coefficient, i.e., $P_{DGR} = \alpha_{DGR}P_{DE}$ where $0 < \alpha_{DGR} < 1$ which depends on the specifications of the generator-rectifier set. The same approach is also considered for the set of battery-converter. As a result, $P_{BC} = \alpha_{BC}P_B$ where $0 < \alpha_{BC} < 1$. Since, the efficient region in the SFC curve is a wide area, this approximation does not affect the optimality of the process, significantly.

The power share assigned at time k that should be delivered by DGR set j over horizon N_E is denoted as $P_{DGR_j}(k|k)$, $P_{DGR_j}(k+1|k)$, ..., $P_{DGR_j}(k+i-1|k)$. Similarly, the assigned power to be delivered by the battery-converter set is $P_{BC}(k|k)$, $P_{BC}(k+1|k)$, ..., $P_{BC}(k+i-1|k)$ over the horizon N_E . Considering these sets, the following relationships are consistent:

$$\begin{aligned} P_{DG_i}(k+i-1|k) &= v_{DC}I_{G_{jdc}}(k+i-1|k) \\ P_{BC}(k+i-1|k) &= v_{DC}i_{BC}(k+i-1|k), \end{aligned} \quad (6.2)$$

where v_{DC} is the DC voltage of the power network, which must be kept constant around a certain value and $I_{G_{jdc}}$ and i_{BC_i} are current shares provided by DGR i and battery-converter sets, respectively.

The efficient delivered power by diesel engine i is denoted as P_{eff_i} and defined as:

$$P_{eff_i} = \arg \min_{P_{m_i}} (SFC(P_{m_i})). \quad (6.3)$$

As a result, the first goal of the algorithm is to keep $\frac{P_{DGR_j}(k+i-1|k)}{\alpha_{DGR}}$ around P_{eff_j} .

It is assumed that the different sets of diesel-generators can have different specifications with different P_{eff_i} and maximum power that they can deliver. Since the power demand changes over the operation time, first the set of active DGRs should be determined using specifications of DGRs (i.e., P_{eff_i} and their power ratings) as well as the power demand $P_d(k)$. For this goal, a set of optimization problems needs to be solved over the prediction horizon. The optimization problems for charge and discharge modes are different. For the battery discharge mode, we have:

$$\mathcal{P}_{DGR_d}^l : \min_{\phi_i^k} J_{DGR_i}(\phi_1^l, \dots, \phi_m^l) \quad (6.4)$$

subject to

$$\frac{\phi_1^l}{\alpha_{\text{DGR}_1}} P_{\text{eff}_1} + \dots + \frac{\phi_m^l}{\alpha_{\text{DGR}_m}} P_{\text{eff}_m} + P_{\text{BC}}(l|k) \geq P_d(l|k) \quad (6.5)$$

$$\forall l \in [k, k+i-1], \forall i \in [0, N]$$

The optimization problems in battery charge mode are:

$$\mathcal{P}_{\text{DGR}_c}^l : \min_{\phi_i^l} J_{\text{DGR}_l}(\phi_1^l, \dots, \phi_m^l) \quad (6.6)$$

subject to

$$\frac{\phi_1^l}{\alpha_{\text{DGR}_1}} P_{\text{eff}_1} + \dots + \frac{\phi_m^l}{\alpha_{\text{DGR}_m}} P_{\text{eff}_m} \geq P_d(l|k) \quad (6.7)$$

$$\forall l \in [k, k+i-1], \forall i \in [0, N]$$

Note that for the charge mode, P_{BC} is included in P_d . Function J_{DGR_l} is defined as:

$$J_{\text{DGR}_l}(P_{\text{eff}_1}, \dots, P_{\text{eff}_m}) = \phi_1^l SFC_1(P_{\text{eff}_1}) + \dots + \phi_m^l SFC_m(P_{\text{eff}_m}), \quad (6.8)$$

where m is the overall number of DGR sets and $\phi_1, \phi_2, \dots, \phi_m$ are binary numbers with 0 or 1 values. If $\phi_j^l = 1$ then DGR set j is considered active during the sample time period t_k . Since the number of DRG sets on-board of a ship is limited, the above optimization problems are trivial. Note that for the charge mode, P_{BC} is negative.

For constructing the main objective function in this part, we define the following function using (6.1):

$$S_j(I_{Gjdc}(k+i-1|k)) = \frac{\alpha_{\text{DGR}_j} a_j}{v_{\text{DC}} I_{Gjdc}(k+i-1|k)} + \frac{b_j}{\alpha_{\text{DGR}_j}} v_{\text{DC}} I_{Gjdc}(k+i-1|k), \quad (6.9)$$

where a_j and b_j are SFC coefficients of diesel engine j defined in (6.1). Suppose \mathbb{I}_{DGR} is the set of $i_{\text{DGR}_j}(k+i-1|k)$ for all $j \in [1, m]$ and $i \in [0, N]$, then by employing (6.9), the cost function for the PEM problem can be formulated as:

$$J_{\text{pm}}(\mathbb{I}_{\text{DGR}}) = \sum_{i=0}^N \sum_{j=1}^m \phi_i^j S_i(I_{Gjdc}(k+i-1|k)). \quad (6.10)$$

The inequality constraints are divided into two types. The first type of constraints are used to keep the energy sources operating in a safe predefined zones. The second type of constraints are employed to prohibit occurrence of major changes in loading condition of energy sources in short intervals to prevent instability in the DC power network. Take

$\text{var}(\cdot)$ as the variance operator, then the inequality constraints are as below:

$$\begin{aligned}
 & \text{var}(\phi_1^k I_{G1dc}(k|k), \dots, \phi_1^{(k+N-1)} I_{G1dc}(k+N-1|k)) \leq M_1 \\
 & \vdots \\
 & \text{var}(\phi_m^k I_{Gmdc}(k|k), \dots, \phi_m^{(k+N-1)} I_{Gmdc}(k+N-1|k)) \leq M_m \\
 & I_{G1dc}(k|k), \dots, I_{G1dc}(k+N-1|k) \leq i_{M_1} \\
 & \vdots \\
 & I_{Gmdc}(k|k), \dots, I_{Gmdc}(k+N-1|k) \leq i_{M_m}.
 \end{aligned} \tag{6.11}$$

The battery constraints depend on its operation mode, i.e., charge or discharge. During discharge the following constrains must be handled.

$$\begin{aligned}
 & \text{var}(i_{BC}(k|k), \dots, i_{BC}(k+N-1|k)) \leq M_{BC}^d \\
 & i_{BC}(k|k), \dots, i_{BC_m}(k+N-1|k) \leq i_{M_{BC}}^d.
 \end{aligned} \tag{6.12}$$

Similarly for the charge mode, the constrains are as follows:

$$\begin{aligned}
 & \text{var}(i_{BC}(k|k), \dots, i_{BC}(k+N-1|k)) \leq M_{BC}^c \\
 & i_{BC}(k|k), \dots, i_{BC_m}(k+N-1|k) \geq i_{M_{BC}}^c
 \end{aligned} \tag{6.13}$$

where M_{BC}^d , M_{BC}^c and $i_{M_{BC}}^d$ are positive and $i_{M_{BC}}^c$ is negative.

The equality constrains are established to keep the sum of power shares equal to the demanded power:

$$\begin{aligned}
 & \phi_1^k P_{DGR_1}(k|k) + \dots + \phi_m^k P_{DGR_m}(k|k) + P_{BC}(k|k) = P_d(k|k) \\
 & \vdots \\
 & \phi_1^{(k+N-1)} P_{DGR_1}(k+N-1|k) + \dots + \phi_m^{(k+N-1)} P_{DGR_m}(k+N-1|k) \\
 & + P_{BC}(k+N-1|k) = P_d(k+N-1|k)
 \end{aligned} \tag{6.14}$$

where $P_{DGR_j}(\cdot)$ and $P_{BC}(\cdot)$ are calculated using (6.2). Now, the optimization problem can be formulated as:

$$\mathcal{P}_{pm} : \min_{\mathbb{I}_{DGR}} J(\mathbb{I}_{DGR}) \tag{6.15}$$

subject to constraints (6.11), (6.12), (6.13) and (6.14).

Remark 2 The cost function in (6.10) is a sum of multiple convex functions. As a result, it is convex and convex optimization methods can be used for solving the optimization problem in (6.15).

Remark 3 The presented PEM algorithm can guarantee maximum efficiency for any set of DGRs accompanied by a BC set with different power ratings and SFC curves if the maximum charge/discharge power by the battery at the desired voltage v_{dc} is greater or equal

to P_{eff} of the diesel engine with the highest power rating, i.e.,

$$\max\{i_{MBC}^d, |i_{MBC}^c|\} \geq \max\left\{\frac{P_{\text{eff}_1}}{\alpha_{\text{DGR}_1} v_{\text{dc}}}, \dots, \frac{P_{\text{eff}_m}}{\alpha_{\text{DGR}_m} v_{\text{dc}}}\right\}. \quad (6.16)$$

If the above non-equality does not hold, then, finding the optimal split between energy sources using SFC curves is not guaranteed for all time instants kt_k .

The above remark indicates that during the design stage, the on-board energy sources should be chosen with regard to achieving optimal fuel efficiency. If this is not the case and (6.16) does not hold, then, achieving optimal fuel efficiency is not guaranteed.

Remark 4 Using the presented algorithm and based on the predicted power demand over horizon N , the safe turn on/turn off time of DGR sets can be predicted. Since, it takes some time (warm up time) for DGR sets to be able to provide power for the power network, this prediction can lead to increased safety and robustness in the system. However, modeling the warm-up dynamics of the DGR sets are out of the scope of this dissertation and are not considered in the simulation cases.

The energy management controller steps are:

- **Initialization:** Determine the initial charge or discharge mode, $P_d(0)$, and obtain the set of active DGR sets.
1. Depending on the discharge or charge mode of the battery solve the optimization problem in (6.4) or (6.6) to select the active DGR sets.
 2. Solve the optimization problem in (6.15).
 3. Obtain the set of active DGR sets, receive P_d from the maneuvering controller, and go to 1.

Remark 5 Step 1 in the energy management algorithm can be revisited less compared to other steps to avoid activation/deactivation of DGR sets in short time periods. Although this might lead to sub-optimality but it can increase the stability of the network and decreases the maintenance costs and efforts.

Remark 6 If the prediction horizon of the energy management problem N_E is greater than the horizon of the ship maneuvering control problem N , $P_d(k+N)$ can be extended over the remainder of N_E .

In the next section, several simulation experiment results are provided for evaluating the performance of the proposed approach.

6.2. SIMULATION EXPERIMENTS

In this section, several experimental results are presented for evaluation of the presented predictive ship control and energy management approach. The Tito-Neri vessel model, which is presented in Chapter 5, is also adopted here.

For the real size harbor tug a 4.4 MW DC-PPS is considered. On the energy generation side, two diesel engines with 1.8 MW and 1.2 MW maximum deliverable power are considered which are accompanied by a battery-converter set which can deliver up to 1.4 MW of power. On the energy consumption side, two 1.5 MW induction motors for propellers and a 500 kW induction motor for actuating the bow thruster are considered. A schematic view of the DC-PPS is provided in Figure 3.2. The specification of the system components are provided in Appendix A.2.

The combined SFC curve of the overall DC-PPS is provided in Figure 6.1, indicating the fuel efficiency of the overall system. The generated and the demanded power construct the following equality constraint at any time instant k :

$$\alpha_{DGR1} P_{DE1}(k) + \alpha_{DGR2} P_{DE2}(k) + P_{BC}(k) = P_d(k), \quad (6.17)$$

which represents a surface plane if it is included in Figure 6.1. One of the objectives of the proposed PEM algorithm is to guarantee that this surface plane includes the optimal point in the combined SFC curve of Figure 6.1 or passes it at a very short distance, depending on the operating and loading conditions.

In this section, results of three different experiments are presented:

1. In the first experiment, a circular trajectory is considered in which the vessel increases its speed.
2. In the second experiment, the trajectory of a real vessel that is based on Automatic Identification System (AIS) data obtained from the port of Rotterdam Authority is simulated.
3. In the third experiment, the performance of the proposed PEM algorithm is experimented with different operating profiles.

6.2.1. EXPERIMENT I: CIRCULAR TRAJECTORY

The results of the maneuvering control experiment in Section 5.2 is used for this experiment. Maneuvering control experiment results are scaled up using Froude scaling for application to the real-size power and propulsion system.

It is assumed that the real-size tug is under a pull force which increases over time. The simulation results of the energy consumption side are shown in Figure 6.2. The bollard pull force increases from $t=300$ s and it reaches to 420 kN after 620 seconds. As a result, the propelling effort increases which results in a higher shaft speed and electric torque of the propelling induction motors.

During this operation, it is assumed that the battery is in the charge mode which leads to higher load demands. The initial SOC is assumed to be 20%. The simulation results using the predictive energy management algorithm are provided in Figure 6.3. The results indicate that despite of changes in the propulsive load, the optimal engine

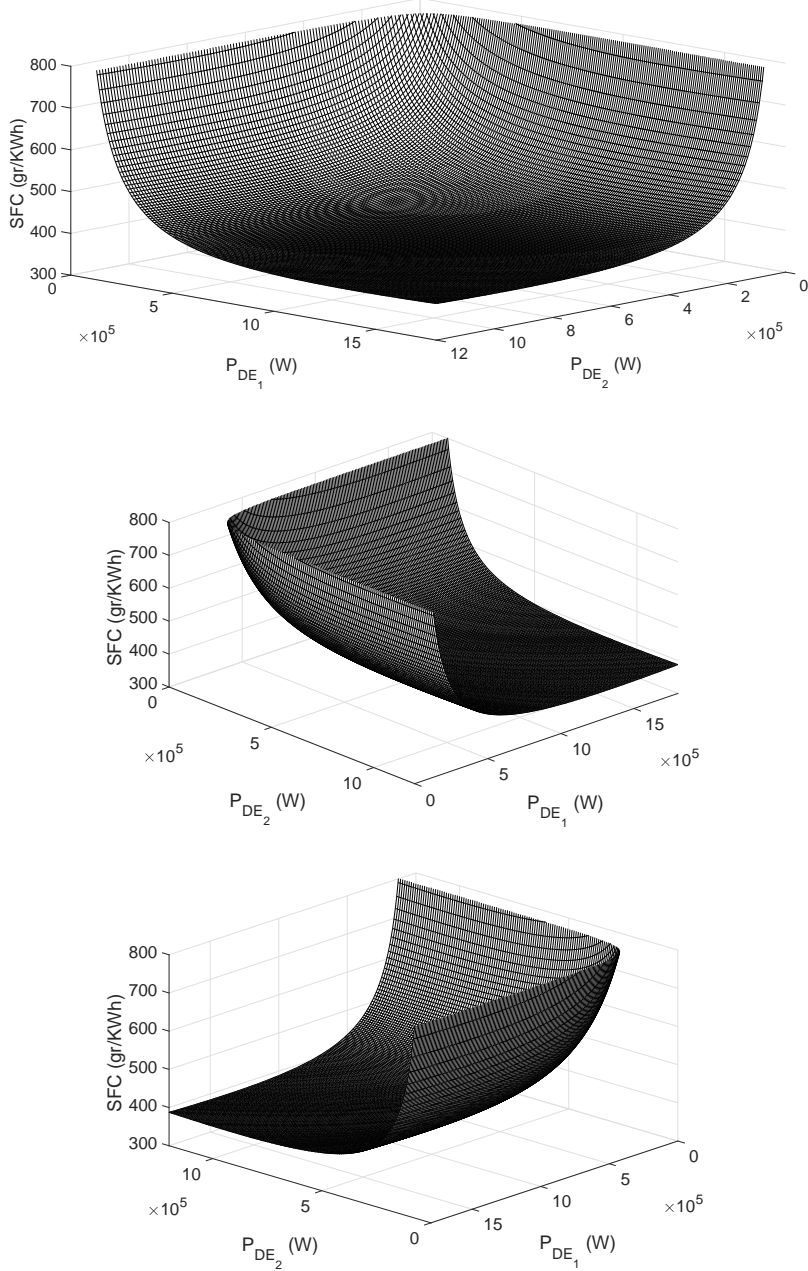
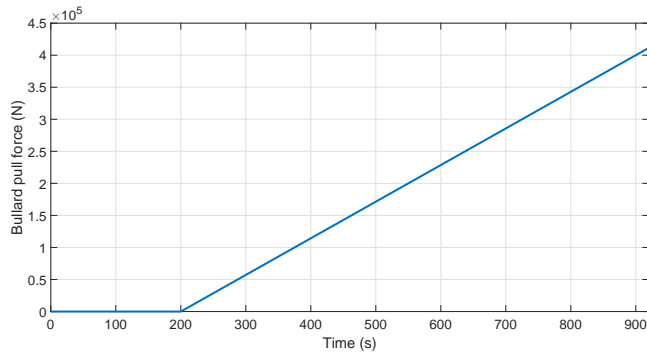
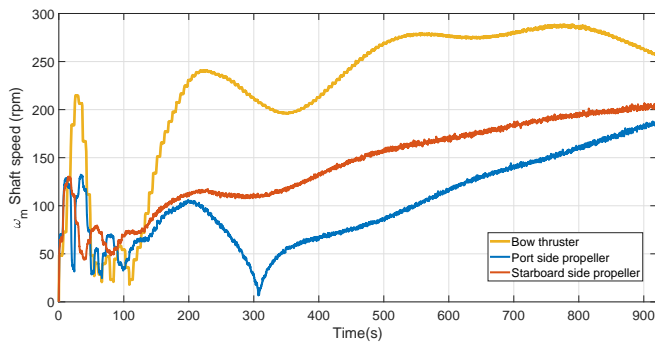


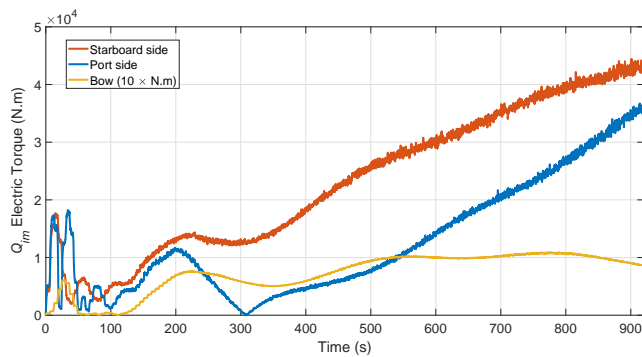
Figure 6.1: Combined SFC curve of the harbor tug from different angles.



(a) Applied bullard pull force.



(b) Shaft speed of the propelling actuators.



(c) Electric torque of the induction motors.

Figure 6.2: Simulation results of the energy consumption side (Experiment I).

Battery mode	Algorithm	Fuel cons. (kg)	Mech. en. (kWh)	SFC	SOC change (%)
Charge	PEM	108.6	567	190.5	23.2
Charge	RB	90	461	195.2	7.2
Discharge	PEM	19.2	101	188.1	-30.4
Discharge	RB	29.1	151.6	192.1	-25.5

Table 6.1: Overall fuel consumption and generated energy (Experiment I).

loading is achieved throughout the operation. In Figure 6.4, the results related to the stability of the DC-PPS are given. The power share of each energy source determined by the energy management algorithm is provided in Figure 6.4a. The voltage of the DC-link capacitor and speed of the diesel-generators are also provided which are stable around their desired values. The battery SOC and fuel consumption rate of the diesel engines are presented in Figure 6.5 which indicate optimal loading consistency.

Experiment I is also carried out in battery discharge mode where the initial SOC is considered to be 80%. The simulation results in this case are shown in Figure 6.6. Furthermore, the results are compared to a conventional Rule-Based (RB) strategy that is no energy source should provide more than 85% of its maximum deliverable power. The simulation results are provided in Figure 6.7. It is observed that the optimal loading of the diesel engines can not be achieved and the engine load varies during the operation. The results are provided in Table 6.1 for comparison. The results suggest that in this voyage, the SFC efficiency of the engines increases in charge and discharge modes if the proposed PEM approach is adopted. In the charging mode, the increase is 2.4% and in discharge mode it is 2.04%. Furthermore, using the proposed algorithm, the saved energy in the battery is more than three times higher.

6.2.2. EXPERIMENT II: VOYAGE IN THE PORT OF ROTTERDAM

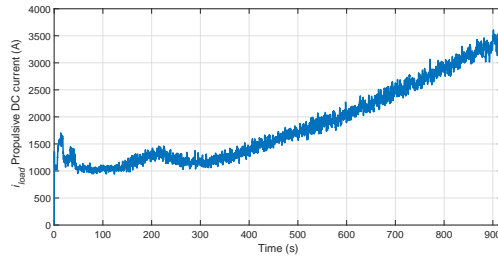
In this experiment, the voyage of an inland vessel is extracted using AIS data of the Oude Maas river in the port of Rotterdam (Figure 4.7). The trajectory is scaled down so that it is applicable to Tito-Neri vessel. This simulation is carried out twice, first using the proposed PEM algorithm and by adopting the conventional rule-based approach. In both cases, it is assumed that at the start of the simulation the battery SOC is at 20%. As a result, the battery is charged up to 80% of its capacity and then is used in discharge mode. In both cases, a full charge and discharge cycle is considered.

The results of the trajectory tracking are provided in Figure 6.8. The shaft speed of the propelling actuators as well as the DC current of their motor-inverter controllers are shown in Figure 6.9.

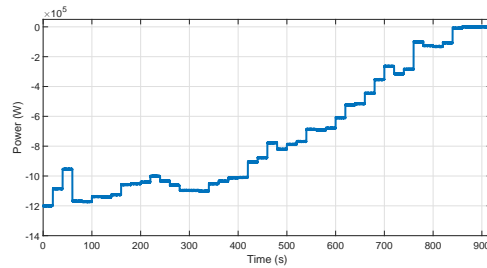
The simulation results of the energy generation side are shown in Figure 6.10. It can be observed that a more optimal engine loading is achieved using the proposed energy management approach. The results are also presented in Table 6.2. The results indicate that using the proposed approach 3% fuel efficiency can be achieved.

6.2.3. EXPERIMENT III: REAL OPERATING PROFILES

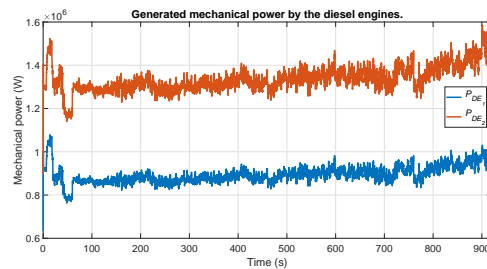
For the third experiment, the operating profile data of an actual harbor tug is used. There are four operating profiles, see Figure 6.11 where the bollard pull force and the vessel



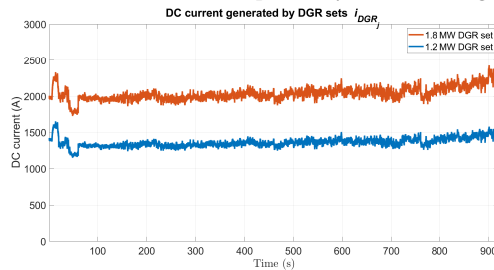
(a) Propulsive load current at DC-link.



(b) Assigned power for battery charging.

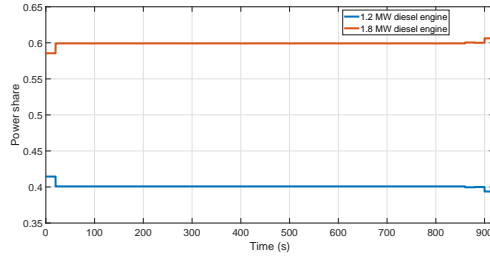


(c) Generated mechanical power by the diesel engines.

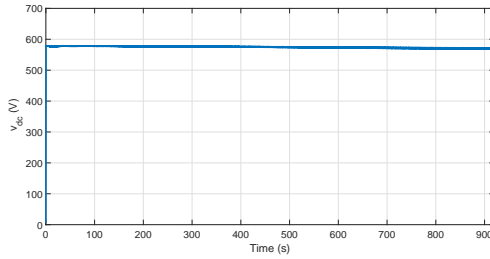


(d) DC current provided by each DRG set.

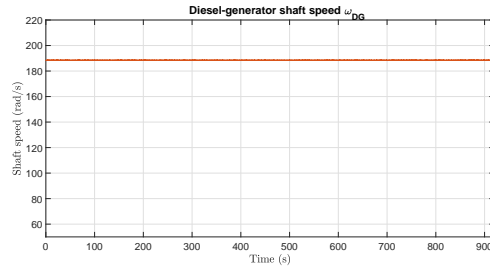
Figure 6.3: Simulation results of the energy generation side (Experiment I).



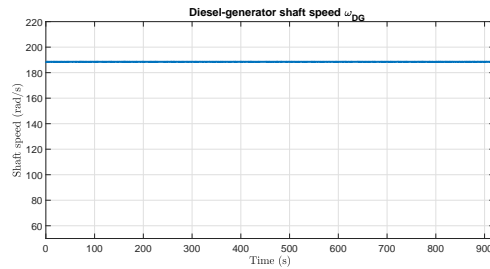
(a) Power share of the DGR sets.



(b) Voltage of the DC-link capacitor.

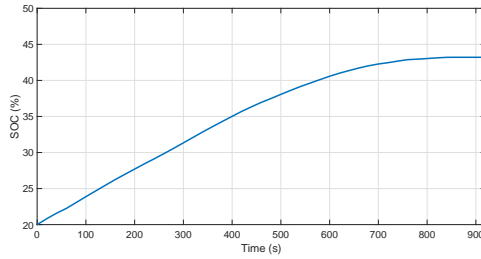


(c) 1.8 MW diesel-generator shaft speed.

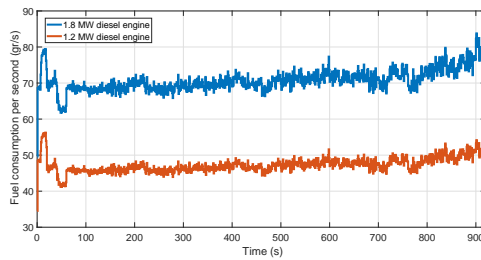


(d) 1.2 MW diesel-generator shaft speed.

Figure 6.4: Stability results of the power system. (Experiment I).



(a) Battery SOC during the voyage.

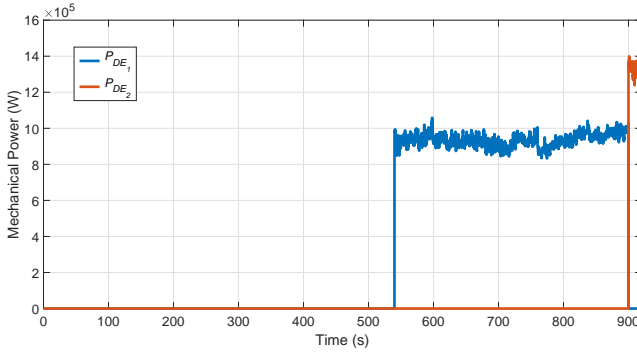


(b) Fuel consumption rate of diesel engines.

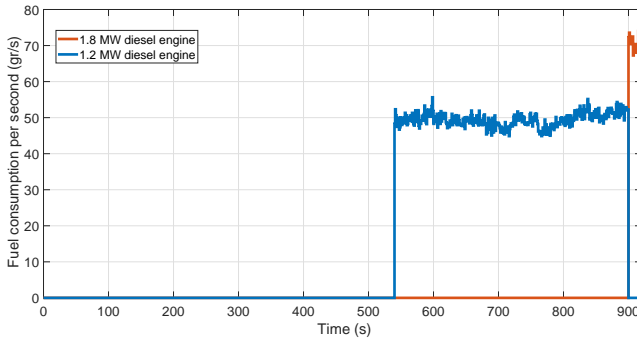
Figure 6.5: Battery SOC and the fuel consumption rate (Experiment I).

Algorithm	Fuel cons. (kg)	Mech. energy (kWh)	SFC
PEM	326	1690	192.8
RB	336	1700	197.6

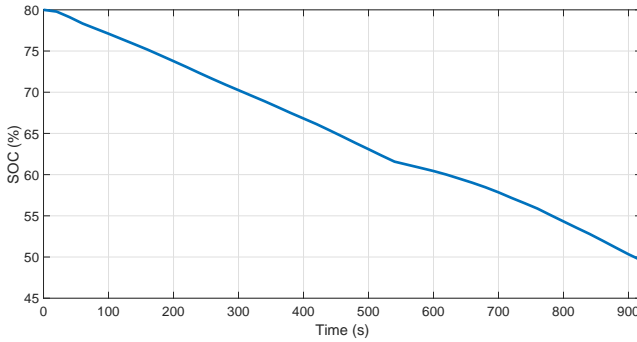
Table 6.2: Performance comparison of algorithms (Experiment II).



(a) Delivered power by the diesel engines.



(b) Fuel consumption rate.



(c) Battery SOC.

Figure 6.6: Simulation results in battery discharge mode using PEM (Experiment I).

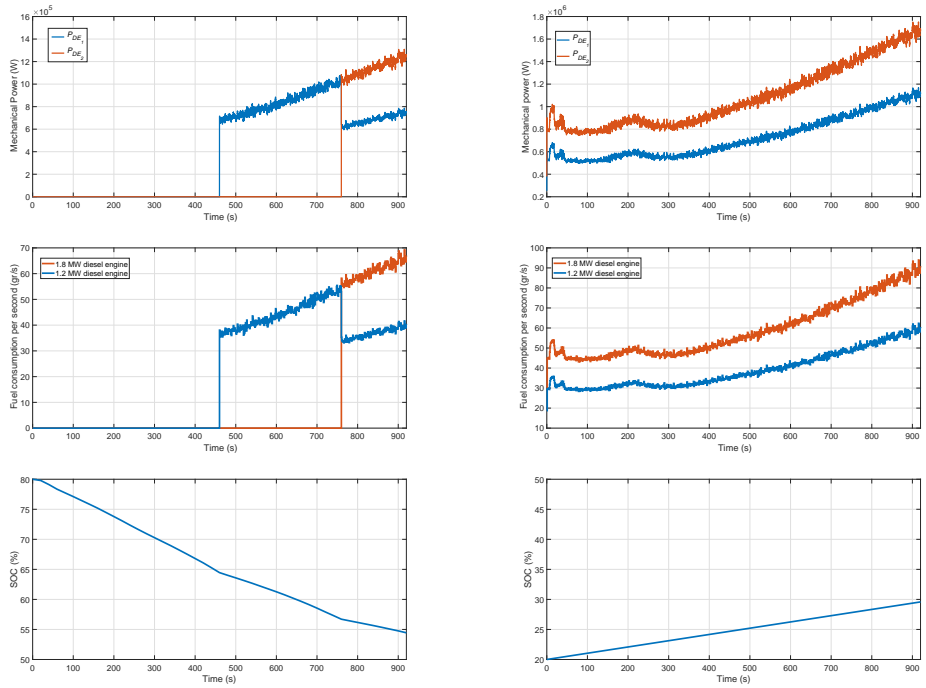


Figure 6.7: Simulation results using the rule-based approach (Experiment I).

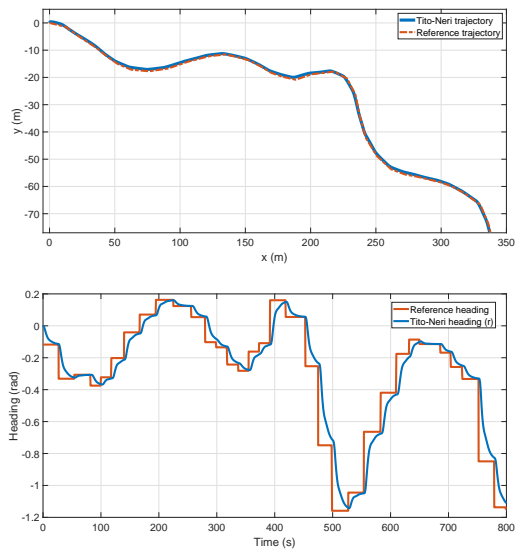
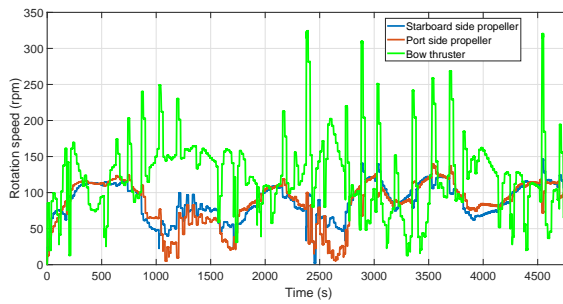
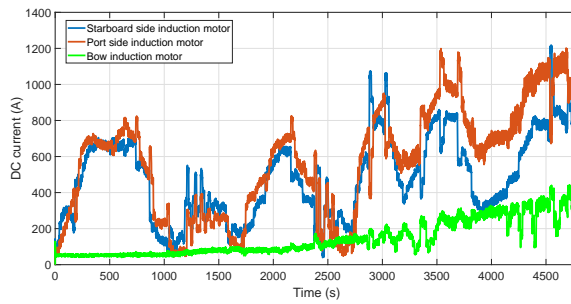


Figure 6.8: Trajectory tracking result (Experiment II).

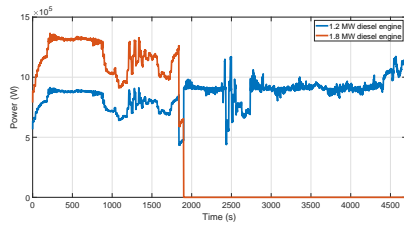


a) Shaft speed of propellers.

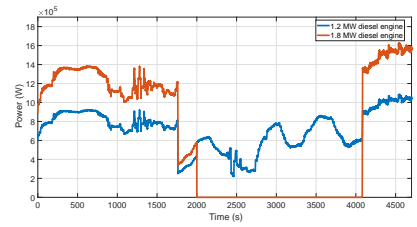


b) Input DC current of motor controller-inverters.

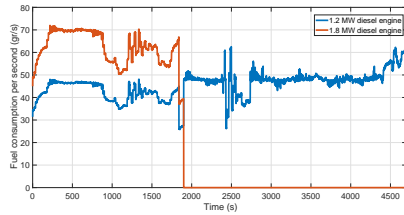
Figure 6.9: Simulation results of propelling actuators (Experiment II).



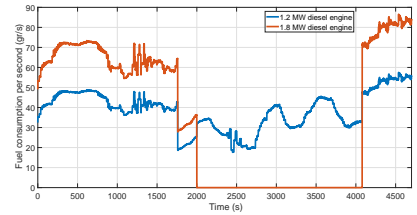
a) Generated power by diesel engines (PEM).



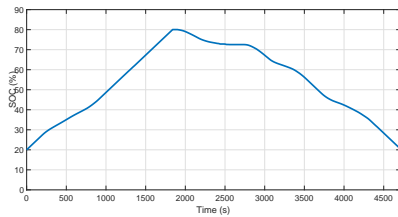
b) Generated power by diesel engines (RB).



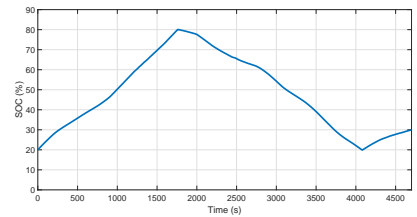
c) Fuel consumption rate (PEM).



d) Fuel consumption rate (RB).



e) Battery SOC (PEM).



f) Battery SOC (RB).

Figure 6.10: Simulation results using PEM and rule-based approaches (Experiment II).

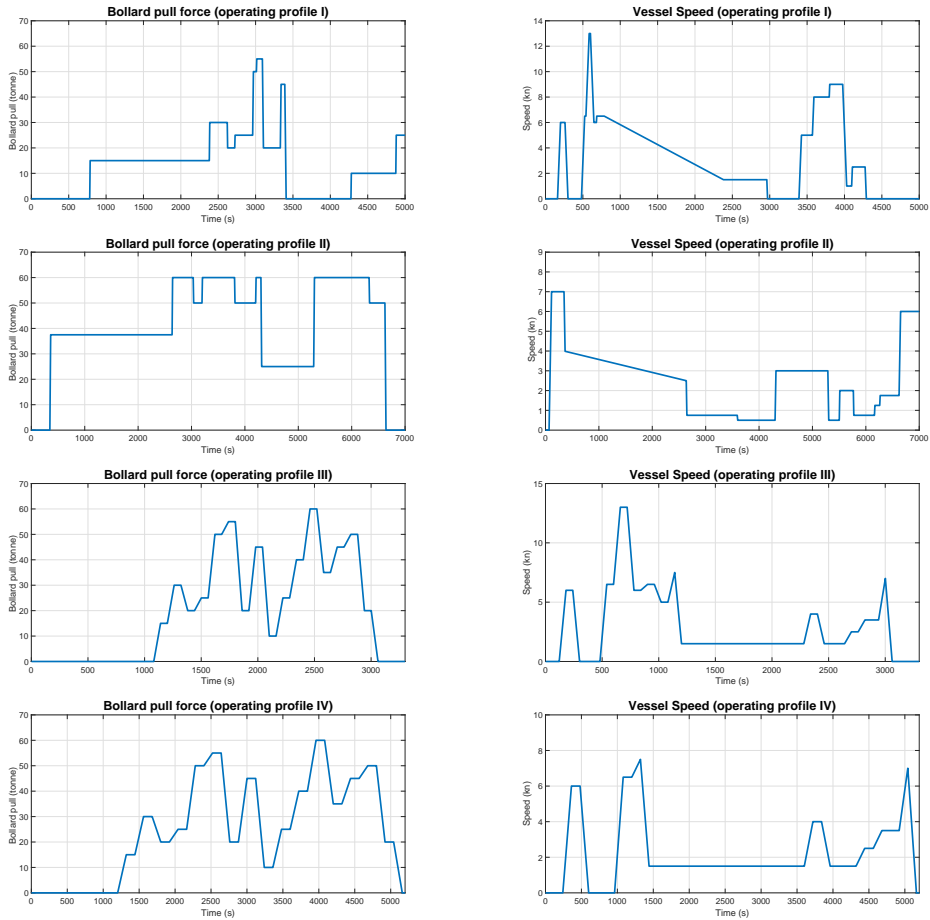


Figure 6.11: Operating profiles (Experiment III).

speed are illustrated over the operation time. The operating profiles are different in terms of load fluctuation and power demand. Profile 1 is a standard profile based on measurements of tugboats in the port of Rotterdam. Profile 2 is a busy profile in which the vessel undergoes a heavy pull operation for relatively a long period. Profile 3 represents an operation where the load fluctuation is high. Profile 4 is an expansion of Profile 3 over time representing a busy profile with high load fluctuation.

The simulation results are provided in Table 6.3. For Profile I, although the fuel consumption is increased using the proposed energy management algorithm, the battery SOC reaches to 68%. This indicates that the available power is handled more efficiently. This can be confirmed by comparing the operation SFCs, where 12% SFC efficiency is obtained using the PEM approach. In the second profile, a complete charge and discharge cycle is not completed. However, the proposed approach offers 3.6% SFC efficiency. In

Profile	Algorithm	Start mode	Fuel cons. (kg)	Mech. en. (kWh)	SFC (gr/kWh)	No. of cycles	Final SOC (%)
I	RB	charge	233.4	1062	219.7	1	20
I	PEM	charge	282.2	1459	193.3	1	68
II	RB	charge	808.2	4108	198.3	0	15
II	PEM	charge	778	4068	191	0	17
III	RB	discharge	151.2	751	201.4	0	32
III	PEM	discharge	148.3	765	193.7	0	35
IV	RB	charge	372.1	1801	206.2	1	33
IV	PEM	charge	350.4	1772	197	1	31

Table 6.3: Simulation results (Experiment III).

the third profile also a complete cycle is not gained due to the short operation time. Using the proposed approach 3.8% and 4.4% SFC efficiency is gained in Profiles 3 and 4, respectively.

6.3. CONCLUSIONS

In this chapter, a Predictive Energy Management (PEM) approach is presented to find the optimal split between different energy sources on-board with objective of maximizing the fuel efficiency. The objective function of the optimization problem is based on SFC curve diesel-generator sets and the prediction of demanded propulsive energy. Through several simulation experiments, the performance of the approach is evaluated and it is shown that its adoption leads to 2-15% fuel efficiency depending on the operating profile.

The results of this chapter provide answers to Research Questions 4, 5, and 6 by proposing an energy management approach which utilizes the propulsive load prediction to guarantee power availability as well as optimal engine loading. In the next chapters, by proposing novel approaches for power generation control, the stability and availability of energy sources are guaranteed. These power generation control approaches use the power split between different on-board energy sources which is determined using the proposed predictive energy management approach in this chapter.

7

CONTROL FOR DIESEL-GENERATOR-RECTIFIER SETS

In the previous chapters, several approaches have been introduced for maneuvering control and energy management to improve the maneuvering performance and fuel efficiency of autonomous all-electric ships. In this chapter, the focus is on improving the stability of the DC-PPS. In Section 7.1, a state space model is introduced for DGR sets. The proposed MPC approach is presented in Section 7.2 and its stability robustness proof is carried out. In Section 7.4, the performance of the approach is evaluated through several simulation-based experiments. The content of this chapter have been partially published in scientific papers.¹

In this chapter, based on the results in [24, 120], a Model Predictive Control approach is proposed to control and stabilize the DC voltage and the shaft speed of the Diesel-Generator-Rectifier (DGR) set. Input-Output Feedback Linearization (IOFL) is adopted for linearization and the design of the proposed algorithm. The advantage of using this strategy lies in the short computation time required for solving the resulting optimization problem. It is shown that this scheme can be made robust by a tube-based MPC algorithm to handle the harmful effects of disturbances and modeling uncertainties [122]. In the proposed methodology, the DC propulsive load current is estimated by employing the mathematical model of propellers as well as the efficiency curve of induction motors. It is shown that if the ship is also controlled using a predictive algorithm, then the DC

¹Parts of this chapter have been published in:

1. A. Haseltalab, M. A. Botto, R. R. Negenborn, "Model Predictive DC Voltage Control for All-Electric Ships," *Control Engineering Practice*, Volume 90, pp. 133-147, 2019.
2. A. Haseltalab, M. A. Botto, R. R. Negenborn, "On-Board Voltage Regulation For All-Electric DC Ships," *IFAC-PapersOnLine*, Volume 51, Issue 29, pp. 341-347, 2018.

propulsive load current can be predicted over a certain horizon. The stability analysis of the proposed algorithm is carried out and a stability criterion is derived. Throughout the chapter, it is shown that the proposed strategy is capable of handling adverse effects of CPLs, fast changes in loading condition and nonlinearities of the system model.

7.1. STATE SPACE MODELING OF DGR SETS

The stability of DGR sets under different loading conditions is a vital issue as if on-board energy sources face any failure, blackout and loss of propulsion are inevitable. As a result, robust control approaches should be adopted to guarantee the stability of the on-board power system under different operating profiles. In this chapter, the focus is on controlling a single DGR set based on the model provided in Chapter 3, i.e.,

$$\begin{aligned}
 \dot{I}_G &= X_G^{-1} S_\omega(\omega_{dg}) X_G I_G + X_G^{-1} R_G I_G \\
 &+ v_{dc} X_G^{-1} \begin{bmatrix} \alpha_{rec} \sin(\arctan(\frac{i_d}{i_q}) - \phi_{rec}) \\ \alpha_{rec} \cos(\arctan(\frac{i_d}{i_q}) - \phi_{rec}) \\ 0 \\ 0 \\ 0 \end{bmatrix} + X_G^{-1} b v_{fd} \\
 \dot{\omega}_{dg} &= \frac{1}{2H} (Q_{en} - I_G X_G^T G_1 I_G + Q'_d) \\
 \dot{v}_{dc} &= \frac{1}{C} (\beta_{rec} \sqrt{I_G^T G_2 I_G} - i_{load} - i_v(v_{dc})) \\
 \dot{Q}_{en} &= -\frac{Q_{en}}{\tau_s} + K_{en} f_{en},
 \end{aligned} \tag{7.1}$$

where i_d , i_q , i_{fd} , i_{kd} , i_{kq} , ω_{dg} , v_{dc} and Q_{en} are the states of the system, v_{fd} and f_{en} are the system inputs and ω_{dg} and v_{dc} are the output variables of the system. Note that i_{load} and $i_v(v_{dc})$ appear as disturbances and state dependent uncertainty to the system.

Remark 7 In most of the research works such as [25],[62],[74],[123], it is assumed that $i_{load} + i_v(v_{dc}) = \frac{P}{v_{dc}}$, where P is the CPL power. However, in this chapter, a more general case is considered where it is presumed that changes in v_{dc} can lead to changes in P as well. As a result, it is assumed that there is no knowledge regarding changes in load current as a result of adverse effects of CPLs.

Remark 8 Load current i_{load} represents the DC load current at the desired voltage v_{ref} . It is assumed measurable and predictable as discussed further in Section 4.

If $\omega = [0, 0, 0, 0, 0, \omega_1, \omega_2, 0]^T$, the equations can be summarized in state-space format as:

$$\begin{aligned}
 \dot{x} &= f(x) + \sum_{j=1}^2 g_j(x) u_j + \omega \\
 y_i &= h_i(x) \quad i = 1, 2,
 \end{aligned} \tag{7.2}$$

where x is the vector of states, u is the vector of system inputs and vector y contains the system outputs. Function $f: \mathbb{R}^8 \rightarrow \mathbb{R}^8$ is the state transition function. Moreover, $g_1(x) = [X_G^{-1}b, 0, 0, 0]^T$, $g_2(x) = [0, 0, 0, K_{en}]^T$, $h_1(x) = \omega_{dg}$, $h_2(x) = v_{dc}$ and $\omega_2 = \omega_v(x) + \omega_{load}$. Note that, $\omega_v(\cdot)$ is $\frac{i_v(\cdot)}{C}$, ω_{load} represents $\frac{i_{load}}{C}$, and $\omega_1 = Q'_d$. The constraints on the input and output variables are:

$$\begin{aligned} u_{\min} &\leq u \leq u_{\max} \\ x_{\min} &\leq x \leq x_{\max}. \end{aligned} \quad (7.3)$$

In the next section, an approach is presented to control and stabilize this highly non-linear system which employs feedback linearization techniques in combination with a receding horizon strategy.

7.2. THE PROPOSED CONTROL STRATEGY

In this section, the proposed strategy to control and stabilize the system is presented. First, the dynamical system is linearized by adoption of feedback linearization technique and then, a receding horizon control strategy is applied. Later, the stability analysis of the algorithm is carried out.

7.2.1. INPUT-OUTPUT FEEDBACK LINEARIZATION

The system under study is a Multi-Input-Multi-Output (MIMO) system, with two inputs and two outputs. For IOFL, we adopt a strategy known as input-output decoupling [124] with which the input-output responses are also decoupled. For this aim, we leave out the disturbances and uncertainties since they are linearly related to v_{dc} .

System (8.4) is said to be input-output feedback linearizable if the vector of relative degrees $\{r_1, r_2\}$ exists under the following conditions:

1. $L_{g_j} L_f^k h_i(x) = 0$ for all $1 \leq i, j \leq 2$ and $k < r_i - 1$ where $L_S R(x) = \frac{d}{dx} R(x) \times S$ is the Lie derivative which is the directional derivative of R with respect to S .
2. The decoupling matrix $\Delta(x)$ should be nonsingular around the operating point of the system x_0 , i.e.,

$$\det(\Delta(x)) \neq 0, \quad |x - x_0| \leq 0 \quad (7.4)$$

where

$$\Delta(x) = \begin{bmatrix} L_{g_1} L_f^{r_1-1} h_1(x) & L_{g_2} L_f^{r_1-1} h_1(x) \\ L_{g_1} L_f^{r_2-1} h_2(x) & L_{g_2} L_f^{r_2-1} h_2(x) \end{bmatrix}. \quad (7.5)$$

By applying the Lie derivative to the system outputs with respect to $f(x)$ successively, the vector of relative degrees is calculated that is $\{2, 2\}$. As a result, by considering the above conditions, the decoupling matrix $\Delta(x)$ is derived as below:

$$\Delta(x) = \begin{bmatrix} \frac{1}{H} I_G^T X_G^T G_1 X_G^{-1} b & \frac{K_{en}}{2H} \\ \frac{I_G^T G_2 X_G^{-1} b}{C \sqrt{I_G^T G_2 I_G}} & 0 \end{bmatrix} \quad (7.6)$$

which is nonsingular around the operating points of the DGR set. Please note that $\|x_0\| \neq 0$.

Since, $\Delta(x)$ is nonsingular, a nonlinear coordinate transformation $\Phi(x) = [\zeta^T, \eta^T]^T$ can be established by choosing the first $r = r_1 + r_2 = 4$ coordinates as:

$$\zeta_l^j = \Phi_l^j(x) = L_f^{j-1} h_l(x), \quad (7.7)$$

with non-negative integers $j \in \{1, 2\}$ and $l \in \{1, 2\}$. The other additional $n - r$ coordinates can be found such that $\Phi(x)$ is invertible [124]. In general, the normal form of the transformed partially linear system is:

$$\begin{aligned} \dot{\zeta}_1^1 &= \zeta_1^2 \\ \dot{\zeta}_1^2 &= v_1 = L_{(f+g_1 u_1 + g_2 u_2)}^2 h_1(x) \\ \dot{\zeta}_2^1 &= \zeta_2^2 \\ \dot{\zeta}_2^2 &= v_2 = L_{(f+g_1 u_1 + g_2 u_2)}^2 h_2(x) \\ \dot{\eta} &= q(\zeta, \eta) \\ y_1 &= \zeta_1^1 \\ y_2 &= \zeta_2^1, \end{aligned} \quad (7.8)$$

where v_1 and v_2 are the system inputs for the transformed linear systems. Vector of nonlinear functions q represents zero-dynamics/internal dynamics where its elements are chosen using the below condition:

$$L_{g_j} \Phi_{r+i}(x) = 0, \quad (7.9)$$

where $1 \leq i \leq 4$ and $1 \leq j \leq 2$. After calculation, we have:

$$\begin{aligned} \zeta_1^1 &= \omega_{\text{dg}} \\ \zeta_1^2 &= \frac{1}{2H} (Q_{\text{en}} - I_G X_G^T G_1 I_G) \\ \zeta_2^1 &= v_{\text{dc}} \\ \zeta_2^2 &= \frac{1}{C} (\sqrt{I_G^T G_2 I_G}). \end{aligned}$$

The relationship between the original system inputs u_1 and u_2 with inputs of the transformed system can be written as:

$$\begin{bmatrix} u_1 \\ u_2 \end{bmatrix} = -\Delta^{-1}(x) \left(\begin{bmatrix} L_f^2 y_1 \\ L_f^2 y_2 \end{bmatrix} + \begin{bmatrix} v_1 \\ v_2 \end{bmatrix} \right). \quad (7.10)$$

For the design of the controller, it is assumed that the rectifier is ideal, i.e., $\beta_{\text{rec}} = 1$ and $\alpha_{\text{rec}} = 1$.

After addition of the disturbances, the decoupled linear systems are:

$$\begin{aligned} \begin{bmatrix} \dot{\zeta}_1^1 \\ \dot{\zeta}_1^2 \end{bmatrix} &= \begin{bmatrix} 0 & 1 \\ 0 & 0 \end{bmatrix} \begin{bmatrix} \zeta_1^1 \\ \zeta_1^2 \end{bmatrix} + \begin{bmatrix} 0 \\ 1 \end{bmatrix} v_1 + \begin{bmatrix} 1 \\ 0 \end{bmatrix} \omega_1 \\ \begin{bmatrix} \dot{\zeta}_2^1 \\ \dot{\zeta}_2^2 \end{bmatrix} &= \begin{bmatrix} 0 & 1 \\ 0 & 0 \end{bmatrix} \begin{bmatrix} \zeta_2^1 \\ \zeta_2^2 \end{bmatrix} + \begin{bmatrix} 0 \\ 1 \end{bmatrix} v_2 + \begin{bmatrix} 1 \\ 0 \end{bmatrix} \omega_2(\zeta_2^1), \end{aligned} \quad (7.11)$$

where $\omega_2(\zeta_2^1) = \omega_v(\zeta_2^1) + \omega_{load}$ and $\omega_1 = Q'_d$,

Remark 9 *The stability of the internal dynamics can be deduced in a straightforward manner. Bearing in mind that $1/\tau_s > 0$, the stability of the engine torque Q_{en} can be determined using (7.1). The stability of the zero electrical dynamics can be determined with (7.1) by recalling that $\min\{L_d, L_{kd}, L_{fd}\} > L_{md}$ and $\min\{L_q, L_{kq}\} > L_{mq}$.*

7.2.2. TUBE-BASED MODEL PREDICTIVE CONTROLLER

In this part, an MPC-based control algorithm is proposed to control the feedback linearized system (7.11) which includes state dependent uncertainty and disturbances as a result the loading condition. Rewriting of (7.11) leads to:

$$\dot{\zeta}_1 = A_1 \zeta_1 + B_1 v_1 + [1, 0]^T \omega_1 \quad (7.12)$$

$$\dot{\zeta}_2 = A_2 \zeta_2 + B_2 v_2 + [1, 0]^T \omega_2(\zeta_2) \quad (7.13)$$

where A_1 and A_2 are state matrices, B_1 and B_2 are input vectors and $\omega_2(\zeta_2) = [1, 0]^T \omega(\zeta_2^1)$. The proposed robust MPC approach is based on a tube-based MPC strategy where first, a nominal trajectory for the system is extracted and then, by a feasible control rule, the system output is kept within a tube. It is shown that with a proper choice for the controller parameters, the disturbances can be handled and the voltage error stays bounded and within a safe range. In this regard, one should focus on the second system in (7.13). Later, it is shown that the same strategy is applicable to the feedback linearized diesel-generator speed dynamics ζ_1 .

Let z_2 and τ_2 be the state vector and the control action of the nominal system, respectively. Then, the nominal system is defined as:

$$\dot{z}_2 = A_2 z_2 + B_2 \tau_2 + [1, 0]^T \omega_{load}. \quad (7.14)$$

The first step for setting up a tube-based MPC strategy is extracting a nominal trajectory. For this aim, the nominal MPC problem is defined as:

$$\mathbb{P}(z_2) : \min_{\tau_2} \left(V_N(z_2, \tau_2) = \sum_{i=k}^{k+N-1} l(z_2(i), \tau_2(i)) + V_f(z_2(k+N)) \right) \quad (7.15)$$

subject to (7.14) with:

$$\begin{aligned} z_{2\min} &\leq z_2(k+i) \leq z_{2\max} \\ \tau_{2\min}(k+i-1) &\leq \tau_2(k+i-1) \leq \tau_{2\max}(k+i-1) \\ \forall i &\in [0, N], \end{aligned} \quad (7.16)$$

where $V_N(\cdot)$ is the MPC cost function, N is the prediction horizon, k is the discrete time step of the system with sample time T_{dc} and $V_f(\cdot)$ is the terminal cost defined as:

$$V_f(z_2^1(N)) = (z_2^1(N) - v_{\text{ref}})^2. \quad (7.17)$$

Moreover,

$$l(z_2^1(k), \tau(k)) = \alpha(z_2^1(k) - v_{\text{ref}})^2 + \beta\tau(k)^2, \quad (7.18)$$

where non-negative parameters α and β are weight factors.

Assumption 6 For all $z_2 \in [z_{2\min}, z_{2\max}]$, the state dependent disturbance $\omega_v(z_2^1) \approx 0$.

The above assumption indicates that if the DC voltage is kept within the desired range, the adverse effects of CPL do not emerge.

Considering (7.14), the error between the nominal system and the real system is:

$$e_2(t) = \zeta_2(t) - z_2(t). \quad (7.19)$$

To keep the error bounded and within the safety range, the below control rule for the actual system (7.13) is adopted [122]:

$$v_2(t) = \kappa_2(z_2(t)) + K_2(\zeta_2(t) - z_2(t)) \quad (7.20)$$

where $\kappa_2(z_2(t))$ is the first element in the solution set of (7.15) after filtering by a zero-order hold block, $t \in [k, k+1)$ and K_2 is a state feedback for the composite system below:

$$\begin{aligned} \dot{\zeta}_2(t) &= A_2\zeta_2(t) + B_2v_2(t) + \omega_2(\zeta_2(t)) \\ \dot{z}_2(t) &= A_2z_2(t) + B_2\tau_2(t) + [1, 0]^T \omega_{\text{load}} \end{aligned} \quad (7.21)$$

By taking into account (7.19) and (7.20), the error dynamics can be written as:

$$\dot{e}_2(t) = A_{K_2}e_2(t) + [1, 0]^T \omega_v(\zeta_2(t)) \quad (7.22)$$

where $A_{K_2} = A_2 + B_2K_2$. Hence, the objective is to keep $e(t)$ within a safe bound. Indeed, with this approach, the aim is to keep the disturbed system in a tube whose center is the trajectory of the nominal system. This is obtained by applying $\kappa_2(z_2(t))$, $t \in [k, k+1)$ to the nominal system. The block diagram of the proposed control methodology is shown in Figure 7.1. The proposed control approach contains two loops where the inner loop controls the nominal system with which a reference trajectory is extracted for the actual system and the outer loop steers the state of the system towards the trajectory of the nominal system using the control law (7.20). Please note that the sampling time of the controllers can be different, i.e., the outer loop can have a higher frequency compared to the inner loop. This is advantageous in the sense that solving the optimization problem is a time consuming process and increasing the sample time T_{dc} leads to reduced computational costs. Later, by introducing a strategy, we show that the MPC optimization problem can be solved using quadratic programming to further decrease the computational costs.

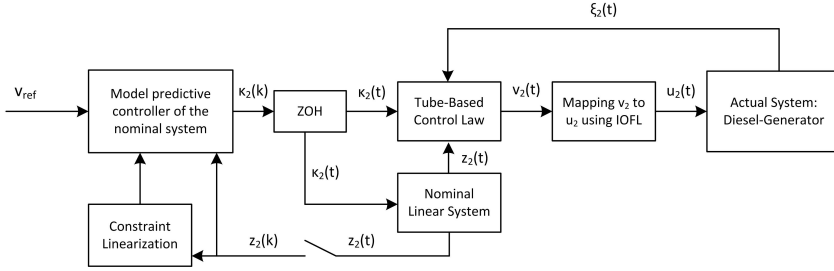


Figure 7.1: The block diagram of the control strategy.

7.2.3. STABILITY PROOF

In this part, the stability analysis of the methodology is carried out. First, it is shown that by proper regulation of control law (7.20), the error e_2 is asymptotically stable.

Before presenting the main stability theorem, the following assumptions are made:

Assumption 7 The load current i_{load} is bounded, i.e., there exists a non-negative integer i_{max} such that $|i_{\text{load}}| \leq i_{\text{max}}$.

Assumption 8 The disturbance function $\omega_v(\cdot)$ is Lipschitz continuous in a compact set centered around v_{ref} with radius ϵ , i.e., there exists a non-negative integer μ such that $|\omega_v(\zeta_2^1) - \omega_v(\zeta_{20}^1)| \leq \frac{\mu}{C} |\zeta_2^1 - \zeta_{20}^1|$, for all $\zeta_2^1, \zeta_{20}^1 \in \mathbb{B}(v_{\text{ref}}, \epsilon)$ where C is the capacitance of the DC-link capacitor.

The above assumptions indicate that the function of generated current as a result of CPLs adverse effects, is continuous around the operating point of the system.

In the following theorem, a criterion is proposed to keep the voltage around the reference voltage when adopting control law (7.20).

Theorem 3 Suppose the tube-based control law for the composite system (7.21) is:

$$v_2(k) = \kappa_2(z_2(k)) + K_2(\zeta_2(k) - z_2(k)) \quad (7.23)$$

and

$$M = \begin{bmatrix} \frac{\mu}{C} & 0 \\ 0 & 0 \end{bmatrix}. \quad (7.24)$$

If vector K_2 is chosen such that A_{K_2} is stable and

$$\lambda\{A_{K_2} + M\} < 0, \quad (7.25)$$

where μ is a Lipschitz constant of $\omega_v(\cdot)$, $\lambda\{A\}$ represents the eigenvalues of A , then e is asymptotically stable for all $t \geq 0$ and the state ζ_2 is bounded.

Proof 4 Consider the following Lyapunov function:

$$V(e) = \frac{1}{2} e_2^T e_2. \quad (7.26)$$

The derivative of V is:

$$\dot{V}(e) = e_2^T A_{K_2} e_2 + \omega_v [1, 0]^T e_2. \quad (7.27)$$

Considering Assumptions 1 and 3, there exists a non-negative integer with which the following equation holds:

$$\dot{V} < e_2^T A_{K_2} e_2 + e_2^T M e_2. \quad (7.28)$$

For correctness of $\dot{V} < 0$, $A_{K_2} + M$ should be negative definite. As a result,

$$\lambda\{A_{K_2} + M\} < 0 \quad (7.29)$$

Which indicates the asymptotic stability of e_2 .

The above result indicates that with a proper choice for K_2 , the origin is asymptotically stable for e_2 . So, the actual state ζ_2 converges to the nominal state z_2 .

Remark 10 The derived design condition (7.29) depends on the Lipschitz constant of ω_v . However, this does not imply that exact knowledge on μ is required since the user has freedom to choose K such that the possible large values of μ are compensated. Moreover, $\tau_{2\min}$ and $\tau_{2\max}$ can be chosen such that v is within an acceptable range [122].

7.2.4. CONSTRAINT LINEARIZATION

For DC voltage regulation and control of the diesel-generator shaft speed, the controllers should be able to calculate the control actions within milliseconds. Since after feedback linearization, linear bounds of the input constraint sets turn into nonlinear bounds of the MPC output, nonlinear methods are necessary for solving the optimization problem which results in increased computational costs and possible latency in the control loop. In this part, based on the results in [120],[119], a strategy is proposed to transform the nonlinear input constraints into linear constraints so that quadratic programming methods are applicable.

Consider the constraints of the original system (7.3). The aim is to translate these constraints so that they can be used by the MPC problem (7.15). Note that the output constraints of the MPC problem (7.16) are identical to the original output constraints in (7.3). However, since

$$v = \begin{bmatrix} v_1 \\ v_2 \end{bmatrix} = \begin{bmatrix} \Psi_1(x, u) \\ \Psi_2(x, u) \end{bmatrix} = \Delta(x)u - \begin{bmatrix} L_f^2 y_1 \\ L_f^2 y_2 \end{bmatrix}, \quad (7.30)$$

the input constraints cannot be found straightforwardly. In the ideal case and by adopting the above relationship, the input constraints of nominal system (7.14) over horizon N for solving MPC problem (7.15) at time constant k are:

$$\begin{aligned} \tau_{2\min}(k+i-1) &\geq v_{2\min}(k+i-1) \\ \tau_{2\max}(k+i-1) &\leq v_{2\max}(k+i-1), \end{aligned} \quad (7.31)$$

where

$$\begin{aligned} v_{2_{\min}}(k+i-1) &= \min_{u_2(k+i-1)} \Psi_2(x(k+i), u(k+i-1)) \\ v_{2_{\max}}(k+i-1) &= \max_{u_2(k+i-1)} \Psi_2(x(k+i), u(k+i-1)), \end{aligned} \quad (7.32)$$

subject to:

$$u_{\min} \leq u(k+i-1) \leq u_{\max}, \forall i \in [0, N]. \quad (7.33)$$

The constraints on nominal system input can be chosen tighter compared to the constraints acting on v so that after applying the control law, v satisfies its constraints [122].

The problem with the exact mapping of constraints is that future values of states x and inputs u are not immediately available and should be found by solving a nonlinear optimization problem which employs predicted values of x over the horizon N . Obviously, this strategy is very time consuming and eliminates the advantages of adopting an MPC-based control strategy. However, the exact mapping of the future input constraints is impractical since $v_{2_{\min}}(k+i)$, $i \in [0, N]$ are not implemented. As a result, a strategy is adopted with which $v_{2_{\min}}(k+i)$ and $v_{2_{\max}}(k+i)$ are approximated over the prediction horizon and $v_{2_{\min}}(k)$ and $v_{2_{\max}}(k)$ represent exact values.

To this end, using (7.32), we have:

$$\begin{aligned} v_{2_{\min}}(k+i-1) &= \min_{u_2(k+i-1)} \Psi_2(x(k), u(k+i-1)) \\ v_{2_{\max}}(k+i-1) &= \max_{u_2(k+i-1)} \Psi_2(x(k), u(k+i-1)) \end{aligned} \quad (7.34)$$

$$\forall i \in [0, N].$$

Solving the above problem is straightforward as $x(k)$ is known and $u(k+i-1)$ appears linearly in function $\Psi(\cdot)$. Using the above equation, it is guaranteed that the implemented control action is within the exact constraints of the actual system. Furthermore, finding the input variable bounds for the rest of the horizon is computationally trivial if (7.34) is adopted.

7.2.5. EXTENSION TO DIESEL-GENERATOR SHAFT SPEED CONTROL

The proposed robust MPC-based control strategy can be adopted for controlling the diesel-generator shaft speed. In this case, the nominal system is defined as:

$$\dot{z}_1 = A_1 z_1 + B_1 \tau_1. \quad (7.35)$$

To extract a desired trajectory for the actual system a similar MPC problem to (7.15) with sampling time T_{dg} should be solved:

$$\mathbb{P}(z_1) : \min_{\tau_1} \left(V_N(z_1, \tau_1) = \sum_{i=k}^{k+N-1} l(z_1(k), \tau_1(k)) + V_f(z_1(N)) \right) \quad (7.36)$$

subject to (7.35) and,

$$\begin{aligned} z_{1\min} &\leq z_1(k+i) \leq z_{1\max} \\ \tau_{1\min}(k+i-1) &\leq \tau_1(k+i-1) \leq \tau_{1\max}(k+i-1) \\ \forall i &\in [0, N] \end{aligned} \quad (7.37)$$

where

$$\begin{aligned} \tau_{1\min}(k+i-1) &\geq v_{1\min}(k+i-1) \\ \tau_{1\max}(k+i-1) &\leq v_{1\max}(k+i-1) \end{aligned} \quad (7.38)$$

and

$$\begin{aligned} v_{1\min}(k+i-1) &= \min_{u_1(k+i-1)} \Psi_1(x(k), u(k+i-1)) \\ v_{1\max}(k+i-1) &= \max_{u_1(k+i-1)} \Psi_1(x(k), u(k+i-1)). \\ \forall i &\in [0, N]. \end{aligned} \quad (7.39)$$

The auxiliary control law to steer the actual states towards the states of the nominal system is:

$$v_1(t) = \kappa_1(z_1(t)) + K_1(\zeta_1(t) - z_1(t)). \quad (7.40)$$

Note that in the case of diesel-generator shaft speed control, the unknown disturbance ω_d is additive and not state dependent. However, ω_d is bounded and lies in a compact set, i.e., $\omega_d \in \mathbb{W}_d$. If \mathbb{W}_d is small enough it can be ensured that $v_{1\min}(k+i-1) \leq v_1(k+i-1) \leq v_{1\max}(k+i-1)$ for all $i \in [0, N]$ [122]. Such an assumption is not uncommon in robust control, since if \mathbb{W}_d is too large, there is no possibility for satisfying the constraints and, as a result, controlling the shaft speed is impossible.

7.3. INTEGRATION WITH MANEUVERING CONTROL

After applying the IOFL rule 5.2 to the solution of the optimization problem in (5.4), a set of input variables over the prediction horizon is obtained that is $\{\tau_s^*(k), \tau_s^*(k+1), \dots, \tau_s^*(k+N_v-1)\}$. Using the mathematical model of propellers, the efficiency curve of induction motors, and measurement of the DC current of other loads on board of the ship at the DC-link, load current i_{load} can be approximated over prediction horizon N_v , that is, $\{i_{\text{load}}^*(k), i_{\text{load}}^*(k+1), \dots, i_{\text{load}}^*(k+N_v-1)\}$. Note that the sampling time of the MPC problem in 5.2 is larger than the sampling time of the MPC problem in (7.15). As a result, the availability of knowledge over i_{load} is guaranteed for voltage regulation.

All in all, the proposed algorithm for the DC voltage regulation and shaft speed control of the diesel-generator, combined with the ship motion control can be presented in the following algorithm.

- **Initialization:** At time $t = 0$, set $z_1(0) = \zeta_1(0)$ and $z_2(0) = \zeta_2(0)$ and receive the initial set of $\{i_{\text{load}}^*(0), i_{\text{load}}^*(1), \dots, i_{\text{load}}^*(N_v-1)\}$.
- 1. **Solving MPC problems:** At time $t = kT_{dc}$, $k = 0, 1, 2, \dots$, solve MPC problem $\mathbb{P}(z_2)$ in (7.15) to obtain nominal control action $\kappa_2(z_2)$ and at time $t = kT_{dg}$, $k = 0, 1, 2, \dots$ solve MPC problem $\mathbb{P}(z_1)$ in (7.36) to gain $\kappa_1(z_1)$.

2. **Computing tube-based control laws:** Compute tube-based control law $v_1(t) = \kappa_1(z_1(t)) + K_1(\zeta_1(t) - z_1(t))$ for $kT_{dg} \leq t < (k+1)T_{dg}$ and $v_2(t) = \kappa_2(z_2(t)) + K_2(\zeta_2(t) - z_2(t))$ for $kT_{dc} \leq t < (k+1)T_{dc}$.
3. **Apply control:** Using the mapping rule (7.10) calculate u and apply it to the system.
4. **Update:** Measure x and go to 3. If $t \geq (k+1)T_{dg}$ or $t \geq (k+1)T_{dc}$ go to 1.

As mentioned in the previous section, the sampling time of the DC voltage controller and diesel-generator shaft speed controller can be different, which is reflected in the algorithm. Moreover, tube-based control laws can be executed several times in between of two consecutive sequence of MPC problems calculation.

In the next section, several experimental results are carried out for evaluating the performance of the controller.

7.4. SIMULATION EXPERIMENTS

The performance of the proposed methodology is assessed using a simulated vessel model from Damen Gorinchem Shipyard. The vessel length is 90m and its displacement at design draft is 2700 ton. For evaluating the performance of the proposed control approach, a high-voltage DC microgrid is considered. The microgrid represents an existing grid, i.e., the mathematical model of components are verified high fidelity models. For propulsion two sets of asynchronous machine-propeller each with 1.8 MW power are considered. The induction motors are controlled by motor controller-inverters that are connected to the DC-link. The specifications of the simulation model components are given in Appendix A.3. The experiments are carried out on a PC with 2.8GHz Intel Core i7-7600U CPU and 8GB RAM. The MATLAB® 2018a Simscape toolbox is partially used for the development of the model. To evaluate the performance of the proposed control approach, three experiments are considered. First, The ship motion is considered with different speeds. The robustness of the proposed approach is evaluated in the second experiment and in the third experiment, the voyage of the ship with a high speed is considered for relatively a long voyage.

7.4.1. MODEL VALIDATION

The diesel engine and synchronous generator models and their performance data are provided by ShipDrive project partner Damen Schelde Naval Shipbuilding. The diesel engine has twelve cylinders and its nominal power and speed are 5400 kw and 16.71 rps, respectively. For more information about the diesel engine model refer to [27]. The synchronous generator is a 6150 kvA machine with 6600 v nominal line-to-line voltage. Based on the standard per-unit (pu) parameters, the fundamental model of the generator is extracted. Then, the model is validated using the generator's performance data. The validation results are illustrated in Figure 7.2. The empirical test results are compared with the results of our model. For this purpose, the generator is connected to a three phase load. The results indicate high accuracy of the model that is less than 1.5 % error for different output powers. The three phase current of the generator is provided in Figure 7.3.

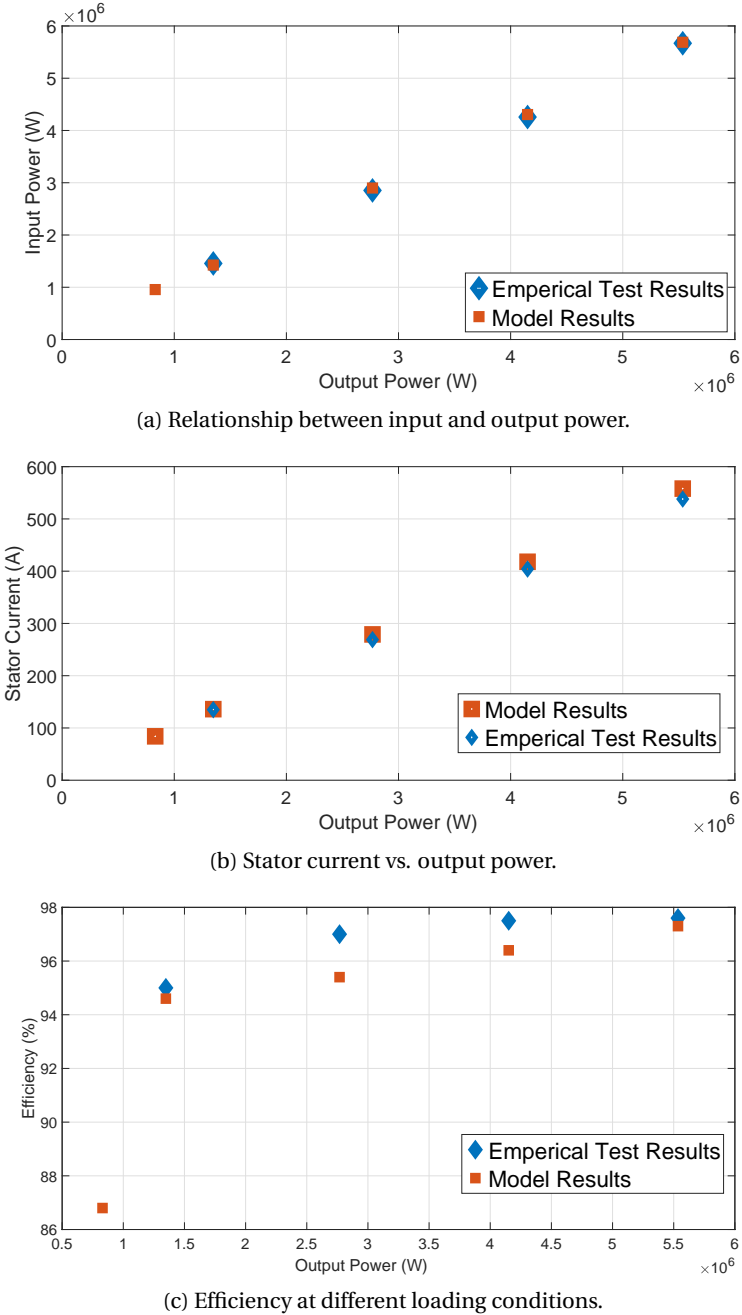


Figure 7.2: Synchronous generator's model results vs. empirical test results.

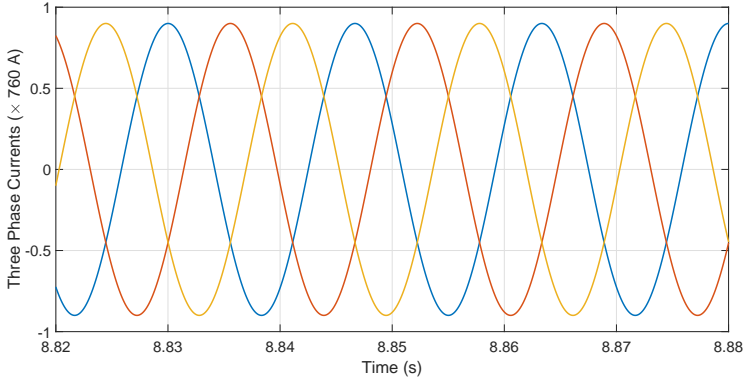


Figure 7.3: Three phase currents at 5535 kw load.

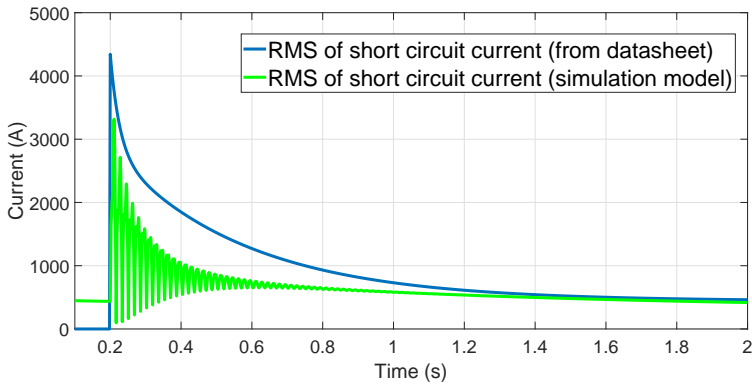


Figure 7.4: Short circuit current: model vs. datasheet.

A symmetric short circuit experiment is also carried out. Based on the transient and subtransient time constants and reactances of the synchronous generator, the short circuit transient response is calculated. The comparison of the Root-Mean-Square (RMS) value of the short circuit current and the computed short circuit current (based on the datasheet) are shown in Figure 7.4. The results indicate sufficient accuracy of the DGR transients.

The evolution of the open loop system eigenvalues is shown in Figure 7.5 when the system is under a 5 MW CPL which changes to 2.5 MW during the simulation. For this purpose, (7.1) is linearized around its operating point. It can be observed that some eigenvalues are positive, some are marginally negative and some change when the loading condition changes. The open loop response of the system is shown in Figure 7.6 where the system is under a 1.4 MW (≈ 0.25 per unit) CPL. The field voltage and the fuel index are $V_f = 1.05$ and $f_{en} = 0.25$ which are chosen based on the synchronous generator

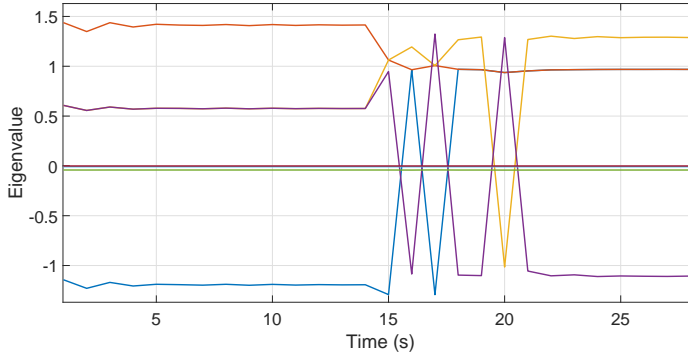


Figure 7.5: The eigenvalues of the DGR set.

data sheet. It is seen that the voltage and speed are falling and do not stay around their desired value. In the remainder of this section, through different experiments, it is shown that the proposed robust MPC controller is capable of keeping the system stable during its operation; in the presence of CPL and sudden changes in the loading conditions.

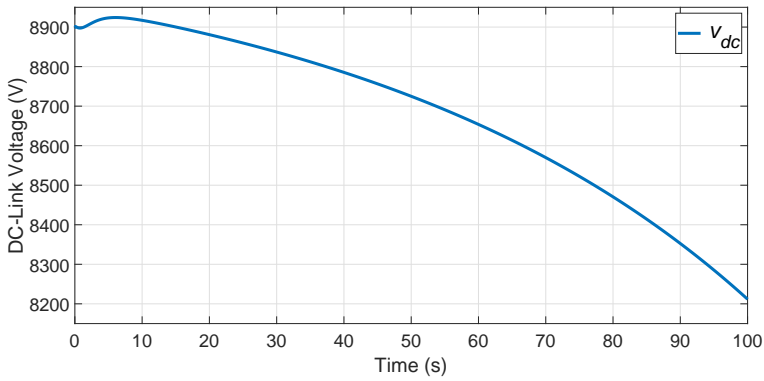
7.4.2. EXPERIMENT I: VOLTAGE CONTROL UNDER VARYING SHIP SPEED

In this experiment, the propelling load in Section 5.2 is applied to the high voltage power system. It is also assumed that other on-board loads are consuming 800 kw of power. The sampling time of the voltage controller is $T_{dc} = 0.01$ s and the sampling time of the engine governor is $T_{dg} = 0.1$ s. Furthermore, $K_1 = [-21 \ -32]$ and $K_2 = [-30 \ -10]$. DC voltage constraints are $8800 \leq V_{dc} \leq 9000$. It is assumed that the sample time of the ship controller is 10 s and its prediction horizon is $N_v = 10$. As explained in Section 4, using the predicted future control inputs, i_{load} is computed for DC voltage regulation purpose. The prediction horizons of the robust predictive controllers of the DC voltage and diesel-generator shaft speed are chosen as $N = 20$.

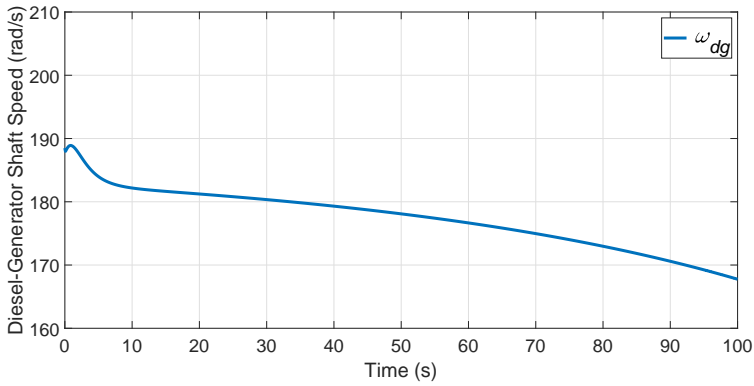
In this experiment, to make the situation for the power system controllers challenging, the ship speed controller is regulated such that it behaves aggressively, i.e., for reaching the desired speed, a very high control input (generated thrust by propellers) is applied and then, as soon as the speed is around the desired speed, the control input effort reduces. Figure 7.7 shows the ship speed and the applied propeller thrust.

The simulation results of the power system are provided in Figure 7.8. The voltage of the DC-link is shown in Figure 7.8a which is stable around its desired value, i.e., 8900 v. The synchronous generator simulation results are provided in pu with line-to-line voltage of 6600 v and 6150 kW apparent power. The field voltage applied to the generator is shown in Figure 7.8b and Figure 7.8c illustrates the generated DC current by the DGR set.

The results of the mechanical variables are shown in Figure 7.9. The diesel-generator's shaft speed is shown in Figure 7.9a which is kept stable around the desired value, i.e., 188 rad/s which is an indication of network frequency stability. The fuel index of the diesel

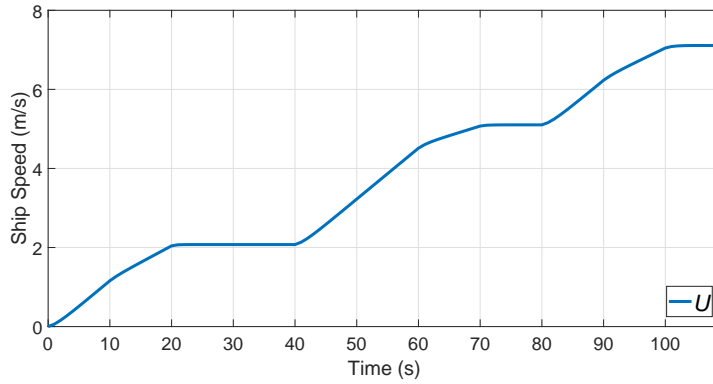


(a) The DC-link voltage.

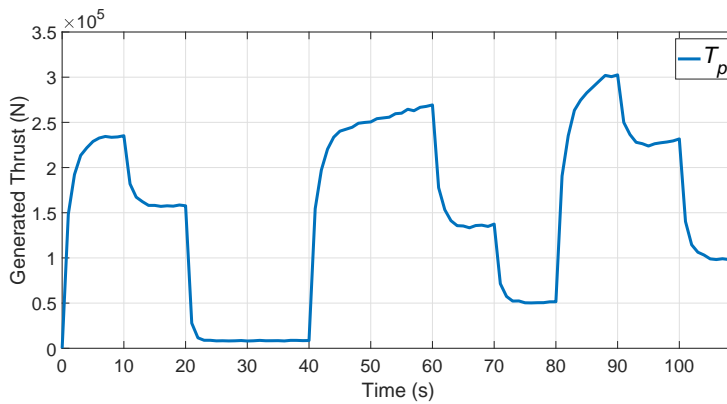


(b) Diesel-generator shaft speed.

Figure 7.6: Open loop response of the system.

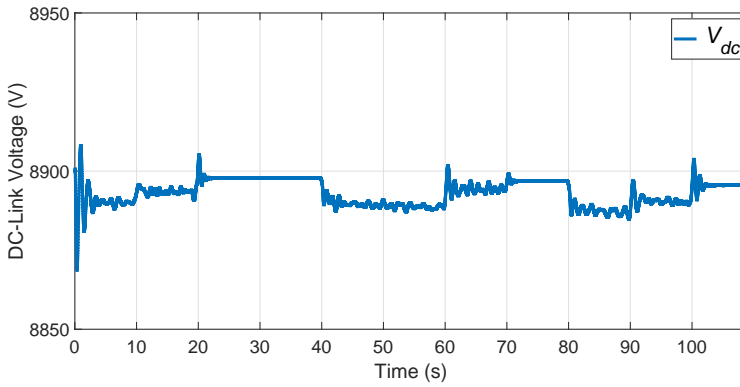


(a) Ship speed increasing during the simulation.

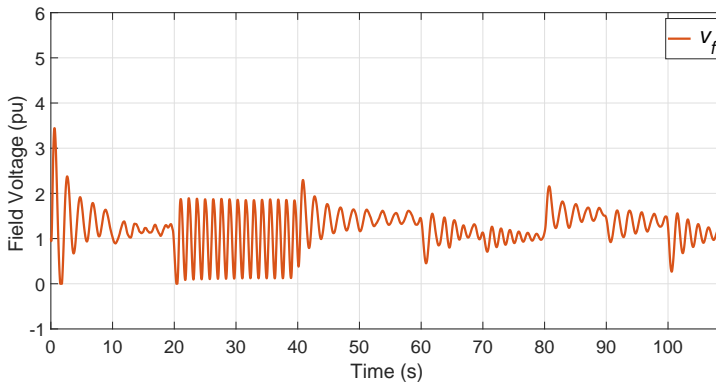


(b) Generated thrust by propellers.

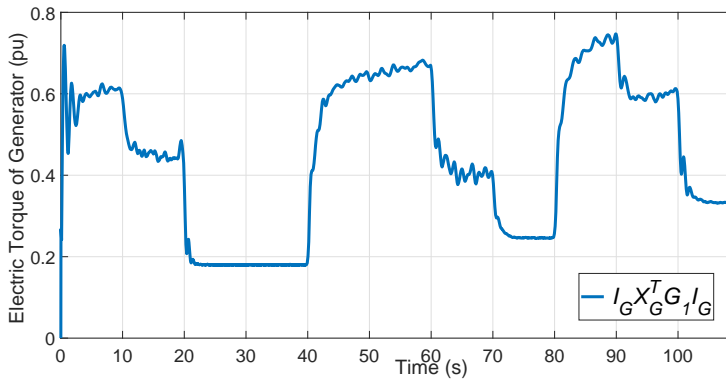
Figure 7.7: The ship speed vs the generated thrust and the propeller shafts speed in Experiment I.



(a) The DC voltage of the capacitor.



(b) Field voltage of the synchronous generator.



(c) Electric torque of the generator.

Figure 7.8: The results of Experiment I using robust MPC approach.

engine is shown in Figure 7.9b and the generated torque by the diesel engine is given in Figure 7.9c.

To compare the results of the proposed control approach with the conventional Proportional Integral (PI)-based approaches, this experiment is carried out using PI control approaches as well. For control of v_{dc} , single voltage-controller approach is used [21], [125]. The block diagram of the controller is represented in Figure 7.10. The controller is regulated using the transient time constant of the generator and the rough estimation of relationship between v_f and terminal voltages of the generator [125]. As a result, $K_p = 294.75$, $K_i = 2.3$, $T_1 = 0.001s$ and $T_2 = 0.01s$. Ziegler-Nichols tuning approach is used to regulate the PI controller acting on the fuel index. For the diesel engine governor, the PI variables are $K_p = 36.2$ and $K_i = 30.4$. The variables are extracted under 2.5 MW loading condition.

The simulation results of the PI-based approach are presented in Figure 7.11. Although, the PI-based control approach is capable of providing stability in this example but the fluctuation of input and output variables are higher than the robust MPC approach. The tracking error of output variables are provided in Figure 7.12.

7.4.3. EXPERIMENT II: FAULT-TOLERANCE UNDER A CPL

In this experiment, the high voltage power system is exposed to a short circuit fault and a sudden load drop. The fault happens between rectifier and the DC-link capacitor at $t = 35.1s$ and ends at $t = 35.15s$. The fault resistance is 0.1 ohm. The sudden load drop happens at $t = 20s$ where the load is dropped from 4 MW to 2 MW. The proposed control approach performance is compared with the conventional PI-based control algorithm.

The results of the experiment are shown in Figure 7.13. In Figure 7.13a, the DC voltage trajectory is shown. The proposed robust MPC approach can keep the voltage around the desired voltage before and after the short circuit. Using the PI scheme, less voltage fall happens during the short circuit compared to the robust MPC approach while the voltage recovery is slower. On the other hand, using the PI controller, the field voltage fluctuation is more and the system is not recovered after the short circuit. The diesel-generator shaft speed results are shown in Figure 7.14 which indicates the success of the proposed strategy in keeping the system stable.

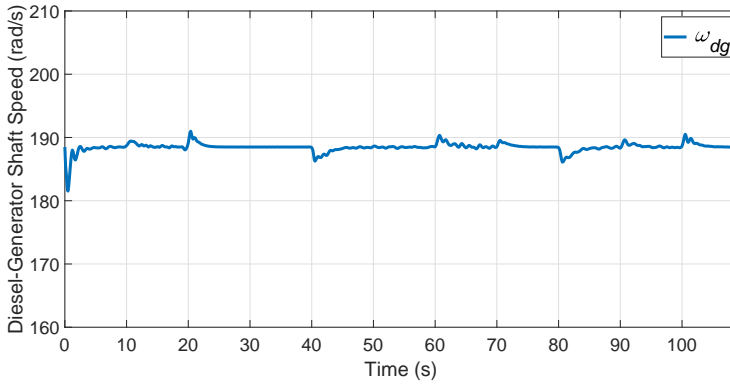
7.4.4. EXPERIMENT III: HIGH SPEED VOYAGE

In this experiment, a voyage of an inland cargo vessel is considered in the port of Rotterdam. The speed data is provided by the port of Rotterdam authority. The real vessel speed is tripled so the it represents a challenging operating profile. The simulation results of the vessel speed is shown in Figure 7.15.

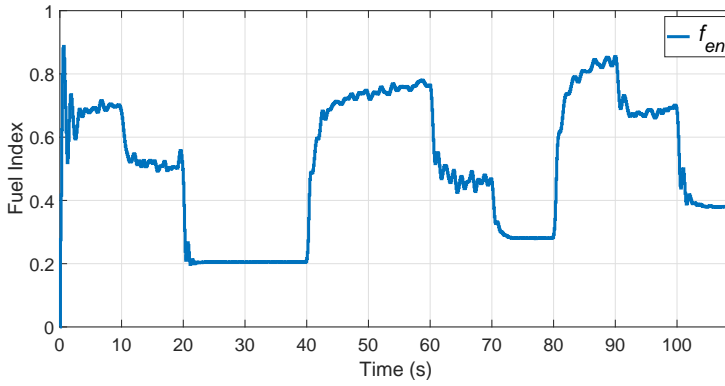
The simulation results of the power system are shown in Figure 7.16. The DC voltage and the shaft speed of the diesel-generator are kept stable close to their reference value using the proposed robust MPC approach.

7.5. CONCLUSIONS

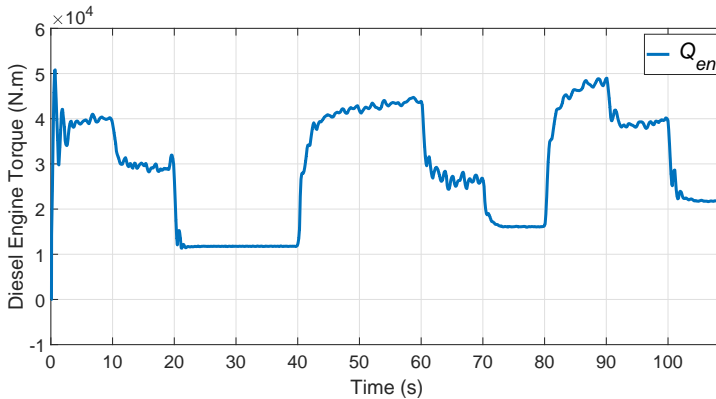
In this chapter, a robust MPC-based algorithm has been presented for stabilization of the DC voltage on board of all-electric ships with a set of diesel-generator connected to



(a) The shaft speed of diesel-generator.



(b) Fuel index.



(c) Diesel engine torque.

Figure 7.9: The results of Experiment III.

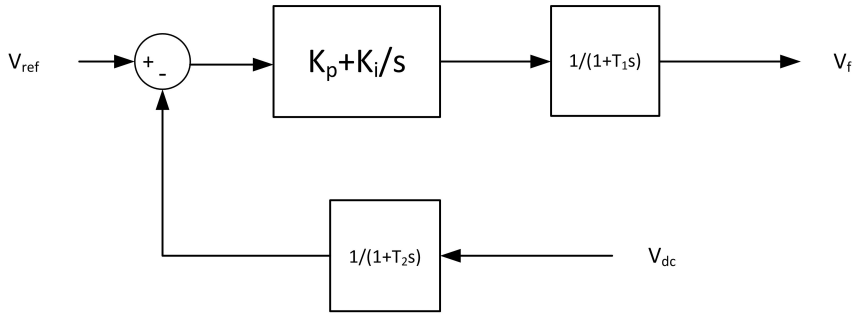
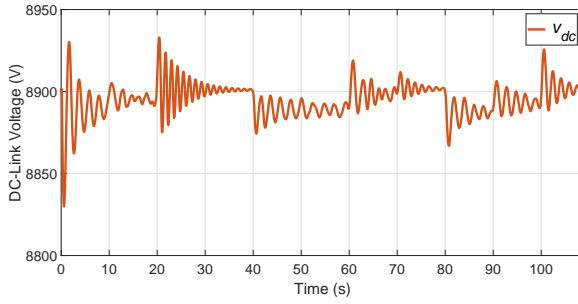


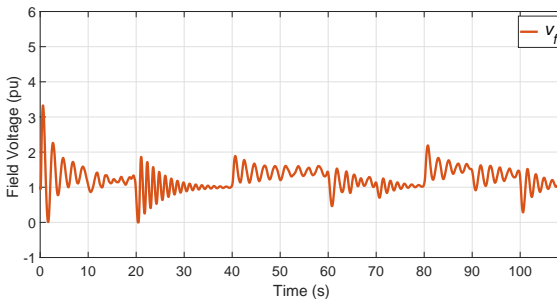
Figure 7.10: The block diagram of the PI-based voltage controller.

an uncontrollable rectifier. The stability proof of the proposed algorithm is carried out and it is shown that it can handle the adverse effects of CPLs as well as sudden changes in the load condition. Moreover, it is shown that the algorithm can be combined with ship motion control algorithm where the predicted propulsive load can be utilized by the proposed control approach. The performance of the approach is evaluated through several simulation experiments that are carried out using a ship model that is provided by Damen Gorinchem Shipyard and power system components that are provided by Damen Schelde Naval Shipbuilding. This research demonstrates the viability of using MPC algorithms for dealing with stability issues of on-board power systems. The results of this research work can also be used in other domains such as electric-hybrid vehicles and local DC microgrids. The results in this chapter provide answers to Research Questions 6 and 7.

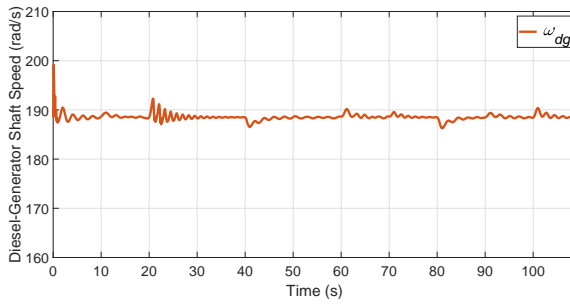
Most of all-electric ships have more than one set of DGR on-board which are combined with a hybrid energy source such as battery. This combination makes the voltage regulation more challenging since different devices are included with different dynamics. As a result, Chapter 8 aims at designing cooperative control algorithms for DC voltage regulation on board of ships with multiple energy sources.



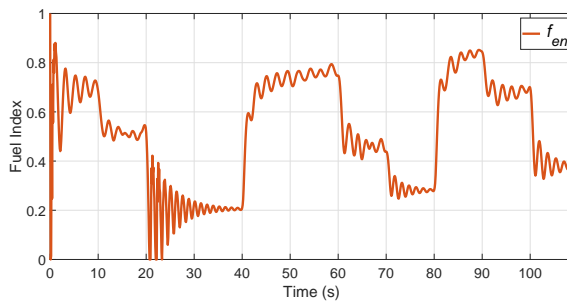
(a) The DC voltage of the capacitor.



(b) Field voltage of the synchronous generator.

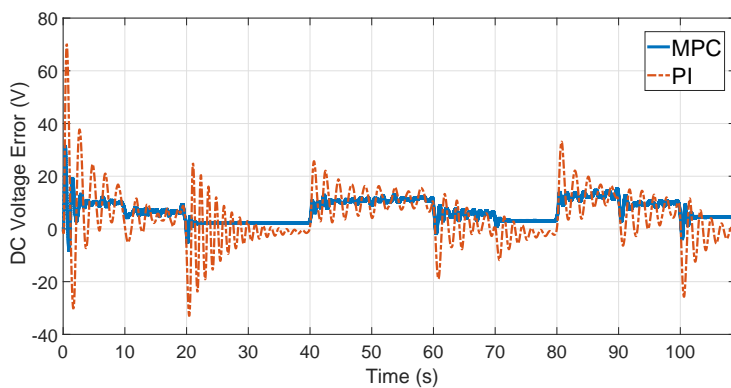


(c) Diesel-generator shaft speed.

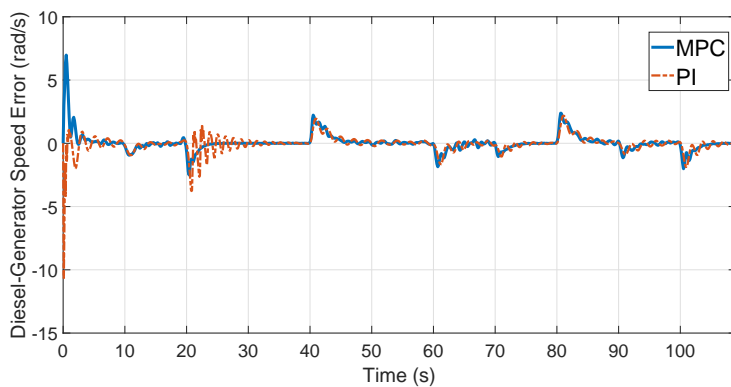


(d) Fuel index.

Figure 7.11: The results of Experiment I using PI-based approach.

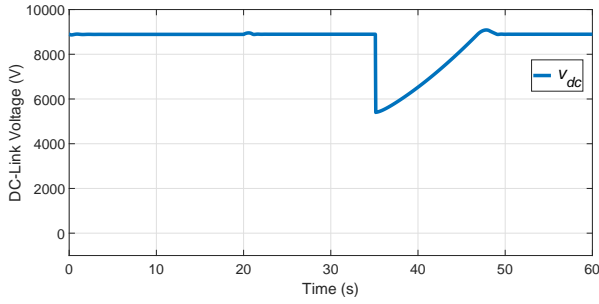


(a) The DC voltage (v_{dc}) tracking error.

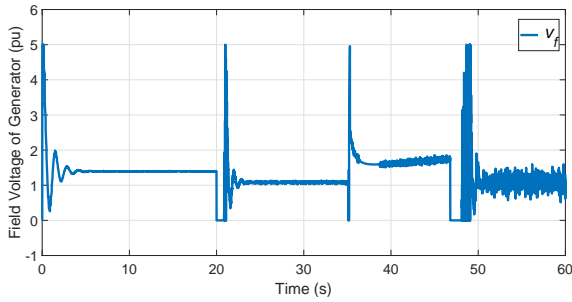


(b) Diesel-generator shaft speed (ω_{dg}) tracking error.

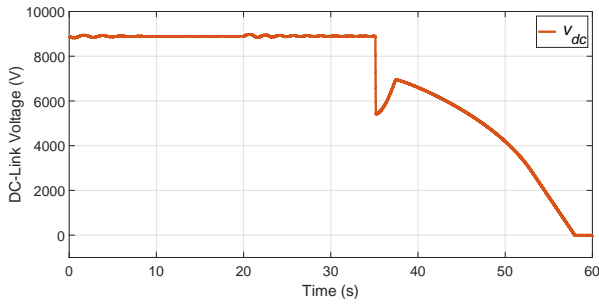
Figure 7.12: The results of Experiment I using PI-based approach.



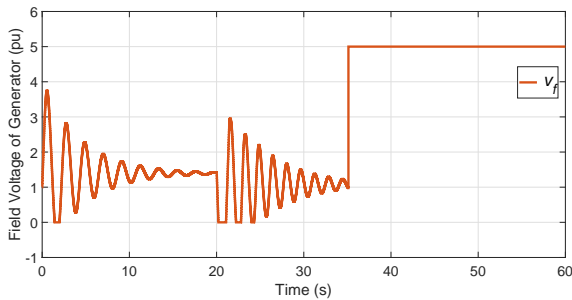
(a) The DC voltage of the capacitor (robust MPC).



(b) Field voltage of the synchronous generator (robust MPC).

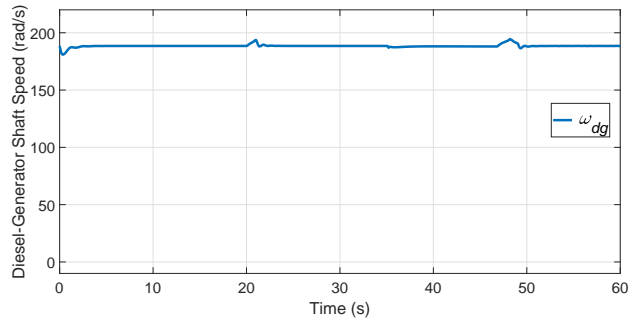


(c) The DC voltage of the capacitor (PI control).

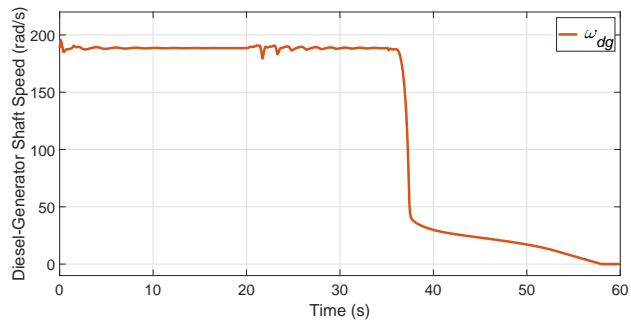


(d) Field voltage of the synchronous generator (PI control).

Figure 7.13: The results of short circuit experiment (MPC vs. PI).

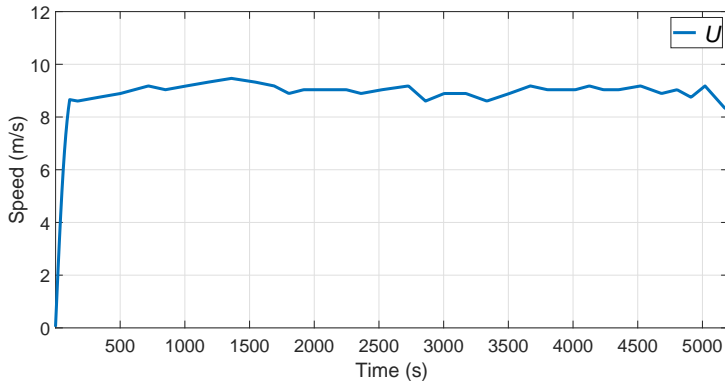


(a) Diesel-generator shaft speed (robust MPC).

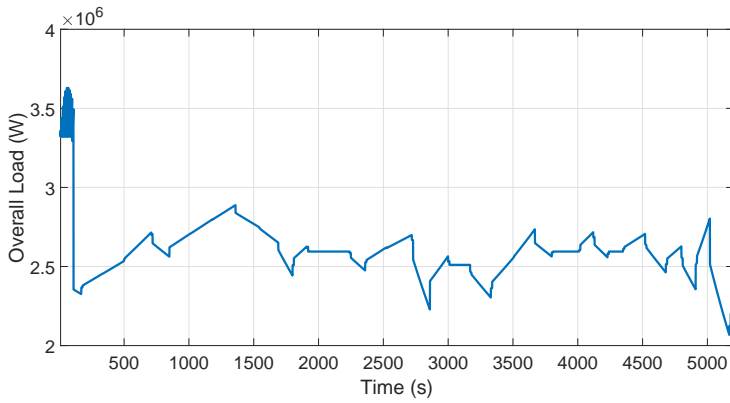


(c) Diesel-generator shaft speed (PI control).

Figure 7.14: The results of short circuit experiment (MPC vs. PI).

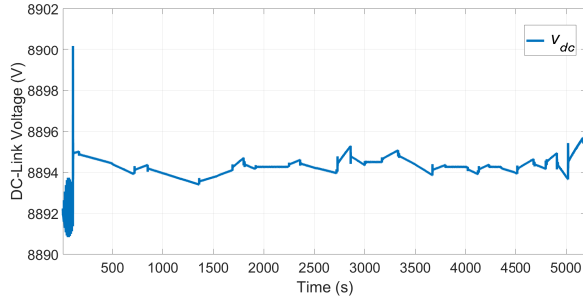


(a) Ship speed.

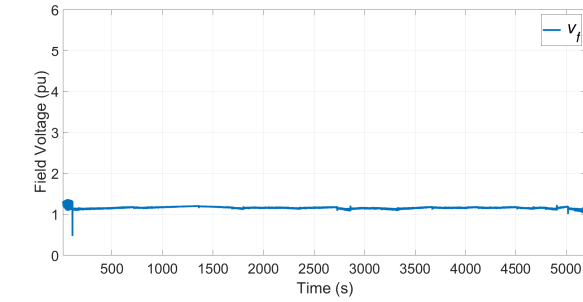


(b) Overall load applied to the DGR set.

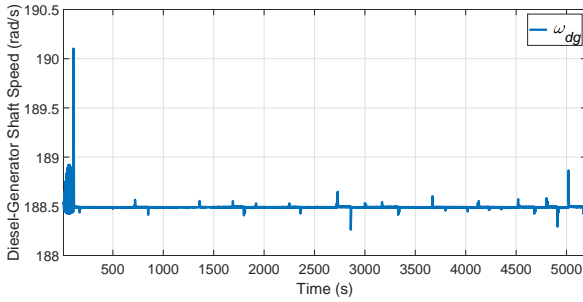
Figure 7.15: Ship speed and propelling thrust during the voyage.



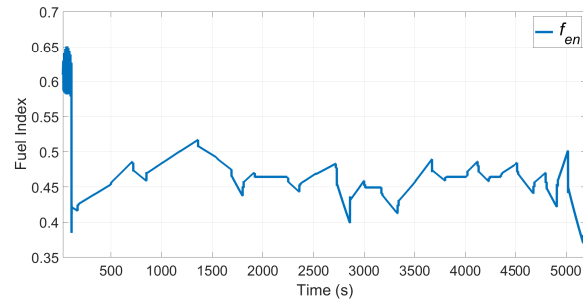
(a) The DC voltage of the capacitor.



(b) Field voltage of the synchronous generator.



(c) Diesel-generator shaft speed.



(d) Fuel index.

Figure 7.16: Results of Experiment III.

8

MULTI-LEVEL CONTROL OF ENERGY GENERATION SIDE

The control and stabilization of DGR sets have been discussed in Chapter 7. In this chapter, by extending the results of Chapter 7, the stability of the overall PPS is under focus where the objective is to control the DC-link voltage as well as speed of the diesel-generator sets in the presence of Constant Power Loads (CPL). The results of Chapter 7 are used for the control of DGR sets. Moreover, it is shown that how the content of this chapter is integrated with the proposed approaches for energy management and maneuvering control. The content of this chapter have been partially published in a scientific paper.¹

For power generation control, an MPC-based multi-level control approach is proposed. On the top level a coordinating controller is considered which is determined to control the voltage of the DC-link capacitor. Through this controller, the reference DC currents are calculated which are sent to the controllers on the second level. These so-called low level controllers aim at controlling the generated current by the energy sources. A tube-based MPC scheme is used for the control of the DC voltage and similar to Chapter 7, Input-Output Feedback Linearization (IOFL) is adopted for linearization. Through simulation experiments, the performance of the algorithm is evaluated. In Section 8.1, the state space model of the system under study is presented. The proposed control strategy is discussed in Section 8.2 and its performance is evaluated in Section 8.3.

¹Parts of this chapter have been published in:

1. A. Haseltalab, F. Wani, R. R. Negenborn, "Multi-level Power Generation Control for All-Electric Ships," Submitted to an international control journal, 2019.

8.1. STATE SPACE MODELING OF ENERGY GENERATION SIDE

In the chapter, the objective is to control the DC-link voltage by controlling the generated DC current by each energy source that is either a DGR set or a battery-converter set. Based on the results in Chapter 3, the mathematical model of the energy generation side is:

$$\begin{aligned}
 \dot{I}_{G_1} &= X_{G_1}^{-1} S_\omega(\omega_{dg_1}) X_{G_1} I_{G_1} + X_{G_1}^{-1} R_{G_1} I_{G_1} \\
 &\quad + v_{dc} X_{G_1}^{-1} E_1 + X_{G_1}^{-1} b v_{fd_1} \\
 \dot{\omega}_{dg_1} &= \frac{1}{2H_1} \left(Q_{en_1} - I_{G_1}^T X_{G_1}^T G_1 I_{G_1} \right) \\
 \dot{Q}_{en_1} &= -\frac{Q_{en_1}}{\tau_{s_1}} + K_{en_1} f_{en_1} \\
 &\quad \vdots \\
 \dot{I}_{G_m} &= X_{G_m}^{-1} S_\omega(\omega_{dg_m}) X_{G_m} I_{G_m} + X_{G_m}^{-1} R_{G_m} I_{G_m} \\
 &\quad + v_{dc} X_{G_m}^{-1} E_m + X_{G_m}^{-1} b v_{fd_m} \\
 \dot{\omega}_{dg_m} &= \frac{1}{2H_m} \left(Q_{en_m} - I_{G_m}^T X_{G_m}^T G_1 I_{G_m} \right) \\
 \dot{Q}_{en_m} &= -\frac{Q_{en_m}}{\tau_{s_m}} + K_{en_m} f_{en_m} \\
 \dot{i}_L &= \frac{d}{L} v_{dc} - \frac{v_b(t)}{L} \\
 \dot{v}_{dc} &= \frac{1}{C} \left(\beta_{rec_1} \sqrt{I_{G_1}^T G_2 I_{G_1}} + \dots + \beta_{rec_m} \sqrt{I_{G_m}^T G_2 I_{G_m}} + D i_L - \frac{P}{v_{dc}} \right),
 \end{aligned} \tag{8.1}$$

where

$$E_j = \begin{bmatrix} \alpha_{rec_j} \sin(\arctan\left(\frac{i_{d_j}}{i_{q_j}}\right) - \phi_{rec_j}) \\ \alpha_{rec_j} \cos(\arctan\left(\frac{i_{d_j}}{i_{q_j}}\right) - \phi_{rec_j}) \\ 0 \\ 0 \\ 0 \end{bmatrix}. \tag{8.2}$$

In the above system, the inputs are $v_{fd_1}, \dots, v_{fd_m}$ and $f_{en_1}, \dots, f_{en_m}$. The system outputs are $\omega_{dg_1}, \dots, \omega_{dg_m}$ and v_{dc} . In this chapter, the objective is to control v_{dc} by controlling the overall generated DC current by the energy sources in a two-level hierarchical MPC-based scheme.

8.2. PROPOSED CONTROL STRATEGY

In this section, the proposed two-level control approach is explained. This strategy is based on determining the required current by a supervisory controller to keep the DC voltage at its nominal value and then, providing the current by controlling the DC current output of the energy sources, i.e., DGR sets and the battery-converter set.

In this section, first, the control approaches for the low level controllers are presented. These modules are responsible for controlling the DC current generated by the energy sources, i.e., DGR sets and the battery-converter set. For this aim, similar to Chapter 7, an MPC accompanied by a IOFL scheme is adopted. Then, the higher control level is discussed which aims at determining feasible desired DC current that should be generated by energy sources. A schematic diagram of the overall control approach is shown in Figure 8.1.

8.2.1. CONTROL OF THE DGR SETS

In this part, the proposed approach for the control of DGR sets is explained. The mathematical model of DGR set j is:

$$\begin{aligned}\dot{I}_{G_j} &= X_{G_j}^{-1} S_{\omega}(\omega_{dg_j}) X_{G_j} I_{G_j} + X_{G_j}^{-1} R_{G_j} I_{G_j} \\ &\quad + v_{dc} X_{G_j}^{-1} E_j + X_{G_j}^{-1} b v_{fd_j} \\ \dot{\omega}_{dg_j} &= \frac{1}{2H_j} (Q_{en_j} - I_{G_2}^T X_{G_j}^T G_j I_{G_j}) \\ \dot{Q}_{en_j} &= -\frac{Q_{en_j}}{\tau_{s_j}} + K_{en_j} f_{en_j},\end{aligned}\tag{8.3}$$

where $y_1^j = \omega_{dg_j}$ and $y_2^j = I_{G_j dc} = \beta_{rec_j} \sqrt{I_{G_j}^T G_2 I_{G_j}}$ are the outputs to be controlled by the controller. The system inputs are f_{en_j} and v_{fd_j} . The overall number of states is $n = 7$ with generator's currents I_{G_j} , diesel-generator shaft speed ω_{dg_j} , and diesel engine torque Q_{en_j} being the states of the system.

The above system can be represented as,

$$\begin{aligned}\dot{x}_j &= f_j(x) + \sum_{i=1}^2 g_i^j(x) u_i^j \\ y_i^j &= h_i^j(x) \quad i = 1, 2,\end{aligned}\tag{8.4}$$

where x_j is the vector of states and u_1^j and u_2^j are the system inputs. Function $f_j : \mathbb{R}^7 \rightarrow \mathbb{R}^7$ is the state transition function. Moreover, $g_1^j(x) = [X_{G_j}^{-1} b, 0, 0]^T$, $g_2^j(x) = [0, 0, K_{en_j}]^T$.

System (8.3) is said to be input-output feedback linearizable if the vector of relative degrees exists under Conditions 1 and 2 presented in Section 7.2.1. By applying the Lie derivative to the system outputs, the decoupling matrix is calculated as,

$$\Delta(x_j) = \begin{bmatrix} \frac{1}{H_j} I_{G_j}^T X_{G_j}^T G_1 X_{G_j}^{-1} b & \frac{K_{en_j}}{2H_j} \\ \frac{I_{G_j}^T G_2 X_{G_j}^{-1} b}{\sqrt{I_{G_j}^T G_2 I_{G_j}}} & 0 \end{bmatrix},\tag{8.5}$$

with $\{2, 1\}$ as the vector of relative degrees. Note that the above matrix is nonsingular around the operating points of the system. As a result, a nonlinear coordinate transformation can be established by choosing the first $r = r_1 + r_2 = 3$ coordinates as,

$$\zeta_l^i = \Phi_l^i(x_j) = L_{f_j}^{i-1} h_l(x_j),\tag{8.6}$$

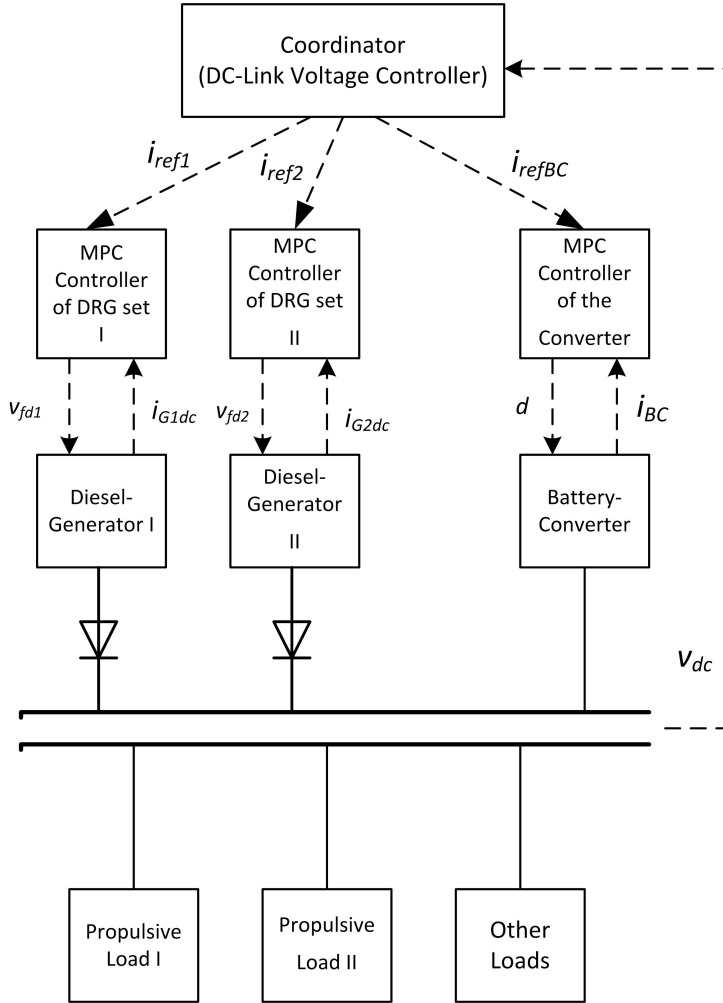


Figure 8.1: The block diagram of the proposed control approach.

with non-negative integers $i \in \{1, 2\}$ and $l \in \{1, 2\}$. The other additional $n - r$ coordinates can be found such that $\Phi_j(x_j)$ is invertible [124]. In general, the normal form of the transformed partially linear system is:

$$\begin{aligned}
 \dot{\zeta}_1^1 &= \zeta_1^2 \\
 \dot{\zeta}_1^2 &= v_1 = L^2_{(f_j+g_1^j u_1^j+g_2^j u_2^j)} h_1^j(x) \\
 \dot{\zeta}_2^1 &= v_2^j = L^1_{(f_j+g_1^j u_1^j+g_2^j u_2^j)} h_2^j(x_j) \\
 \dot{\eta}_j &= q(\zeta_j, \eta_j) \\
 y_1^j &= \zeta_1^1 \\
 y_2^j &= \zeta_2^1,
 \end{aligned} \tag{8.7}$$

where v_1 and v_2 are the system inputs for the transformed linear systems. Vector of nonlinear functions q represents zero-dynamics/internal dynamics where its elements are chosen using the below condition:

$$L_{g_j} \Phi_{r+i}(x) = 0, \tag{8.8}$$

where $1 \leq i \leq 4$ and $1 \leq j \leq 2$. After calculation, we have:

$$\begin{aligned}
 \zeta_1^1 &= \omega_{dg_j} \\
 \zeta_1^2 &= \frac{1}{2H_j} (Q_{enj} - I_{G_2}^T X_{G_j}^T G_j I_{G_j}) \\
 \zeta_2^1 &= \beta_{rec_j} \sqrt{I_{G_j}^T G_2 I_{G_j}}.
 \end{aligned}$$

The relationship between the original system inputs u_1^j and u_2^j with inputs of the transformed system can be written as:

$$\begin{bmatrix} u_1^j \\ u_2^j \end{bmatrix} = -\Delta^{-1}(x_j) \left(\begin{bmatrix} L^2_{f_j} y_1^j \\ L^1_{f_j} y_2^j \end{bmatrix} + \begin{bmatrix} v_1^j \\ v_2^j \end{bmatrix} \right). \tag{8.9}$$

Then, the decoupled linear systems are defined as:

$$\begin{aligned}
 \begin{bmatrix} \dot{\zeta}_1^1 \\ \dot{\zeta}_1^2 \end{bmatrix} &= \begin{bmatrix} 0 & 1 \\ 0 & 0 \end{bmatrix} \begin{bmatrix} \zeta_1^1 \\ \zeta_1^2 \end{bmatrix} + \begin{bmatrix} 0 \\ 1 \end{bmatrix} v_1^j \\
 \dot{\zeta}_2^1 &= v_2^j.
 \end{aligned} \tag{8.10}$$

To control the DGR set two MPC problems should be solved; one for the speed control and the second one for the current generation control.

After discretization, the following MPC problem is defined for controlling the speed of the diesel-generator.

$$\mathbb{P}_1^j(\zeta_1^1) : \min_{v_1^j} \left(V_N(\zeta_1^1, v_1^j) = \sum_{i=k}^{k+N-1} S(\zeta_1^1(i), \omega_{ref}^j(i), v_1^j(i)) + S_f(\zeta_1^1(k+N)) \right) \tag{8.11}$$

subject to (8.10) with:

$$\begin{aligned} \zeta_{1\min}^1 &\leq \zeta_1^1(k+i) \leq \zeta_{1\max}^1 \\ v_{1\min}^j(k+i-1) &\leq v_1^j(k+i-1) \leq v_{1\max}^j(k+i-1) \\ \forall i &\in [0, N], \end{aligned} \quad (8.12)$$

where $V_N(\cdot)$ is the MPC cost function, N is the prediction horizon, k is the discrete time step of the system with sample time T_{dc}^j and $V_f(\cdot)$ is the terminal cost defined as:

$$V_f(z_2^1(N)) = (\zeta_1^1(N) - \omega_{ref}^j(N))^2. \quad (8.13)$$

Moreover,

$$S(\zeta_1^1(k), \omega_{ref}^j(k), v_1^j(k)) = \alpha(\zeta_1^1(k) - \omega_{ref}^j(k))^2 + \beta v_1^j(k)^2, \quad (8.14)$$

where non-negative parameters α and β are weight factors.

Similar to the diesel-generator speed control, the following MPC problem is defined for the generated DC current control of DGR set j .

$$\mathbb{P}_2^j(\zeta_2^1) : \min_{v_2^j} \left(V_N(\zeta_2^1, v_2^j) = \sum_{i=k}^{k+N-1} S(\zeta_2^1(i), I_{jref}(i), v_2^j(i)) + S_f(\zeta_2^1(k+N)) \right) \quad (8.15)$$

subject to (8.10) with:

$$\begin{aligned} \zeta_{2\min}^1 &\leq \zeta_2^1(k+i) \leq \zeta_{2\max}^1 \\ v_{2\min}^j(k+i-1) &\leq v_2^j(k+i-1) \leq v_{2\max}^j(k+i-1) \\ \forall i &\in [0, N]. \end{aligned} \quad (8.16)$$

Remark 11 *To increase the robustness of the proposed methodology, the tube-based MPC control approach can be applied for the control of DGR sets.*

CONSTRAINT LINEARIZATION

Although the systems in (8.10) are linear but due to the nonlinearity of constraints in (8.12) and (8.16), quadratic programming schemes can not be used for solving the optimization problems in (8.11) and (8.15). In this part, similar to Chapter 7 and by using the results in [119, 120], a strategy is proposed to transform the nonlinear input constraints into linear constraints so that quadratic programming approaches are applicable.

The input constraints of the system cannot be found straightforward way since,

$$\begin{bmatrix} v_1^j \\ v_2^j \end{bmatrix} = \begin{bmatrix} \Psi_1^j(x_j, u_j) \\ \Psi_2^j(x_j, u_j) \end{bmatrix} = \Delta(x_j)u_j - \begin{bmatrix} L_{f_j}^2 y_1^j \\ L_{f_j} y_2^j \end{bmatrix}. \quad (8.17)$$

The problem with the exact mapping of constraints is that future values of states x_j and inputs u_1^j and u_2^j are not immediately available and should be found by solving a nonlinear optimization problem which employs predicted values of x_j over the horizon N . Obviously, this strategy is very time consuming and eliminates the advantages of

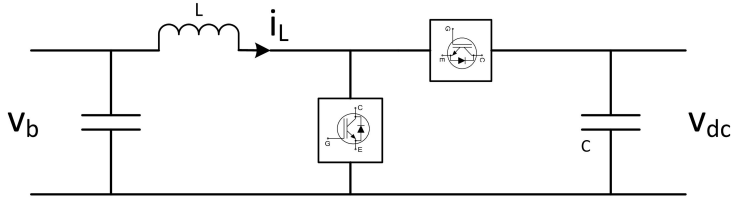


Figure 8.2: The circuit diagram of the bidirectional converter.

adopting an MPC-based control strategy. However, the exact mapping of the future input constraints is impractical since $v_1^j(k+i)$ and $v_2^j(k+i)$, $i \in [0, N]$ are not implemented. As a result, a strategy is adopted with which $v_{1\min}^j(k+i)$, $v_{1\max}^j(k+i)$, $v_{2\min}^j(k+i)$, and $v_{2\max}^j(k+i)$ are approximated over the prediction horizon and $v_{1\min}^j(k)$, $v_{1\max}^j(k)$, $v_{2\min}^j(k)$, and $v_{2\max}^j(k)$ represent exact values.

To this end, the following optimization problems are defined.

$$\begin{aligned}
 v_{1\min}^j(k+i-1) &= \min_{v_1^j(k+i-1)} \Psi_1^j(x_j(k), u^j(k+i-1)) \\
 v_{1\max}^j(k+i-1) &= \max_{v_1^j(k+i-1)} \Psi_1^j(x_j(k), u^j(k+i-1)) \\
 v_{2\min}^j(k+i-1) &= \min_{v_2^j(k+i-1)} \Psi_2^j(x_j(k), u^j(k+i-1)) \\
 v_{2\max}^j(k+i-1) &= \max_{v_2^j(k+i-1)} \Psi_2^j(x_j(k), u^j(k+i-1))
 \end{aligned} \tag{8.18}$$

$$\forall i \in [0, N].$$

Solving the above problem is straightforward as $x_j(k)$ is known and $u^j(k+i-1)$ appears linearly in functions $\Psi_1^j(\cdot)$ and $\Psi_2^j(\cdot)$. Using the above equation, it is guaranteed that the implemented control action is within the exact constraints of the actual system. Furthermore, finding the input variable bounds for the rest of the horizon is computationally trivial if (8.31) is adopted.

8.2.2. CONTROL OF THE BATTERY-CONVERTER SET

In this part, the objective is to control the DC current generated by the battery-converter set. To this end, and in order to handle constraints and utilize the prediction of the required propulsive load, an MPC approach is proposed.

As mentioned, in this thesis, a non-isolated converter model is adopted for DC/DC conversion stage. The structure of the converter is shown in Figure 8.2.

The dynamical model of the converter is:

$$\begin{aligned}
 \dot{i}_L &= \frac{d(t)}{L} v_{dc}(t) - \frac{v_b(t)}{L} \\
 i_{BC} &= D i_L,
 \end{aligned} \tag{8.19}$$

where d is the control input and i_{BC} is the output. The relationship between the input and output is linear, if v_{dc} is constantly measured and kept constant around its nominal value. Note that changes in v_b are very slow and negligible.

To control i_{BC} , the following MPC problem is defined:

$$\mathbb{P}_{BC}(i_{BC}) : \min_d \left(V_N(i_{BC}, d) = \sum_{i=k}^{k+N-1} S(i_{BC}(i), I_{BC_{ref}}(i), d(i)) + S_f(i_{BC}(k+N)) \right) \quad (8.20)$$

subject to (8.19) and

$$\begin{aligned} I_{BC_{min}} &\leq \zeta_1^1(k+i) \leq I_{BC_{max}} \\ 0 &\leq d(k+i-1) \leq 1 \\ \forall i &\in [0, N]. \end{aligned} \quad (8.21)$$

8.2.3. COORDINATOR: CONTROL FOR THE DC-LINK VOLTAGE

In this section, the high level control approach is presented. This module is responsible for determining a current with which the DC voltage is kept around its nominal value:

The dynamics of the DC-link can be represented as

$$\dot{v}_{dc} = \frac{1}{C}(I_{G1dc} + \dots + I_{Gmdc} + i_{BC} - \frac{P}{v_{dc}}) = \frac{1}{C}(i_{dc} - \frac{P}{v_{dc}}), \quad (8.22)$$

where i_{dc} is considered as the system input and v_{dc} is the system output.

Let the solution of controlling v_{dc} be $i_{ref_{dc}}$. Note that, in reality, there is no active controller at the rectification stage and $i_{ref_{dc}}$ is provided by the energy sources. However, $i_{ref_{dc}}$ can not be exactly tracked by i_{dc} . This tracking error is formulated as:

$$e_{i_{dc}} = i_{ref_{dc}} - i_{dc}, \quad (8.23)$$

Due to the correctness of control methods presented in Sections 8.2.1 and 8.2.2, $e_{i_{dc}}$ is bounded. Therefore, (8.22) can be written as:

$$\dot{v}_{dc} = \frac{1}{C}(i_{ref_{dc}} - \frac{P}{v_{dc}} + e_{i_{dc}}), \quad (8.24)$$

where $i_{ref_{dc}}$ is regarded as the system input and $e_{i_{dc}}$ as a bounded additive disturbance. Due to the presence of a CPL, the above system has nonlinear dynamics. In order to control this system, similar to Section 8.2.1, an auxiliary control input is defined for establishing a linear relationship between system input and output as:

$$v_i = \frac{1}{C}(i_{ref_{dc}} - \frac{P}{v_{dc}}) \quad (8.25)$$

which leads to the following transformed system:

$$\dot{v}_{dc} = v_i + \frac{e_{i_{dc}}}{C}. \quad (8.26)$$

To control (8.26), based on the results in [122], a robust tube-based MPC approach is proposed. This approach is based on extracting a trajectory for a nominal system and

then, by adopting a linear control law, the trajectory of the system is steered towards the trajectory of the nominal system. The nominal system is defined as,

$$\dot{z}_{dc} = \tau_{dc} \quad (8.27)$$

where z_{dc} is the state and τ_{dc} is the system input. To generate the nominal trajectory, the following MPC problem is defined:

$$\mathbb{P}_{DC}(z_{dc}) : \min_d \left(V_N(z_{dc}, \tau_{dc}) = \sum_{i=k}^{k+N-1} S(z_{dc}(i), v_{dc_{ref}}(i), \tau_{dc}(i)) + S_f(z_{dc}(i)(k+N)) \right), \quad (8.28)$$

subject to (8.27) with:

$$\begin{aligned} z_{dc_{min}} &\leq z_{dc}(k+i) \leq z_{dc_{max}} \\ \tau_{dc_{min}}(k+i-1) &\leq \tau_{dc}(k+i-1) \leq \tau_{dc_{max}}(k+i-1) \\ \forall i &\in [0, N]. \end{aligned} \quad (8.29)$$

To steer the actual system's trajectory towards the trajectory of the nominal system, the following control rule is defined:

$$v_i(t) = \kappa_{dc}(z_{dc}(t)) + K_{dc}(v_{dc}(t) - z_{dc}(t)) \quad (8.30)$$

where $\kappa_{dc}(\cdot)$ is the solution of the MPC problem in (8.28) and $K_{dc} \leq 0$ is the feedback gain.

Similar to Section 8.2.1, the constraints in (8.29) are found by solving the following optimization problems:

$$\begin{aligned} \tau_{dc_{min}}(k+i-1) &= \min_{i_{ref_{dc}}(k+i-1)} v_i(v_{dc}(k), i_{ref_{dc}}(k+i-1)) \\ \tau_{dc_{max}}(k+i-1) &= \max_{i_{ref_{dc}}(k+i-1)} v_i(v_{dc}(k), i_{ref_{dc}}(k+i-1)) \\ \forall i &\in [0, N]. \end{aligned} \quad (8.31)$$

Similar to the tube-based approach in Chapter 7, the bounds on the input variables can be considered tighter.

Remark 12 *The relationship between the maneuvering controller and the proposed power generation control approach is established similar to Section 7.3. As a result, $P(k)$, $P(k+1)$, ..., $P(k+N)$ are realizable.*

Remark 13 *The integration of the energy management module and the power generation controller is established by sharing the reference current $i_{ref_{dc}}$ between the energy sources as:*

$$i_{ref_{dc}} = \xi_{DGR_1} i_{ref_{dc}} + \dots + \xi_{DGR_m} i_{ref_{dc}} + \xi_{BC} i_{ref_{dc}} \quad (8.32)$$

where $i_{ref_1} = \xi_{DGR_1} i_{ref_{dc}}$, ..., $i_{ref_m} = \xi_{DGR_m} i_{ref_{dc}}$, and $i_{ref_1} = \xi_{BC} i_{ref_{dc}}$.

8.3. SIMULATION EXPERIMENTS

In this part, the performance of the proposed control approach is evaluated through simulation experiments. First, the simulation model is discussed and then, the experiment results are presented. For evaluating the performance of the proposed approach, two simulation-based experiments are considered:

1. Voltage control under a varying load.
2. Short circuit experiment under a CPL.

8.3.1. SIMULATION MODEL VALIDATION

The simulation model is established based on the component models that are provided by the ShipDrive project partner Damen Schelde Naval Shipbuilding. The overall energy generation side can deliver 10606 kW which is provided by two DGR sets and a battery-converter sets. In order to show the applicability of the control approach to different component models, two non-similar diesel-generators are considered for the energy generation side. The first diesel-generator is a 6150 kW, 6600 V, 60 Hz and the second one is a 3456 kW, 6600, 60 Hz. Both models represent existing diesel-generators.

The validation experiments and results of the first diesel engine and synchronous generator are discussed in Section 7.4.1. Validation results of the second diesel generator are presented in this section. In Figure 8.3, the validation test results of the second synchronous generator are given. It is shown that the efficiency of the developed model tracks the real generator's efficiency over different loading rates with maximum error of 1.5%. The comparison of the Root-Mean-Square (RMS) value of the short circuit current and the computed short circuit current (based on the datasheet) are shown in Figure 8.3c. The results indicate sufficient accuracy of the DGR transients.

The maximum torque of the smaller diesel engine is 36.668 kN.m at the rated speed of 15 rps. For the voltage conversion stages, a rectifier model with 96% of efficiency is considered.

8

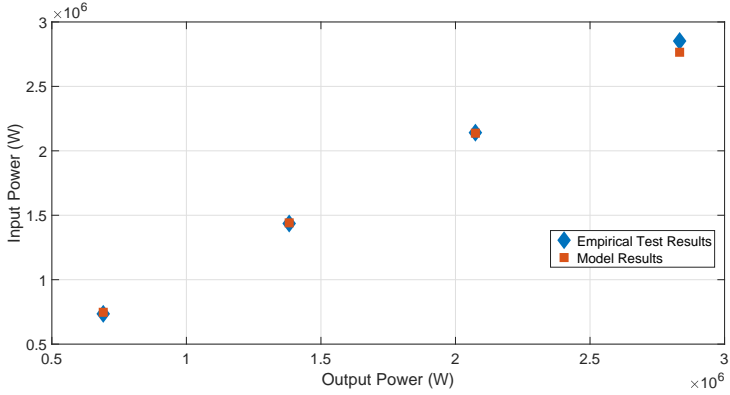
For this simulation model, a 1 MWh battery is considered with internal resistance of 0.01 ohm. The bidirectional converter data is provided in Appendix A.3.

The experiments are carried out on a PC with 2.8GHz Intel Core i7-7600U CPU and 8GB RAM. The MATLAB® 2018a Simscape toolbox is partially used for the development of the model.

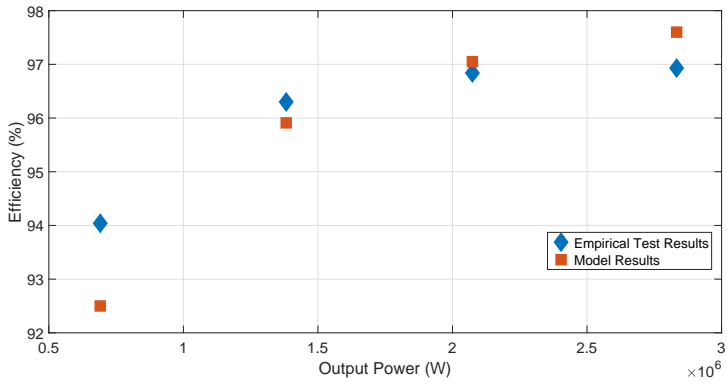
8.3.2. EXPERIMENT I: VOLTAGE CONTROL UNDER VARYING LOAD

In this experiment, a CPL with varying power P over time is applied to the system. Both DGR sets and the battery-converter set are online and providing power. The power splits between energy sources are $\zeta_{DGR_1} = 0.6$, $\zeta_{DGR_2} = 0.3$, and $\zeta_{BC} = 0.1$. The load applied to the power system is shown in Figure 8.4.

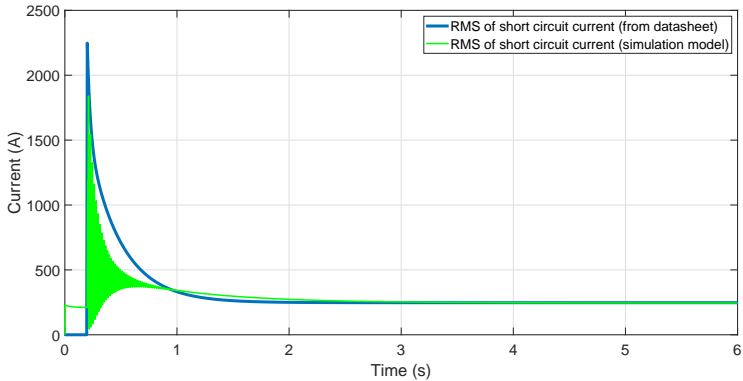
It is assumed that the prediction horizon of the model predictive controller of the coordinator is $N = 20$ with sampling time $T_{dc} = 0.1s$. Similar setting is used for the DC current controllers of the DGR sets and the converter. Similar to Chapter 7, a tube-based rule is adopted to increase the robustness of the low level controllers. For the diesel-generators shaft speed control, the controller's prediction horizons are chosen as $N_\omega = 10$.



(a) Relationship between input and output power.



(b) Efficiency at different loading conditions.



(c) Short circuit current: model vs. datasheet.

Figure 8.3: Synchronous generator's model results versus empirical test results.

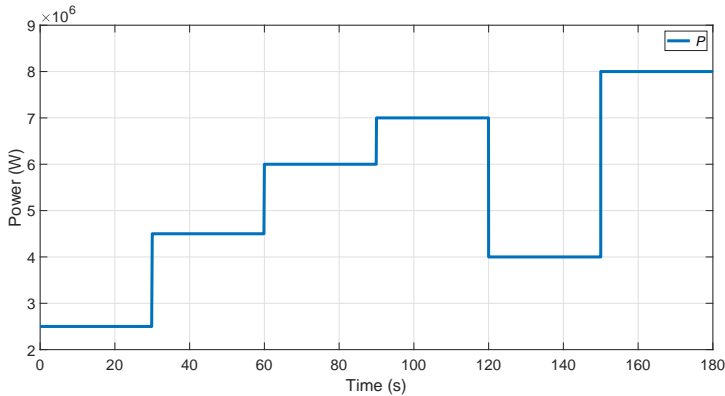


Figure 8.4: The varying load applied to the power system (Experiment I).

The simulation results of the voltage stability are shown in Figures 8.5. It is shown that the energy sources respond actively to the load changes and as a result, the voltage stays around its nominal value. Moreover, the power splits between different sources stays around the desired values. The simulation results of the mechanical variables are shown in Figure 8.6. It is shown that the shaft speed of diesel-generators are kept around the desired value by injecting feasible amount of fuel. The response of the engine torque is shown in Figure 8.6b which represents the load changes during the simulation time. The simulation results of the synchronous generator's electrical variables are presented in Figure 8.7. The SOC of the battery is shown in Figure 8.8.

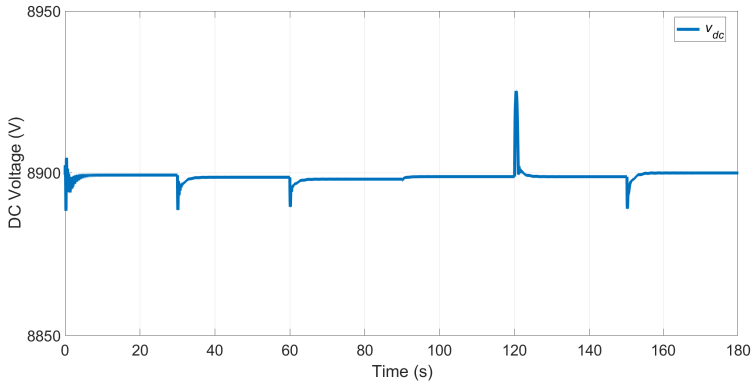
8.3.3. EXPERIMENT II: SHORT CIRCUIT TEST

In this section, the tolerance of the proposed control approach is evaluated against a short circuit fault. Moreover, the performance of the two-level MPC controller is compared with the conventional droop control methods.

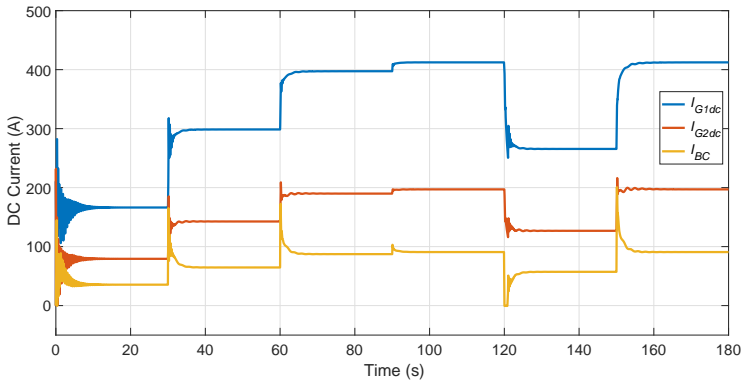
A 7.5 MW CPL is considered as a load which drops to 4.5 MW at $t = 50$ s. The DC-link short circuit fault happens at $t = 15.1$ s and stops at $t = 15.15$ s. Similar settings are considered for the proposed two-level MPC controller.

The simulation results are presented in Figure 8.9. It is shown that the DC-link voltage can recover after the short circuit. This happened by increasing the generated DC current by the controllers. Figure 8.9c, represents the controllers effort to keep the DC-link voltage stable.

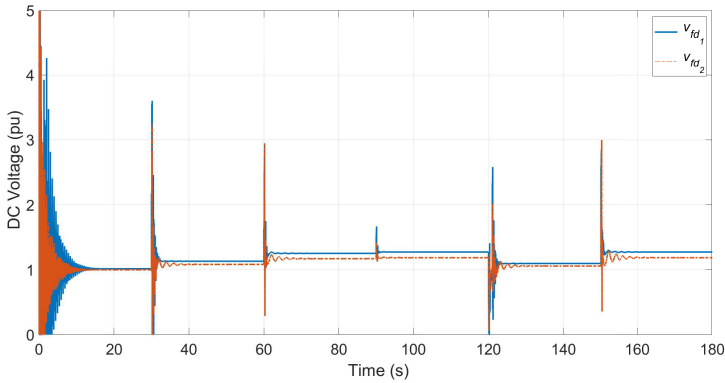
This experiment is also carried out using conventional droop control approach. In this approach, the diesel-generator controllers are PI-based. For voltage regulation, the PI values of the first synchronous generator are $K_{P_1} = 294.75$ and $K_{I_1} = 2.3$. For the second synchronous generator, these values are $K_{P_2} = 121.1$ and $K_{I_2} = 2.9$. The PI values are estimated by using the transient time constant of the synchronous generators and the rough estimation of relationships between $v_{fd_{1,2}}$ and the terminal voltages of the generators [125]. The simulation results of PI-based droop control scheme are shown in Figure 8.10 which indicates the failure of the control approach since after the short circuit inci-



(a) The DC-link voltage.

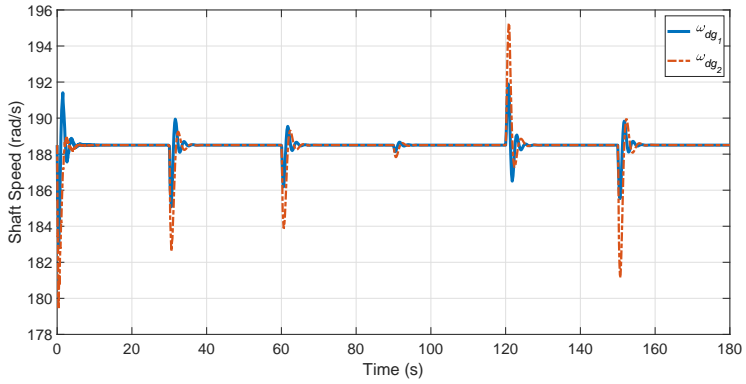


(b) DC currents provided by the energy sources.

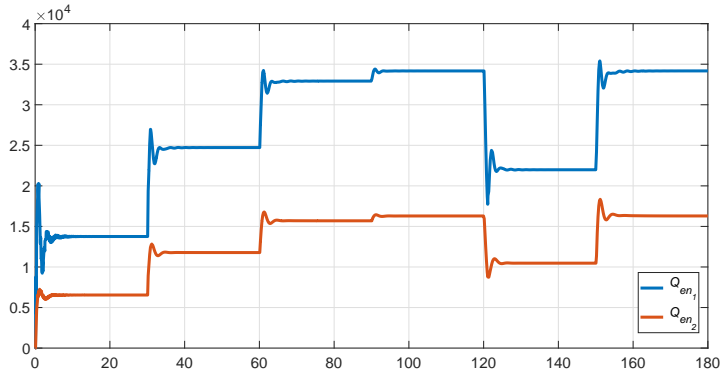


(c) Field voltage of the synchronous generators.

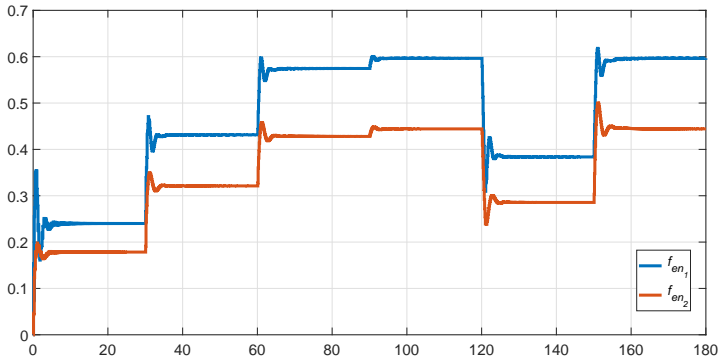
Figure 8.5: DC-link voltage stability simulation results (Experiment I).



(a) Shaft speed of diesel-generators.

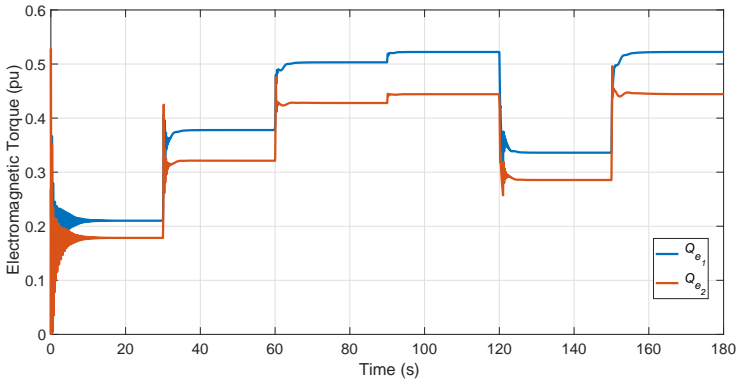


(b) Diesel engine torques.

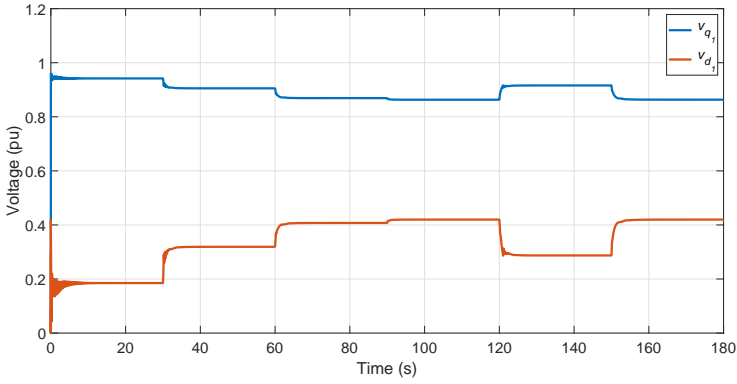


(c) Fuel index of the diesel engines.

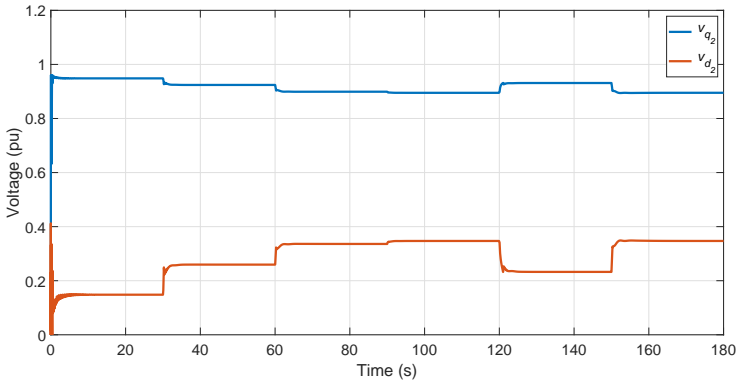
Figure 8.6: Simulation results of the mechanical variables (Experiment I).



(a) Electromagnetic torque of the synchronous generators.



(b) dq voltages of the first synchronous generators.



(c) dq voltages of the second synchronous generators.

Figure 8.7: Simulation results of the mechanical variables (Experiment I).

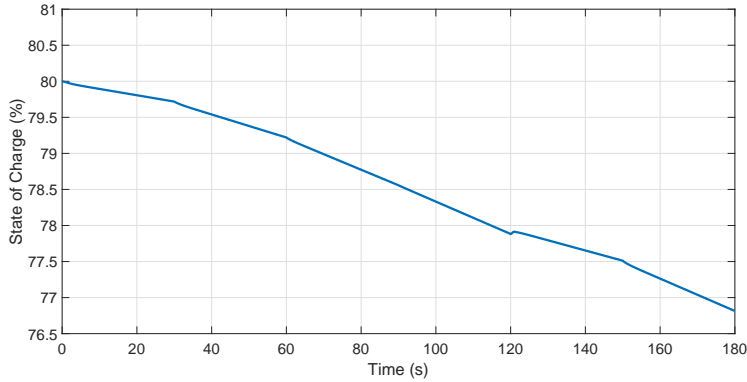


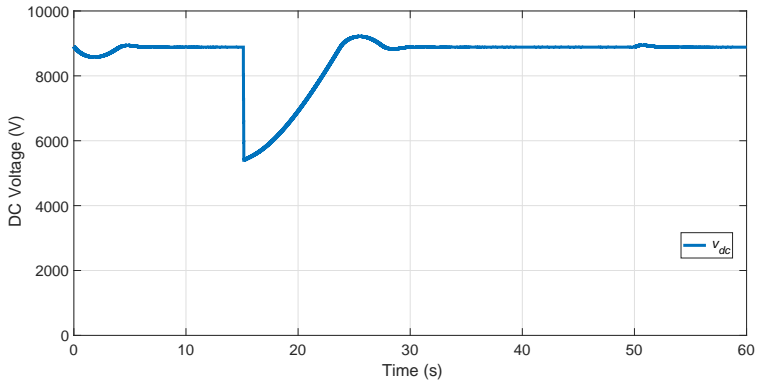
Figure 8.8: The SOC of the battery during simulation (Experiment I).

dent, the voltage could not be recovered.

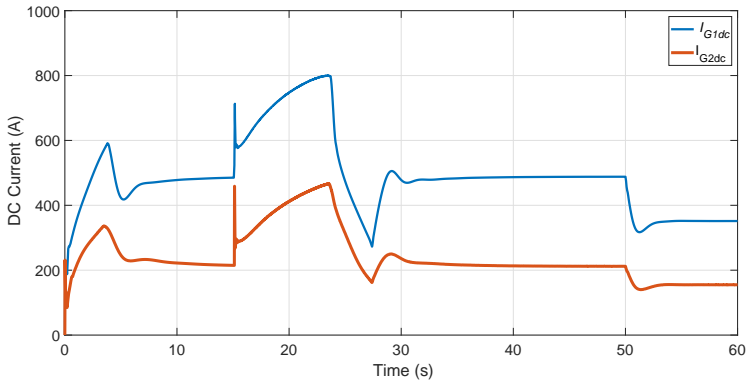
8.4. CONCLUSIONS

In this chapter, a novel control approach has been proposed for power generation control on-board of all-electric ships with DC-PPS. The proposed approach is a two-level MPC-based approach. A coordinator is considered on the top level which determines the amount of DC current to be generated by the energy sources for keeping the DC-link voltage around its nominal value. Low-level controllers fulfill the current generation requests by the coordinator. Through simulation experiments the performance of the proposed control approach has been evaluated.

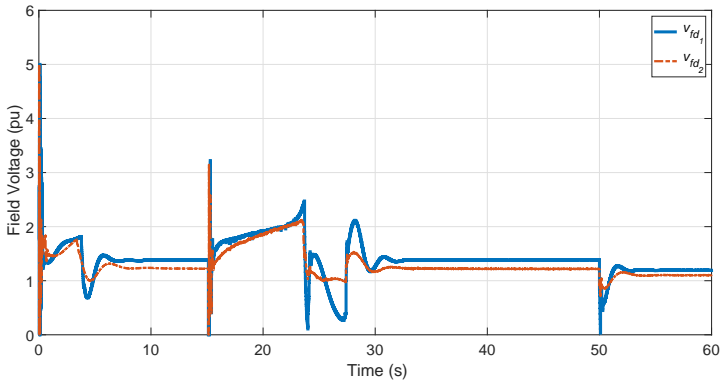
By proposing a novel power generation control approach to guarantee stability, the results in this chapter provide an answer to Research Question 8.



(a) DC-link Voltage.

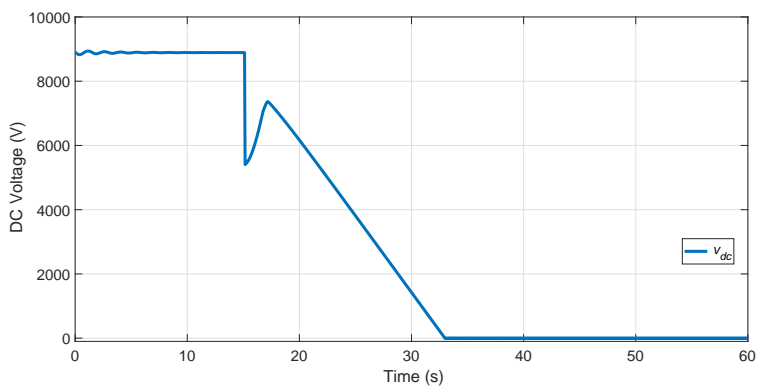


(b) Generated currents by the energy sources.

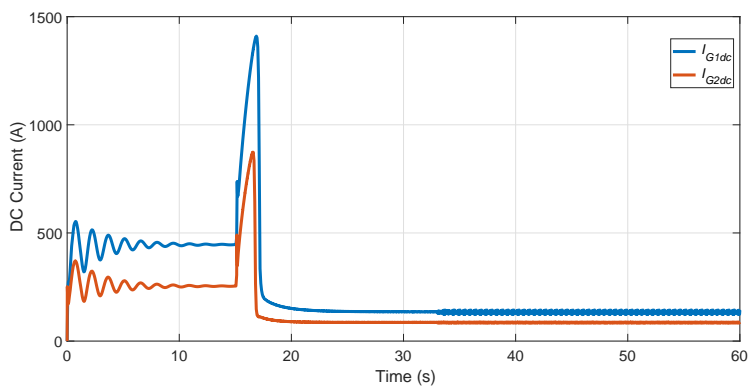


(c) Field voltage of the synchronous generators.

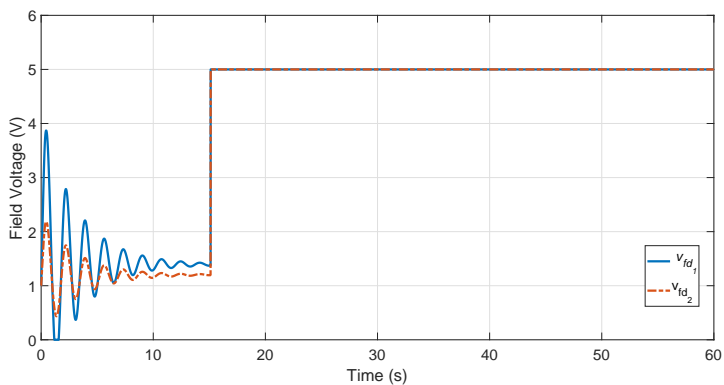
Figure 8.9: Simulation results of Experiment II using the proposed two-level MPC controller.



(a) DC-link Voltage.



(b) Generated currents by the energy sources.



(c) Field voltage of the synchronous generators.

Figure 8.10: Simulation results of Experiment II using the PI-based droop control scheme.

9

CONCLUSIONS AND FUTURE RESEARCH

In this chapter, the concluding remarks about the contributions of this thesis are presented. The research questions of Chapter 1 are revisited and it is discussed how each question is answered based on the research results within the thesis. Furthermore, in-detail discussions are provided regarding future research directions.

9.1. ADDRESSING THE RESEARCH QUESTIONS

The ultimate goal in this thesis has been answering the following overall question: *How can the performance and efficiency of autonomous all-electric ships be improved using novel control approaches?* This goal has been achieved by breaking this question to different sub-questions and providing an answer/solution for each of them.

In this section, the research questions presented in Chapter 1 are subsequently answered. The research questions are related to different ship control domains, namely, maneuvering control, energy management, and power generation control as well as the integration of them.

1. What are the feasible approaches for the maneuvering control of autonomous ships?

Considering the rich literature of control for dynamical systems, this question is about the problem of choice. In the literature, there are numerous control approaches for non-linear systems. Moreover, in the field of maneuvering control of autonomous ships, these control approaches have been employed to address maneuvering challenges. In this thesis, these challenges have been identified and studied. Unlike the results in the literature which have studied maneuvering control independently and only in relation with environmental conditions, in this thesis, maneuvering control challenges are studied in relation with other on-board challenges including energy management and power generation control. In this regard, the maneuvering control challenges are related to (i) uncertainties within the maneuvering model, (ii) uncertainties that are a result of environmental disturbances (iii) subjective constraint handling (iv) effective integration

with energy management and power generation control. Based on these challenges, the control approaches in Chapters 4 and 5 are proposed for maneuvering control. Adaptive and model predictive approaches are chosen for handling uncertainties, constraint handling, and integration with energy management and power generation control.

2. How to handle environmental disturbances and model uncertainties in the maneuvering model?

In this thesis, first the sources of model uncertainty are identified. It is shown that the thrusters and propellers, drag forces, and the added mass matrix are among the sources of uncertainties. Based on the results in the literature, it is discussed how the propeller's model undergo a significant uncertainty during maneuvering. In this thesis, an adaptive control approach is proposed for handling uncertainties within the propellers and the maneuvering model. The stability analysis of the proposed control approach is carried out and through several control experiments the success of the control approach is shown. In simulation experiments of Chapter 4, it is shown that the proposed approach can lead to lower trajectory tracking error compared to conventional PID-based approaches.

3. How to guarantee small trajectory tracking errors, constraints handling, and the prediction of future required propulsive energy?

To address the challenges mentioned in the question, a Model Predictive Control (MPC) approach is proposed for trajectory tracking control. An Input-Output Feedback Linearization (IOFL) is employed to decrease the computation costs. A method for constraints linearization is adopted to enable the use of quadratic programming approaches and effective handling of uncertainties. Using the mathematical model of propellers and thrusters, and the prediction of future required thrust, the propulsive power is estimated over a finite horizon. This information can be utilized by the energy management and power generation controllers to determine the optimal split between energy sources (see Chapter 6) and improve power system stability (see Chapters 7 and 8). The simulation experiment results suggest that the proposed approach is capable of reducing the trajectory tracking error up to 60% in comparison to the conventional PID-based approaches.

4. In what ways can the prediction of required future propulsive energy be used for increasing the operation robustness and efficiency of vessels?

In this thesis, a maneuvering control approach is proposed with which the prediction of future required propulsive power is enabled. By designing MPC-based control approaches, this information is actively used for energy management and power generation control. For energy management, the prediction is used to determine the optimal split between on-board energy sources and prohibit diesel-generators to experience sudden changes in the loading condition. The prediction of the future required propulsive power is used by the proposed power generation control approach to increase the precision of the prediction model which is used by the MPC-based power generation controllers.

5. How can optimal engine loading, fuel efficiency, and efficiency of energy generation be maximized?

In this thesis, an energy management approach is proposed which aims at maximizing fuel efficiency. This energy management approach utilizes the prediction of the future required power for finding the optimal split between different on-board energy sources. The cost function of the optimization problem is built using the Specific Fuel Consumption (SFC) curve of the diesel engines. The proposed approach guarantees that if a diesel-generator is active, its delivering power is around the optimal point in its SFC curve. As a result, the energy generation efficiency is maximized and optimal engine loading can be achieved. Moreover, using this approach and by introducing a variance-based cost function to the main cost function, fast and extreme changes in the loading condition of the DGR sets are limited. The simulation experiment results suggest that, in comparison to conventional rule-based approaches, the proposed approach is capable of increasing the fuel efficiency between 2-15%, depending on the operating profile.

6. How can propulsive power availability be guaranteed?

In the proposed approaches in this thesis, power availability is guaranteed using two different approaches on different levels. The first approach is incorporated within the energy management approach. Using this approach which utilizes the prediction of the required propulsive power, the number of online Diesel-Generator-Rectifier (DGR) sets is determined such that providing optimal power is guaranteed. The second approach guarantees the availability of power by maximizing the stability of the power system using robust control methodologies for controlling the DGR sets, the battery-converter set, and the DC-link voltage.

7. Can advanced control approaches increase the stability of DC-PPS? If yes, what approach is suitable?

In Chapter 7 of this thesis, the stability of the power system and the adoption of advanced control approaches for power generation control are analyzed. It is shown that the adoption of advanced control algorithms is necessary to increase the robustness of the power system. As a result, a robust control approach is adopted for power generation control. The approach is a tube-based MPC scheme which guarantees the stability in the presence of Constant Power Loads (CPL) and rapid changes in the loading condition. It also utilizes the prediction of future propulsive power over a finite horizon. IOFL accompanied by a methodology to linearize the constraints are adopted in order to enable the use of quadratic programming approaches. The simulation results indicate that using the proposed approach the voltage and shaft speed fluctuations decrease (Figure 7.12).

8. How can the adoption of cooperative control approaches lead to the increased stability and robustness of DC-PPS?

In Chapter 8 of this thesis, a multi-level control approach is proposed for power generation control and control of energy sources in the presence of CPLs. In this approach, a high level controller acts as a coordinator to determine the referenced current values for on-board energy sources. Then, the low level controllers control the current generation and the shaft speed of diesel-generators using the the desired DC current values. The proposed control scheme is a multi-level MPC-based approach which utilizes an

IOFL rule and a constraint linearization methodology to enable the use of quadratic programming approaches. Furthermore, the propulsive load prediction is also utilized to increase the precision of prediction model. The simulation experiment results suggest that proposed control approach is capable of handling CPLs and varying loads. Moreover, in comparison to conventional PI-based approaches, the proposed approach is capable of re-stabilizing the power system after occurrence of a fault.

9. In what ways can maneuvering, energy management, and power generation controllers interact and how this interaction can lead to a more effective performance?

Throughout this thesis, the integration of different controllers is explained. The maneuvering controller not only controls the trajectory tracking of the vessel but also predicts the required propulsive load over a finite horizon. This prediction data is used by the energy management module and the power generation controller. Moreover, after determining the optimal power split between different sources, load share of each energy source is utilized by the coordinator of the power generation controller as explained in Chapter 8.

Overall research question: How can the performance and efficiency of autonomous all-electric ships be improved using novel control approaches?

The results of this thesis improve the maneuvering performance, fuel efficiency, and PPS robustness of autonomous all-electric ships. Proposed maneuvering control approaches enable trajectory tracking in the presence of uncertainties and constraints. The adoption of the proposed predictive energy management approach can lead to higher fuel efficiency. Moreover, the proposed power generation control approach can improve the robustness of the PPS.

The International Maritime Organization (IMO) has commenced work to look into how safe, secure and environmentally sound Maritime Autonomous Surface Ships (MASS) operations may be addressed in IMO instruments. The results of this thesis are aligned with the concerns of IMO as they lead to major improvements in the performance of autonomous all-electric ships. Using the proposed approaches in this thesis, as the results of Chapters 4 and 5 indicate, the maneuvering performance of autonomous ships in the presence of disturbances and uncertainties improves. Moreover, using the proposed energy management approach in Chapter 6, fuel efficiency increases between 2-15%. The problem of power and propulsion system stability is addressed in Chapters 7 and 8 by proposing control approaches which guarantee the voltage stability on-board.

9.2. CONTRIBUTIONS OF THE THESIS

In this thesis, several control approaches have been proposed for different challenges in realizing autonomous ships with all-electric power and propulsion system. It has also been explained how these control approaches, which act on different control domains, can be integrated to create a general framework for controlling all-electric ships. In brief, the contributions of the thesis can be summarized as follows:

- In Chapter 2, a literature review on integrating maneuvering, energy management, and power generation control has been presented.

- In Chapter 3, a mathematical model has been given for different components on-board of an all-electric ship. Then, by combining the models, the overall ship with the DC Power and Propulsion System (DC-PPS) has been modeled in state space format. Parts of this chapter have been published in:
 1. A. Haseltalab, R. R. Negenborn, Model predictive maneuvering control and energy management for all-electric autonomous ships, *Applied Energy*, Volume 251, pp. 1-27, 2019.
 2. A. Haseltalab, M. A. Botto, R. R. Negenborn, Model Predictive DC Voltage Control for All-Electric Ships, *Control Engineering Practice*, Volume 90, pp. 133-147, September 2019.
 3. A. Haseltalab, R. R. Negenborn, G. Lodewijks, Multi-Level Predictive Control for Energy Management of Hybrid Ships in the Presence of Uncertainty and Environmental Disturbances, *IFAC-PapersOnLine*, Volume 49, Issue 3, 2016, Pages 90-95.
- In Chapter 4, an adaptive control approach has been proposed for trajectory tracking control of autonomous ships in the presence of model uncertainties and environmental disturbances. Using several simulation experiments, it has been shown that the proposed approach can steer the ship along its reference trajectory while state dependent uncertainties exist. Parts of this chapter have been published in:
 1. A. Haseltalab, R. R. Negenborn, Adaptive Control for a Class of Partially Unknown Non-Affine Systems: Applied to Autonomous Surface Vessels, *IFAC-PapersOnLine*, Volume 50, Issue 1, 2017, Pages 4252-4257.
 2. A. Haseltalab, R. R. Negenborn, Adaptive Control for Autonomous Ships with Uncertain Model and Unknown Propeller Dynamics, *Control Engineering Practice*, Volume 91, 2019.
- In Chapter 5, a model predictive trajectory tracking control approach has been proposed which is designed using an IOFL rule and a method to linearize constraints so that quadratic programming algorithms can be used for solving the optimization problem of the MPC problem. Using this approach, trivial trajectory tracking error, constraints handling, and the prediction of future required propulsive power is guaranteed. Parts of this chapter have been published in:
 1. A. Haseltalab, R. R. Negenborn, Model predictive maneuvering control and energy management for all-electric autonomous ships, *Applied Energy*, Volume 251, 2019.
- In Chapter 6, an energy management approach has been proposed for achieving optimal power split between different on-board energy sources. The approach aims at enabling optimal engine loading and maximizing fuel efficiency. Several simulation experiments have been carried out to evaluate the performance of the proposed energy management approach. It has been shown that using the proposed approach, the fuel efficiency increases between 2% to 15% depending on the operating profile. Parts of this chapter have been published in:

1. A. Haseltalab, R. R. Negenborn, "Model predictive maneuvering control and energy management for all-electric autonomous ships," *Applied Energy*, Volume 251, pp. 1-27, 2019.
 2. A. Haseltalab, R. R. Negenborn, "Predictive on-board power management for all-electric ships with DC distribution architecture," in the proceedings of OCEANS 2017, Aberdeen, pp. 1-8, 2017.
- In Chapter 7, the stability of a single DGR set connected to propulsive loads has been analyzed and then, a tube-based MPC control algorithm has been proposed for controlling the DC-link voltage and the shaft speed of the diesel-generator. This approach is designed using IOFL and an MPC constraint linearization method. The stability proof of the control approach has been carried out and throughout several simulation experiments on high fidelity model, it is shown that the proposed approach is capable of guaranteeing stability in the presence of CPLs and varying loads. Parts of this chapter have been published in:
 1. A. Haseltalab, M. A. Botto, R. R. Negenborn, "Model Predictive DC Voltage Control for All-Electric Ships," *Control Engineering Practice*, Volume 90, Pages 133-147, 2019.
 2. A. Haseltalab, M. A. Botto, R. R. Negenborn, "On-Board Voltage Regulation For All-Electric DC Ships," *IFAC-PapersOnLine*, Volume 51, Issue 29, Pages 341-347, 2018.
 - In Chapter 8, the results of Chapter 7 have been extended to the case of a DC-PPS with multiple DGR sets and a battery-converter set. In this chapter, a hierarchical MPC approach is proposed for controlling the DC-link voltage and the shaft speed of diesel-generators. Through several simulation experiments, it has been shown that this so called power generation control approach is capable keeping the overall system stable in the presence of CPLs.
 - Throughout this thesis, a framework for integrating maneuvering, energy management, and power generation controllers have been proposed. Parts of this chapter have been published in:
 1. A. Haseltalab, F. Wani, R. R. Negenborn, "Multi-level Power Generation Control for All-Electric Ships," Submitted to an international journal, 2019.

9.3. RECOMMENDATIONS FOR FUTURE RESEARCH DIRECTION

In this section, several recommendations for future research are presented. The recommendations are proposed aiming at enabling autonomous all-electric ships with robust DC-PPS. The recommendations are related to maneuvering, energy management, power generation control and their integration.

9.3.1. MANEUVERING CONTROL OF AUTONOMOUS SHIPS

As discussed in Chapters 2, 3, and 4 of this thesis, several control approaches are presented in the literature for maneuvering control of ships. Most of these research works

are experimented in simulation or using small scale vessel. It is necessary to for academics and their industrial partners to test these novel approaches in practice using real size boats/vessels. A novel approach for maneuvering control should be capable of handling model uncertainties, environmental disturbances, and constraints of input and output variables. Moreover, it should be capable of predicting the future required propulsive power and guaranteeing trivial tracking error.

To fully enable autonomous shipping, the interaction of autonomous ships with their surrounding environment should be studied as well. Autonomous vessels should be able to cooperate with each other and other transport infrastructures (e.g., bridges and sluices) to carry out different operations and tasks. Moreover, they should be able to communicate and collaborate with non-autonomous vessels. As a result, perception algorithms, control approaches, and communication protocols should be developed to enable the interaction of autonomous ships with each other and their surrounding environment.

9.3.2. ENERGY MANAGEMENT FOR ALL-ELECTRIC SHIPS

The proposed energy management in this thesis aims at guaranteeing optimal engine loading during diesel engine's operation and is designed to be replaced by conventional rule-based approaches. This approach should be tested in practice with different operating profiles. This approach is designed for DC-PPS, however, in future researches, this approach should be extended to AC all-electric and hybrid power and propulsion systems for guaranteeing optimal engine loading. In case of autonomous vessels, the proposed energy management approach should be studied and tested in accordance with the maneuvering control module as discussed in this thesis.

9.3.3. POWER GENERATION CONTROL

The conventional control approaches for DC power systems should be revisited and analyzed critically again. In the literature, it is shown that conventional droop control schemes are not reliable for power generation control in the presence of CPLs and varying loads. Novel control approaches should be tested in practice using scaled components in the laboratory environment. The integration of the energy management approaches with the power generation schemes should be implemented and tested empirically.

Due to limited resources in academia for implementing, testing, and evaluating the novel approaches for control of autonomous ships, it is necessary that industrial partners take part in testing and implementing novel approaches.

To increase the autonomy level of vessels, reliability and robustness of the power and propulsion system is critical. Fault-detection and isolation approaches should be investigated to deal with different faults that might happen on-board. Reconfiguration approaches should also be investigated to recover the system after occurrence of a fault and to avoid loss of propulsion.

BIBLIOGRAPHY

- [1] Central Intelligence Agency (CIA), “The world factbook 2017,” url: <https://www.cia.gov/library/publications/download/download-2017/index.html>, Accessed: March 2019.
- [2] Allianz Global Corporate and Specialty, “Safety and shipping review 2015,” url: <https://www.agcs.allianz.com/news-and-insights/news/safety-shipping-review-2015.html>, Accessed: March 2019.
- [3] United Nations, “Review of maritime transport,” in *United Nations Conference on Trade and Transport*, Switzerland, 2017.
- [4] J. E. Manley, “Unmanned surface vehicles: 15 years of development,” in proceedings of *OCEANS 2008*, pp. 1–4, Quebec City, Canada, September 2008.
- [5] H. Zheng, R. R. Negenborn, and G. Lodewijks, “Predictive path following with arrival time awareness for waterborne AGVs,” *Transportation Research Part C: Emerging Technologies*, vol. 70, pp. 214 – 237, 2016.
- [6] S. Li, *Coordinated Planning of Inland Vessels for Large Seaports*. PhD thesis, Delft University of Technology, 2016.
- [7] V. Hassani and S. V. Lande, “Path planning for marine vehicles using bezier curves,” *IFAC-PapersOnLine*, vol. 51, no. 29, pp. 305–310, 2018.
- [8] G. Bitar, M. Breivik, and A. M. Lekkas, “Energy-optimized path planning for autonomous ferries,” *IFAC-PapersOnLine*, vol. 51, no. 29, pp. 389–394, 2018.
- [9] A. Haseltalab and R. R. Negenborn, “Adaptive control for a class of partially unknown non-affine systems: Applied to autonomous surface vessels,” *IFAC-PapersOnLine*, vol. 50, no. 1, pp. 4252–4257, 2017.
- [10] H. Zheng, R. R. Negenborn, and G. Lodewijks, “Fast ADMM for distributed model predictive control of cooperative waterborne AGVs,” *IEEE Transactions on Control Systems Technology*, Vol. 25, No. 4, pp. 1406–1413, 2017.
- [11] H. Zheng, R. R. Negenborn, and G. Lodewijks, “Robust distributed predictive control of waterborne AGVs –a cooperative and cost-effective approach,” *IEEE Transactions on Cybernetics*, vol. 48, no. 8, pp. 2449–2461, 2018.
- [12] L. Chen, H. Hopman, and R. R. Negenborn, “Distributed model predictive control for vessel train formations of cooperative multi-vessel systems,” *Transportation Research Part C: Emerging Technologies*, vol. 92, pp. 101–118, 2018.

- [13] R. D. Geertsma, R. R. Negenborn, K. Visser, and J. Hopman, "Design and control of hybrid power and propulsion systems for smart ships: A review of developments," *Applied Energy*, Vol. 194, pp. 30–54, 2017.
- [14] M. Kalikatzarakis, R. Geertsma, E. Boonen, K. Visser, and R. R. Negenborn, "Ship energy management for hybrid propulsion and power supply with shore charging," *Control Engineering Practice*, Vol. 76, pp. 133–154, 2018.
- [15] J. Hou, Z. Song, H. Park, H. Hofmann, and J. Sun, "Implementation and evaluation of real-time model predictive control for load fluctuations mitigation in all-electric ship propulsion systems," *Applied Energy*, Vol. 230, pp. 62–77, 2018.
- [16] J. Zhou, Y. Yang, Z. Zhao, and S. X. Ding, "A fault detection scheme for ship propulsion systems using randomized algorithm techniques," *Control Engineering Practice*, Vol. 81, pp. 65–72, 2018.
- [17] M. Babaei, J. Shi, and S. Abdelwahed, "A survey on fault detection, isolation, and reconfiguration methods in electric ship power systems," *IEEE Access*, Vol. 6, pp. 9430–9441, 2018.
- [18] W. Li, A. Monti, and F. Ponci, "Fault detection and classification in medium voltage DC shipboard power systems with wavelets and artificial neural networks," *IEEE Transactions on Instrumentation and Measurement*, Vol. 63, pp. 2651–2665, November 2014.
- [19] International Maritime Organization (IMO), "International convention for the prevention of pollution from ships (MARPOL)," 2011.
- [20] R. D. Geertsma, K. Visser, and R. R. Negenborn, "Adaptive pitch control for ships with diesel mechanical and hybrid propulsion," *Applied Energy*, Vol. 228, pp. 2490–2509, 2018.
- [21] B. Zahedi and L. Norum, "Modeling and simulation of all-electric ships with low-voltage dc hybrid power systems," *IEEE Transactions on Power Electronics*, Vol. 28, pp. 4525–4537, October 2013.
- [22] A. Haseltalab and R. R. Negenborn, "Predictive on-board power management for all-electric ships with dc distribution architecture," in proceedings of *OCEANS 2017*, pp. 1–8, June 2017.
- [23] B. Zahedi, L. E. Norum, and K. B. Ludvigsen, "Optimized efficiency of all-electric ships by dc hybrid power systems," *Journal of Power Sources*, Vol. 255, pp. 341–354, 2014.
- [24] A. Haseltalab, M. A. Botto, and R. R. Negenborn, "On-board voltage regulation for all-electric DC ships," *IFAC-PapersOnLine*, Vol. 51, No. 29, pp. 341–347, 2018.
- [25] A. Emadi, A. Khaligh, C. H. Rivetta, and G. A. Williamson, "Constant power loads and negative impedance instability in automotive systems: definition, modeling, stability, and control of power electronic converters and motor drives," *IEEE Transactions on Vehicular Technology*, vol. 55, pp. 1112–1125, July 2006.

- [26] X. Feng, K. Butler-Purry, and T. Zourntos, "Multi-agent system-based real-time load management for all-electric ship power systems in DC zone level," *IEEE Transactions on Power Systems*, vol. 27, pp. 1719–1728, November 2012.
- [27] R. D. Geertsma, R. R. Negenborn, K. Visser, M. Loonstijn, and H. Hopman, "Pitch control for ships with diesel mechanical and hybrid propulsion: Modelling, validation and performance quantification," *Applied Energy*, Vol. 206, pp. 1609–1631, 2017.
- [28] R. D. Geertsma, *Autonomous Control for Adaptive Ships with Hybrid Propulsion and Power Generation*, PhD thesis, Delft University of Technology, 2019.
- [29] G. J. van den Bogerd, P. M. A. de Groot, J. D. van de Ketterij, A.T. de Nooijer, and W. J. Treurniet, "Waypoint tracking control of the grey Seabax model ship using GPS-IMU data," BSc end project report, Delft University of Technology, 2019.
- [30] M. Abdelaal, M. Franzle, and A. Hahn, "Nonlinear model predictive control for trajectory tracking and collision avoidance of underactuated vessels with disturbances," *Ocean Engineering*, vol. 160, pp. 168–180, 2018.
- [31] B. S. Park, "Adaptive formation control of underactuated autonomous underwater vehicles," *Ocean Engineering*, vol. 96, no. 0, pp. 1–7, 2015.
- [32] Z. Zhao, W. He, and S. S. Ge, "Adaptive neural network control of a fully actuated marine surface vessel with multiple output constraints," *IEEE Transactions on Control Systems Technology*, Vol. 22, pp. 1536–1543, July 2014.
- [33] R. Skjetne, y. N. Smogeli, and T. I. Fossen, "A nonlinear ship manoeuvring model: identification and adaptive control with experiments for a model ship," *Modeling, Identification and Control*, vol. 25, no. 1, pp. 3–27, 2004.
- [34] T. I. Fossen, *Handbook of Marine Craft Hydrodynamics and Motion Control*. Wiley, West Sussex, UK, 2011.
- [35] T. Jonker, B. Blankenaar, K. van Ekeren and J. Verhagen, "Control, navigation and path planning for autonomous vessels," BSc end project report, Delft University of Technology, 2016.
- [36] M. Verbeij. D. Blaauw, G. Hoogendoorn, and E. van Wijk, "Path following control for Delfia-1*," BSc end project report, Delft University of Technology, 2018.
- [37] G. Zhang, X. Zhang, and Y. Zheng, "Adaptive neural path-following control for underactuated ships in fields of marine practice," *Ocean Engineering*, Vol. 104, pp. 558–567, 2015.
- [38] K. Do and J. Pan, "Global robust adaptive path following of underactuated ships," *Automatica*, Vol. 42, No. 10, pp. 1713–1722, 2006.
- [39] H. Xu and C. G. Soares, "Vector field path following for surface marine vessel and parameter identification based on LS-SVM," *Ocean Engineering*, Vol. 113, pp. 151–161, 2016.

- [40] D. Belleter, C. Paliotta, M. Maggiore, and K. Pettersen, "Path following for underactuated marine vessels," *IFAC-PapersOnLine*, Vol. 49, No. 18, pp. 588–593, 2016.
- [41] M. Maghenem, D. Belleter, C. Paliotta, and K. Pettersen, "Observer based path following for underactuated marine vessels in the presence of ocean currents: A local approach," *IFAC-PapersOnLine*, Vol. 50, No. 1, pp. 13654–13661, 2017.
- [42] P. Encarnação, A. Pascoal, and M. Arcaç, "Path following for autonomous marine craft," *IFAC PapersOnline*, Vol. 33, No. 21, pp. 117–122, 2000.
- [43] M. Abdelaal, M. Fränzle, and A. Hahn, "NMPC-based trajectory tracking and collision avoidance of underactuated vessels with elliptical ship domain," *IFAC-PapersOnLine*, Vol. 49, No. 23, pp. 22–27, 2016.
- [44] R. R. Negenborn, H. Zheng and G. Lodewijks, "Trajectory tracking of autonomous vessels using model predictive control," *IFAC-PapersOnLine*, Vol. 19, June 2013.
- [45] S. L. Dai, M. Wang, and C. Wang, "Neural learning control of marine surface vessels with guaranteed transient tracking performance," *IEEE Transactions on Industrial Electronics*, Vol. 63, pp. 1717–1727, March 2016.
- [46] Y. Qu, B. Xiao, Z. Fu, and D. Yuan, "Trajectory exponential tracking control of unmanned surface ships with external disturbance and system uncertainties," *ISA Transactions*, Vol. 78, pp. 47–55, 2018.
- [47] M. E. Serrano, G. J. E. Scaglia, S. A. Godoy, V. Mut, and O. A. Ortiz, "Trajectory tracking of underactuated surface vessels: A linear algebra approach," *IEEE Transactions on Control Systems Technology*, Vol. 22, pp. 1103–1111, May 2014.
- [48] J. Velagic, Z. Vukic, and E. Omerdic, "Adaptive fuzzy ship autopilot for track-keeping," *Control Engineering Practice*, vol. 11, no. 4, pp. 433 – 443, 2003. MCMC00.
- [49] M. E. N. Sørensen and M. Breivik, "Comparing nonlinear adaptive motion controllers for marine surface vessels," *IFAC-PapersOnLine*, vol. 48, no. 16, pp. 291–298, 2015.
- [50] M. Chen, S. S. Ge, B. V. E. How, and Y. S. Choo, "Robust adaptive position mooring control for marine vessels," *IEEE Transactions on Control Systems Technology*, Vol. 21, pp. 395–409, March 2013.
- [51] Y. Yang, J. Du, H. Liu, C. Guo, and A. Abraham, "A trajectory tracking robust controller of surface vessels with disturbance uncertainties," *IEEE Transactions on Control Systems Technology*, vol. 22, pp. 1511–1518, July 2014.
- [52] L. Consolini and M. Tosques, "A minimum phase output in the exact tracking problem for the non-minimum phase underactuated surface ship," *IEEE Transactions on Automatic Control*, Vol. 57, pp. 3174–3180, December 2012.

- [53] R. Yu, Q. Zhu, G. Xia, and Z. Liu, "Sliding mode tracking control of an underactuated surface vessel," *IET Control Theory Applications*, Vol. 6, pp. 461–466, February 2012.
- [54] H. Ashrafiuon, K. R. Muske, L. C. McNinch, and R. A. Soltan, "Sliding-mode tracking control of surface vessels," *IEEE Transactions on Industrial Electronics*, Vol. 55, pp. 4004–4012, November 2008.
- [55] H. Zheng, R. R. Negenborn, and G. Lodewijks, "Closed-loop scheduling and control of waterborne agvs for energy-efficient inter terminal transport," *Transportation Research Part E: Logistics and Transportation Review*, Vol. 105, pp. 261–278, 2017.
- [56] A. Pavlov, H. Nordahl, and M. Breivik, "MPC-based optimal path following for underactuated vessels," *IFAC-PapersOnline*, Vol. 42, No. 18, pp. 340–345, 2009.
- [57] P. Schulten, *The interaction between diesel engines, ship and propellers during maneuvering*, PhD thesis, Delft University of Technology, 2005.
- [58] A. Haseltalab and R. R. Negenborn, "Predictive on-board power management for all-electric ships with DC distribution architecture," in *OCEANS 2017*, pp. 1–8, Aberdeen, Scotland, June 2017.
- [59] M. Butcher, R. Maltby, and P. Parvin, "Compact DC power and propulsion systems - the definitive solution?," in proceedings of *Electric Ship Technologies Symposium*, pp. 521–528, April 2009.
- [60] R. O'Rourke, "Navy DDG-51 and DDG-1000 destroyer programs: Background and issues for congress", CRS report, 2019.
- [61] J. Hou, J. Sun, and H. Hofmann, "Adaptive model predictive control with propulsion load estimation and prediction for all-electric ship energy management," *Energy*, vol. 150, pp. 877–889, 2018.
- [62] A. Kwasinski and C. N. Onwuchekwa, "Dynamic behavior and stabilization of DC microgrids with instantaneous constant power loads," *IEEE Transactions on Power Electronics*, Vol. 26, pp. 822–834, March 2011.
- [63] X. Feng, Z. Ye, K. Xing, F. C. Lee, and D. Borojevic, "Impedance specification and impedance improvement for dc distributed power system," in *30th Annual IEEE Power Electronics Specialists Conference*, Vol. 2, pp. 889–894, July 1999.
- [64] I. Gadoura, V. Grigore, J. Hatonen, J. Kyyra, P. Vallittu, and T. Suntio, "Stabilizing a telecom power supply feeding a constant power load," in *INTELEC - Twentieth International Telecommunications Energy Conference*, pp. 243–248, Oct 1998.
- [65] R. S. Balog, W. W. Weaver, and P. T. Krein, "The load as an energy asset in a distributed DC smartgrid architecture," *IEEE Transactions on Smart Grid*, vol. 3, pp. 253–260, March 2012.

- [66] M. Weiming, H. An, L. Dezhi, and Z. Gaifan, "Stability of a synchronous generator with diode-bridge rectifier and back-EMF load," in proceedings of *IEEE Power Engineering Society Winter Meeting*, vol. 1, pp. 609–615, Jan 2000.
- [67] T. H. Helland, "Stability analysis of diode bridge rectifier-loaded synchronous generators characterized with high values of reactances," MSc thesis, Norwegian University of Science and Technology, 2015.
- [68] P. Liutanakul, A. Awan, S. Pierfederici, B. Nahid-Mobarakeh, and F. Meibody-Tabar, "Linear stabilization of a DC bus supplying a constant power load: A general design approach," *IEEE Transactions on Power Electronics*, Vol. 25, pp. 475–488, February 2010.
- [69] J. Wang and D. Howe, "A power shaping stabilizing control strategy for DC power systems with constant power loads," *IEEE Transactions on Power Electronics*, Vol. 23, pp. 2982–2989, November 2008.
- [70] S. Singh, V. Kumar, and D. Fulwani, "Mitigation of destabilising effect of CPLs in island DC micro-grid using non-linear control," *IET Power Electronics*, Vol. 10, No. 3, pp. 387–397, 2017.
- [71] J. You, M. Vilathgamuwa, and N. Ghasemi, "DC bus voltage stability improvement using disturbance observer feedforward control," *Control Engineering Practice*, Vol. 75, pp. 118 – 125, 2018.
- [72] A. Riccobono and E. Santi, "Positive feedforward control of three-phase voltage source inverter for dc input bus stabilization with experimental validation," *IEEE Transactions on Industry Applications*, vol. 49, pp. 168–177, January 2013.
- [73] G. Sulligoi, D. Bosich, G. Giadrossi, L. Zhu, M. Cupelli, and A. Monti, "Multiconverter medium voltage DC power systems on ships: constant power loads instability solution using linearization via state feedback control," *IEEE Transactions on Smart Grid*, Vol. 5, pp. 2543–2552, September 2014.
- [74] L. Herrera, W. Zhang, and J. Wang, "Stability analysis and controller design of DC microgrids with constant power loads," *IEEE Transactions on Smart Grid*, Vol. 8, pp. 881–888, March 2017.
- [75] M. K. Zadeh, B. Zahedi, M. Molinas, and L. E. Norum, "Centralized stabilizer for marine DC microgrid," in *39th Annual Conference of the IEEE Industrial Electronics Society*, pp. 3359–3363, November 2013.
- [76] Y. Murphey, J. Park, L. Kiliaris, M. Kuang, M. Masrur, A. Phillips, and Q. Wang, "Intelligent hybrid vehicle power control, part ii: Online intelligent energy management," *IEEE Transactions on Vehicular Technology*, Vol. 62, pp. 69–79, January 2013.
- [77] F. Chen, R. Burgos, D. Boroyevich, and W. Zhang, "A nonlinear droop method to improve voltage regulation and load sharing in dc systems," in proceedings of *IEEE First International Conference on DC Microgrids (ICDCM)*, pp. 45–50, June 2015.

- [78] L. Meng, T. Dragicevic, J. C. Vasquez, and J. M. Guerrero, "Tertiary and secondary control levels for efficiency optimization and system damping in droop controlled DC-DC converters," *IEEE Transactions on Smart Grid*, vol. 6, pp. 2615–2626, November 2015.
- [79] I. Kiaei and S. Lotffard, "Tube-based model predictive control of energy storage systems for enhancing transient stability of power systems," *IEEE Transactions on Smart Grid*, pp. 1–1, 2018.
- [80] A. Iovine, T. Rigaut, G. Damm, E. D. Santis, and M. D. D. Benedetto, "Power management for a DC microgrid integrating renewables and storages," *Control Engineering Practice*, Vol. 85, pp. 59–79, 2019.
- [81] N. Noroozi, S. Trip, and R. Geiselhart, "Model predictive control of DC microgrids: current sharing and voltage regulation," *IFAC-PapersOnLine*, Vol. 51, No. 23, pp. 124 – 129, 2018.
- [82] J. Kumar, A. Agarwal, and V. Agarwal, "A review on overall control of DC microgrids," *Journal of Energy Storage*, Vol. 21, pp. 113–138, 2019.
- [83] A. G. Tsikalakis and N. D. Hatziargyriou, "Centralized control for optimizing microgrids operation," *IEEE Transactions on Energy Conversion*, Vol. 23, pp. 241–248, March 2008.
- [84] R. A. F. Ferreira, H. A. C. Braga, A. A. Ferreira, and P. G. Barbosa, "Analysis of voltage droop control method for DC microgrids with Simulink: Modelling and simulation," in *10th IEEE/IAS International Conference on Industry Applications*, pp. 1–6, November 2012.
- [85] C. Chen, S. Duan, T. Cai, B. Liu, and G. Hu, "Smart energy management system for optimal microgrid economic operation," *IET Renewable Power Generation*, Vol. 5, pp. 258–267, May 2011.
- [86] D. Wu, F. Tang, T. Dragicevic, J. M. Guerrero, and J. C. Vasquez, "Coordinated control based on bus-signaling and virtual inertia for islanded DC microgrids," *IEEE Transactions on Smart Grid*, Vol. 6, pp. 2627–2638, November 2015.
- [87] T. Dragicevic, X. Lu, J. C. Vasquez, and J. M. Guerrero, "DC microgrids part i: A review of control strategies and stabilization techniques," *IEEE Transactions on Power Electronics*, Vol. 31, pp. 4876–4891, July 2016.
- [88] R. R. Negenborn, Z. Lukszo, and H. Hellendoorn, *Intelligent Infrastructures*. Springer, Dordrecht, The Netherlands, 2010.
- [89] M. Yazdani and A. Mehrizi-Sani, "Distributed control techniques in microgrids," *IEEE Transactions on Smart Grid*, Vol. 5, pp. 2901–2909, November 2014.
- [90] R. R. Negenborn, *Multi-Agent Model Predictive Control with Applications to Power Networks*. PhD thesis, Delft University of Technology, 2007.

- [91] D. Dam and H. Lee, "A power distributed control method for proportional load power sharing and bus voltage restoration in a DC microgrid," *IEEE Transactions on Industry Applications*, Vol. 54, pp. 3616–3625, July 2018.
- [92] K. Sun, L. Zhang, Y. Xing, and J. M. Guerrero, "A distributed control strategy based on DC bus signaling for modular photovoltaic generation systems with battery energy storage," *IEEE Transactions on Power Electronics*, Vol. 26, pp. 3032–3045, October 2011.
- [93] C. De Persis, E. R. Weitenberg, and F. Dörfler, "A power consensus algorithm for DC microgrids," *Automatica*, Vol. 89, pp. 364–375, 2018.
- [94] S. Boudoudouh and M. Maârroufi, "Multi-agent system solution to microgrid implementation," *Sustainable Cities and Society*, Vol. 39, pp. 252–261, 2018.
- [95] A. Armellini, S. Daniotti, P. Pinamonti, and M. Reini, "Evaluation of gas turbines as alternative energy production systems for a large cruise ship to meet new maritime regulations," *Applied Energy*, Vol. 211, pp. 306–317, 2018.
- [96] L. van Biert, M. Godjevac, K. Visser, and P. V. Aravind, "A review of fuel cell systems for maritime applications," *Journal of Power Sources*, Vol. 327, pp. 345–364, 2016.
- [97] S. Wen, H. Lan, Y.-Y. Hong, D. C. Yu, L. Zhang, and P. Cheng, "Allocation of ESS by interval optimization method considering impact of ship swinging on hybrid PV/diesel ship power system," *Applied Energy*, vol. 175, pp. 158–167, 2016.
- [98] H. Liu, Q. Zhang, X. Qi, Y. Han, and F. Lu, "Estimation of PV output power in moving and rocking hybrid energy marine ships," *Applied Energy*, Vol. 204, pp. 362–372, 2017.
- [99] R. Izadi-Zamanabadi and M. Blanke, "A ship propulsion system as a benchmark for fault-tolerant control," *Control Engineering Practice*, Vol. 7, No. 2, pp. 227–239, 1999.
- [100] D. K. P. Barnitsas, M. M.; Ray, "Kt, Kq and efficiency curves for the Wageningen B-series propellers," technical report, Department of Naval Architecture and Marine Engineering, University of Michigan, Ann Arbor, 1981.
- [101] P. C. Krause, O. Wasynczuk, and S. Pekarek, *Analysis of Electric Machinery and Drive Systems, 3rd Edition*, Wiley-IEEE press, 2013.
- [102] H. T. Grimmeliuss, E. Mesbahi, P. J. M. Schulten, and D. Stapersma, "The use of diesel engine simulation models in ship propulsion plant design and operation," in proceedings *CIMAC World Congress*, Vienna, 2007.
- [103] M. Blanke and J. Andersen, *On dynamics of large two stroke Diesel Engines: new results from identification*. 1984.
- [104] O. N. Smogeli, *Control of marine propellers*. PhD thesis, Norwegian University of Science and Technology, 2006.

- [105] J. Jatskevich, S. D. Pekarek, and A. Davoudi, "Parametric average-value model of synchronous machine-rectifier systems," *IEEE Transactions on Energy Conversion*, vol. 21, pp. 9–18, March 2006.
- [106] G. L. Plett, "Extended Kalman filtering for battery management systems of Lipb-based HEV battery packs: Part 1. background," *Journal of Power Sources*, Vol. 134, No. 2, pp. 252–261, 2004.
- [107] T. H. Syverud, "Modeling and control of a DC-grid hybrid power system with battery and variable speed diesel generators," MSc thesis, Norwegian University of Science and Technology, 2016.
- [108] F. L. Lewis, A. Yesildirak, and S. Jagannathan, *Neural Network Control of Robot Manipulators and Nonlinear Systems*. Bristol, PA, USA: Taylor & Francis, Inc., 1998.
- [109] K. Hornik, M. Stinchcombe, and H. White, "Multilayer feedforward networks are universal approximators," *Neural Networks*, vol. 2, pp. 359–366, July 1989.
- [110] M. H. Stone, "The generalized Weierstrass approximation theorem," *Mathematics Magazine*, vol. 21, no. 4, pp. 167–184, 1948.
- [111] P. V. Oossanen and M. Oosterveld, "Further computer-analyzed data of the Wageningen B-screw series," *International Shipbuilding Progress*, Vol. 22, No. 251, 1975.
- [112] H. Klein Woud and D. Stapersma, *Design of Propulsion and Electric Power Generation Systems*, IMarEST, 2002.
- [113] F. Gutsche, *The Study of Ships' Propellers in Oblique Flow*, DRIC translation, 1975.
- [114] G. Kuiper, M. Grimm, B. McNeice, B. Noble, and M. Krikke, "Propeller inflow at full scale during a maneuver," in *24th Symposium on Naval Hydrodynamics, Fukuoka, Japan*, 2002.
- [115] H. Nijmeijer and A. van der Schaft, *Nonlinear Dynamical Control Systems*. Springer-Verlag, New York, 1990.
- [116] J. D. Boskovic, L. Chen, and R. K. Mehra, "Multivariable adaptive controller design for a class of non-affine models arising in flight control," in *Decision and Control, 2001. in proceedings of the 40th IEEE Conference on*, Vol. 3, pp. 2442–2447, 2001.
- [117] A. Das and F. L. Lewis, "Distributed adaptive control for synchronization of unknown nonlinear networked systems," *Automatica*, Vol. 46, No. 12, pp. 2014–2021, 2010.
- [118] B. J. Yang and A. J. Calise, "Adaptive control of a class of non-affine systems using neural networks," *IEEE Transactions on Neural Networks*, Vol. 18, pp. 1149–1159, July 2007.
- [119] M. J. Kurtz and M. A. Henson, "Input-output linearizing control of constrained nonlinear processes," *Journal of Process Control*, Vol. 7, No. 1, pp. 3–17, 1997.

-
- [120] H. A. B. te Braake, M. A. Botto, H. J. L. van Can, J. S. da Costa, and H. B. Verbruggen, "Linear predictive control based on approximate input-output feedback linearisation," in proceedings of *Control Theory and Applications*, vol. 146, pp. 295–300, July 1999.
- [121] R. R. Groenewegen, D. J. J. B. Bruggink, Q. C. Cremer, and A. G. C. Klokgieters, "Differentiation of maneuvering coefficients for scaled model vessels," BSc end project report, Delft University of Technology, 2018.
- [122] J. R. Rawlings and D. Q. Mayne, *Model Predictive Control: Theory and Design*. Nob Hill Publishing, 2009.
- [123] J. Liu, W. Zhang, and G. Rizzoni, "Robust stability analysis of dc microgrids with constant power loads," *IEEE Transactions on Power Systems*, vol. 33, pp. 851–860, Jan 2018.
- [124] M. A. Henson and D. E. Seborg, eds., *Nonlinear Process Control*. Upper Saddle River, NJ, USA: Prentice-Hall, Inc., 1997.
- [125] T. H. Syverud, "Modeling and control of a DC-grid hybrid power system with battery and variable speed diesel generators," MSc, Norwegian University of Science and Technology, 2016.

A

APPENDIX

A.1. MANEUVERING MODEL OF TITO-NERI

The parameters of the maneuvering model are provided in Table A.1. The drag forces are estimated using the graphs in Figure A.1. Moreover, $\tau_{\text{drag}\theta} = \frac{1}{3}\tau_{\text{drag}_y}(\frac{\pi}{2}, \frac{2v_r}{3})$. For more information regarding the Tito-Neri model, see [121].

A.2. SPECIFICATIONS OF THE LOW VOLTAGE PPS

A.2.1. DIESEL ENGINE

- I. 1.8 MW DGR set: $K_{\text{en}} = 2.2 \times 10^4$, rated speed: 188.5 rad/s , $a = 6.45 \times 10^7 \text{ gr.kWh}$, $b = 3.45 \times 10^{-5} \text{ gr/kWh}^2$, $c = 96.21 \text{ gr/kWh}$.
- II. 1.2 MW DGR set: $K_{\text{en}} = 1.4 \times 10^4$, rated speed: 188.5 rad/s , $a = 3.68 \times 10^7 \text{ gr.kWh}$, $b = 4.40 \times 10^{-5} \text{ gr/kWh}^2$, $c = 109.60 \text{ gr/kWh}$.

A.2.2. SYNCHRONOUS GENERATORS

- I. 1.8 MW DGR set: 1.8 MW, 460 v, 60 Hz, 4 poles, $J = 112.8$, $r_s = 0.0008$, $r_{fd} = [0.00015, r_{kd} = 0.016, r_{kq} = 0.0021, L_d = 0.0077, L_{md} = 1.273 \times 10^{-5}, L_{kd} = 0.00054, L_{fd} = 8.7 \times 10^{-5}, L_q = 0.00052, L_{mq} = 0.00051 \text{ and } L_{kq} = 5.2 \times 10^{-5}$.
- II. 1.2 MW DGR set: 1.2 MW, 460 v, 60 Hz, 4 poles, $J = 96.4$, $r_s = 0.0011$, $r_{fd} = 0.00045$, $r_{kd} = 0.034$, $r_{kq} = 0.0041$, $L_d = 0.012$, $L_{md} = 0.00014$, $L_{kd} = 0.0011$, $L_{fd} = 0.0017$, $L_q = 0.00091$, $L_{mq} = 0.0013 \text{ and } L_{kq} = 0.00013$.

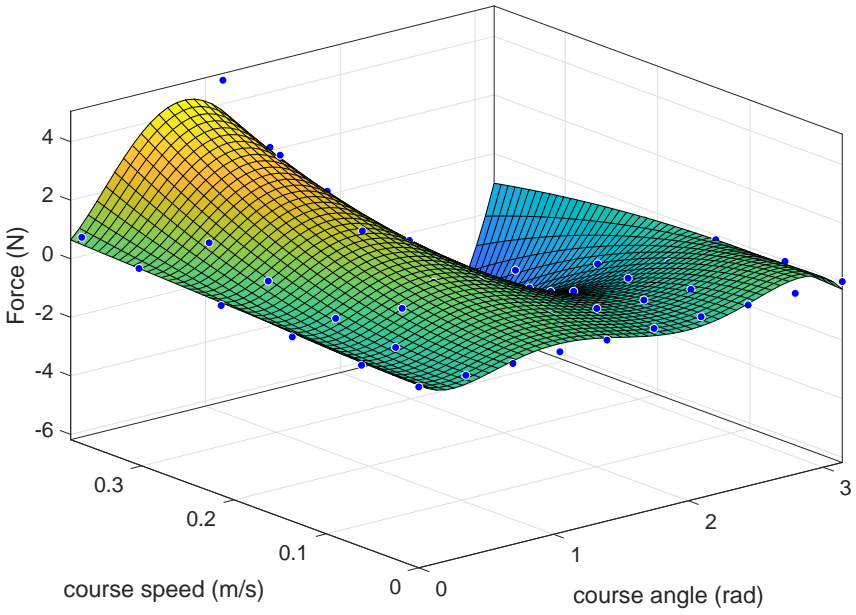
Resistance values are in ohms and inductance values are in Henry.

A.2.3. RECTIFIER

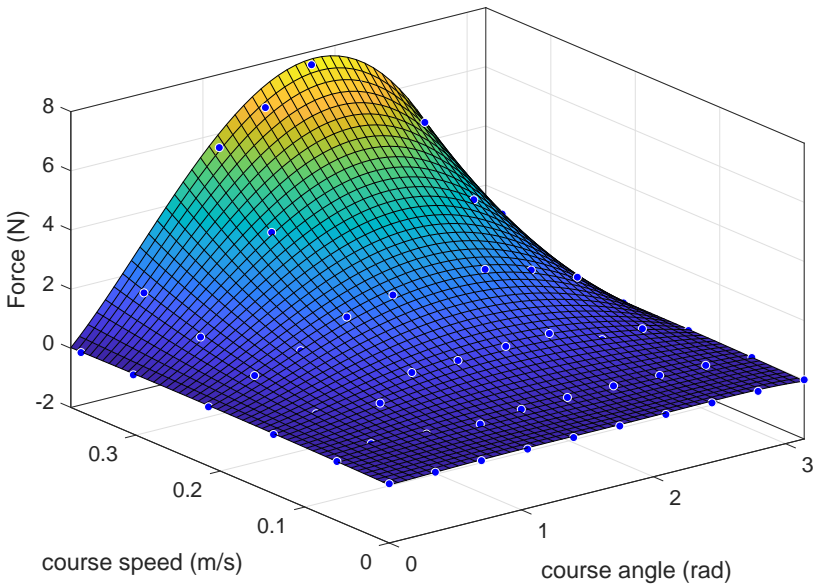
Snubber values of six-pulse rectifiers, $r_{\text{sn}} = 100 \text{ ohms}$ and $C_{\text{sn}} = 1e-5 \text{ F}$

A.2.4. DC-LINK

$C = 0.05 \text{ F}$



(a) Longitudinal drag forces in the body-fixed frame.



(b) Lateral drag forces in the body-fixed frame.

Figure A.1: The graph of Tito-Neri drag forces.

Parameter	Symbol	Value	Unit
Mass of the ship	m_b	16.9	kg
Mass matrix	M_{RB}	$\begin{bmatrix} 16.9 & 0 & 0 \\ 0 & 16.9 & 0 \\ 0 & 0 & 0.51 \end{bmatrix}$	$\begin{bmatrix} kg \\ kg \\ kg * m^2 \end{bmatrix}$
Added mass matrix	M_A	$\begin{bmatrix} 1.2 & 0 & 0 \\ 0 & 49.2 & 0 \\ 0 & 0 & 1.8 \end{bmatrix}$	$\begin{bmatrix} kg \\ kg \\ kg * m^2 \end{bmatrix}$
Length ship	l	0.97	m
Width ship	w	0.3	m
Center of gravity	CoG	$\begin{bmatrix} 0 \\ 0 \end{bmatrix}$	$\begin{bmatrix} m \\ m \end{bmatrix}$
Port-thruster location	-	$\begin{bmatrix} -0.42 \\ -0.08 \end{bmatrix}$	m
Starboard-thruster location	-	$\begin{bmatrix} -0.42 \\ 0.08 \end{bmatrix}$	m

Table A.1: Maneuvering model parameters.

A.2.5. INDUCTION MOTOR

I. Induction motors of propellers: 1.5 MW, 460 v, 60 Hz, 4 poles, $J_m = 4.2$, $r_{sm} = 0.0001818$, $r_{rm} = 0.0009956$, $L_{sm} = 0.00099$, $L_{mm} = 0.0009415$, $L_{rm} = 0.00096$.

II. Induction motor of the bow thruster: 0.5 MW, 460 v, 60 Hz, 4 poles, $J_m = 3.1$, $r_{sm} = 0.0148$, $r_{rm} = 0.00929$, $L_{sm} = 0.0108$, $L_{mm} = 0.0104$, $L_{rm} = 0.0105$.

Resistance values are in ohms and inductance values are in Henry. Direct torque control is used for the control of induction motors [Krause, P. C. Analysis of Electric Machinery. New York: McGraw-Hill, 1986.].

A.2.6. PROPELLING ACTUATORS

I. Propellers: $K_T = 0.59$, $K_Q = 0.046$, $D = 2.4$ m, $\rho = 1024$ kg/m³.

II. Bow thruster: $K_T = 0.56$, $K_Q = 0.041$, $D = 1$ m, $\rho = 1024$ kg/m³.

A.2.7. BATTERY

$C_n = 2000$ Ah, $\eta_i = 0.96$ (charge mode), $v_b = 400$ V.

A.2.8. BIDIRECTIONAL CONVERTER

$C_c = 267$ μ F, $L_c = 516$ μ H, $R_c = 19$ ohm, $n = 3$.

A.3. SPECIFICATIONS OF THE HIGH VOLTAGE PPS

- **The ship model:** Length: 90 m, deadweight at design draught: 425 ton, Displacement at design draught 2565 ton.
- **Induction motors:** 1.8 MW, 6600 V, 60 Hz, four poles.
- **Diesel Engine I:** $K_{en} = 57295$, twelve cylinders, 5.4 MW, diesel-generator gear ratio: $\frac{1}{2}$.
- **Diesel Engine II:** $K_{en} = 36668$, twelve cylinders, 3.5 MW, diesel-generator gear ratio: $\frac{1}{2}$.
- **Synchronous generator I:** 6.150 MW, 6600 v, 60 Hz, 10 poles, $H = 0.71$, $r_s = 0.0363$, $r_{fd} = 0.2$, $r_{kd} = 0.722$, $r_{kq} = 0.1072$, $L_d = 0.0323$, $L_{md} = 0.0305$, $L_{kd} = 0.0320$, $L_{fd} = 0.4820$, $L_q = 0.0163$, $L_{mq} = 0.0144$ and $L_{kq} = 0.0163$. Resistance values are in ohm and inductance values are in Henry.
- **Synchronous generator II:** 3.456 MW, 6600 v, 60 Hz, 10 poles, $H = 0.56$, $r_s = 0.0601$, $r_{fd} = 0.177$, $r_{kd} = 1.5049$, $r_{kq} = 0.1726$, $L_d = 0.05768$, $L_{md} = 0.05407$, $L_{kd} = 0.06125$, $L_{fd} = 0.3204$, $L_q = 0.02702$, $L_{mq} = 0.0144$ and $L_{kq} = 0.02341$. Resistance values are in ohm and inductance values are in Henry.
- **Rectifier:** Six-pulse rectifier, $\beta_{rec} = 0.981$.
- **DC-link:** $C = 0.5$ F
- **Bidirectional Converter:** $L = 0.0005$ H, $v_b = 1000$ V.

LIST OF PUBLICATIONS

The scientific results in this thesis have been partially published in:

1. A. Haseltalab, R. R. Negenborn, Adaptive Control for Autonomous Ships with Uncertain Model and Unknown Propeller Dynamics, Control Engineering Practice, Volume 91, 2019.
2. A. Haseltalab, R. R. Negenborn, Model predictive maneuvering control and energy management for all-electric autonomous ships, Applied Energy, Volume 251, pp. 1-27, 2019.
3. A. Haseltalab, M. A. Botto, R. R. Negenborn, Model Predictive DC Voltage Control for All-Electric Ships, Control Engineering Practice, Volume 90, pp. 133-147, September 2019.
4. A. Haseltalab, F. Wani, R. R. Negenborn, "Multi-level Power Generation Control for All-Electric Ships," Submitted to a scientific journal, 2019.
5. A. Haseltalab, M. A. Botto, R. R. Negenborn, "On-Board Voltage Regulation For All-Electric DC Ships," IFAC-PapersOnLine, Volume 51, Issue 29, Pages 341-347, 2018.
6. A. Haseltalab, R. R. Negenborn, Adaptive Control for a Class of Partially Unknown Non-Affine Systems: Applied to Autonomous Surface Vessels, IFAC-PapersOnLine, Volume 50, Issue 1, 2017, Pages 4252-4257.
7. A. Haseltalab, R. R. Negenborn, "Predictive on-board power management for all-electric ships with DC distribution architecture," in the proceedings of OCEANS 2017, Aberdeen, pp. 1-8, 2017.
8. A. Haseltalab, R. R. Negenborn, G. Lodewijks, Multi-Level Predictive Control for Energy Management of Hybrid Ships in the Presence of Uncertainty and Environmental Disturbances, IFAC-PapersOnLine, Volume 49, Issue 3, 2016, Pages 90-95.

CURRICULUM VITÆ

Ali HASELTALAB

Ali Haseltalab is a researcher at Delft University of Technology working towards enabling fuel-efficient and emission free autonomous shipping. His current main areas of interest are Control of marine systems, multi-agent control of transport systems, and networked systems analysis and control. As a researcher in the Department of Maritime and Transport Technology, Haseltalab is involved in several projects including "Gas-Drive: minimizing emissions and energy losses at sea with LNG combined prime movers, underwater exhausts and nano hull materials", "Impulse Autonomous Shipping for Amsterdam", and "ShipDrive: a novel methodology for integrated modeling, control, and optimization of hybrid ship system". Aside from his career, Haseltalab has a great passion for music, philosophy, and literature.

16-04-1989 Born in Tehran, Iran.

EDUCATION

2003–2007	High School Pirouz High School, Tehran, Iran
2007–2011	BSc in Electrical Engineering (Control and Systems) University of Tabriz, Tabriz, Iran
2012–2015	MSc in Electrical and Electronics Engineering (Control and Systems) Boğaziçi University, Istanbul, Turkey
2015–2019	PhD in Maritime and Transport Technology Delft University of Technology, Delft, the Netherlands